TP XXXXXX

Quantifying Underwater Radiated Noise (URN) Effects of Propeller Cages

Prepared for
The Innovation Centre
of
Transport Canada

By
Martec Limited

15 March 2024

TP XXXXXX

Quantifying Underwater Radiated Noise (URN) Effects of Propeller Cages

Report for: Matthew Cooke

Authors: D. Alexander, C. Arisman, C. Boudreau, A. Deeb, K. MacKay

Name of client: The Innovation Centre of Transport Canada

Report no.: TR-24-15

Project no.: 21.28049

Revision no.: 0

15 March 2024

Notices

This report reflects the views of the authors and not necessarily those of the Innovation Centre of Transport Canada or the cosponsoring organizations.

The Innovation Centre and the co-sponsoring agencies do not endorse products or manufacturers. Trade or manufacturers' names appear in this report only because they are essential to its objectives.

Un sommaire français se trouve avant la table des matières.

Publication Data Form

Formule de Données Pour Publication

Summary

Quantifying Underwater Radiated Noise (URN) Effects of Propeller Cages

Project Number: 21.28049

Authors: D. Alexander, C. Arisman, C. Boudreau, A. Deeb, K. MacKay

Report no.:	Revision no.:	Report date:
TR-24-15	0	15 March 2024

Prepared by:	Reviewed by:	Approved by:
Derrick Alexander Lead Technical Specialist	Sydney Ryan Team Lead, Explosion and Fluid Dynamics	David Whitehouse Commercial Manager, Americas Advisory

Registered name:	Martec Limited
Correspondence address:	Martec Limited 237 Brownlow Ave, Suite 200, Dartmouth, NS, Canada, B3B 2C6
Contact:	Derrick Alexander T: +1 (902) 417 2471 E: derrick.alexander@lr.org

Client name and address:
The Innovation Centre of Transport Canada
330 Sparks St, Place De Ville, Tower C, 18th Floor(AHSB)
Ottawa, ON K1A 0N5

Client contact:
Matthew Cooke
T: (343) 543 3497
E: Matthew.Cooke@tc.gc.ca

Document control

Revision history

Revision No.	Date	Revision
0	15 March 2023	Original Release

Proprietary Notice

This report was prepared under a contribution Agreement for Quantifying Underwater Radiated Noise (URN) Effects in conjunction with the Transport Canada Innovation Centre.

The information contained herein may be used by Transport Canada Innovation Centre for their purposes only.

Complete use and disclosure limitations are contained in the Contribution Agreement for Quantifying Underwater Radiated Noise (URN) Effects (No. 164657).

Acknowledgements

The support and cooperation of the Innovation Centre of Transport Canada, are gratefully acknowledged.

Executive summary

Underwater acoustic ambient noise levels in the open ocean have doubled each decade during the period from 1950–2007 due to increasing commercial shipping activity. The increased noise has had notable impacts on marine mammals that rely heavily on self generated underwater acoustic signals as a primary means to communicate, navigate, and forage in the ocean. Transport Canada's Quiet Vessel Initiative recognizes this through their Underwater Radiated Noise (URN) and Green House Gas Reduction Program for Canada's Inshore Fishing Craft. For most ships and boats, the on-board machinery and propeller noise comprises the majority of the generated noise that becomes radiated into the far-field. There is a fair body of work on URN for large commercial and naval ships, but the focus in this project is the URN of small marine craft (fishery vessels, crab vessels, lifeboats, and pleasure craft) fitted with propeller cages. These are used to prevent snagging of lines and limit injury to both people and wildlife. The cages can significantly increase drag which negatively influences boat performance, increases fuel consumption, and generates URN harmful to marine life. Fouling of the cages exasperates these issues, with operators compensating by running the propellers at higher speed generating further cavitation and increased URN. Propeller cage impact on performance is rarely quantified, and no studies of their URN are present in the open literature.

In this project, the impact of propeller cages on URN was quantified by performing experimental measurements for four Cape Islander fishing vessels with bare propellers, propeller cages, and artificially fouled cages. In total 188 trials were conducted (four vessels; ambient, static, dynamic runs; without cage, with cage, with fouled cage). There was significant scatter in the measured URN; however, all vessels exhibited the highest peak near 5 Hz at approximately 160 dB. Generally, the presence of the cage increased the signature (up to 20 dB in some parts of the spectrum). Additionally fouling tended to increase the noise, with a larger impact at the lower speeds. The intention of this project was to generate a data set that may be used to assist in understanding URN interactions. As such the experimental data is freely available.

The second purpose of this project was to provide a validated modelling environment for future assessments of URN generated by propeller cages. Validated numerical models can be used to complement costly trial measurements and determine all desired quantities with a high resolution in space and time. Two vessels (of the four measured) were selected for model generation and noise predictions. Computational fluid dynamics (CFD) simulations were combined with a boundary element method (BEM) to simulate propeller performance and cavitation. Additional models were utilized to obtain noise predictions. The cages themselves were shown to have little noise generation compared to the propeller. The main performance issue was that the cages significantly increased the vessel drag, and hence the propeller required a higher RPM to compensate. Numerical predictions of the noise levels were higher than that determined experimentally. The relative noise levels were replicated by numerical predictions for the bare propeller, propeller cage, and fouled propeller. This would suggest that the relative impacts of propeller cage designs may be determined by the current methodology. Best practices derived from this project and other applicable numerical analyses were presented.

The relative merits of two different propeller cages designs were assessed compared to the baseline propeller cage.

Contents

List of Figures

List of Tables

Glossary

CFD	Computational Fluid Dynamics
URN	Underwater Radiated Noise
TC	Transport Canada
FW-H	Ffowcs-Williams Hawkings acoustic analogy
RANS	Reynold's Averaged Navier Stokes (CFD model methodology in which turbulent processes are modelled)
DNS	Direct Numerical Simulation (CFD model methodology all turbulent processes are resolved)
LES	Large-Eddy Simulation (CFD model methodology where turbulence on the order of the numerical mesh is resolved and sub-grid scale turbulence is modelled)
DES	Detached Eddy Simulation (CFD model methodology where turbulence on the order of the numerical mesh is resolved and sub-grid scale / near-wall turbulence is modelled)

1. Introduction

Earth's oceans are at a critical point in their health. This is relevant to everyone as all of humanity depends on the oceans. A growing body of literature suggests that low-frequency, underwater acoustic ambient noise levels in the open ocean increased approximately 3.3 dB (i.e., a doubling of the levels) each decade during the period from 1950–2007 [1]. This is attributed to increasing commercial shipping activity and its underwater radiated noise (URN).

The increased underwater acoustic ambient noise has had notable impacts on marine mammals (dolphins, seals, whales, etc.) as they rely heavily on self generated underwater acoustic signals as a primary means to communicate, navigate, and forage in the ocean. Increased acoustic ambient noise contributes to shorter ranges and distortions of their transmitted and received signals. This impact can manifest as abnormal behavior for their species. Marine mammals occupy an important niche in the ecosystem as predators and organic ocean fertilizers among other roles. Their health is a direct reflection of the ocean's health.

Transport Canada's Quiet Vessel Initiative recognizes this through their Underwater Radiated Noise (URN) and Green House Gas Reduction Program for Canada's Inshore Fishing Craft. URN from ships and boats are generated through their on-board machinery, propellers, and fluid flow noise. Propeller noise is the result of the hydrodynamic interactions between the propeller and the fluid it works in. Flow noise is created when the fluid interacts with the ship / boat's wetted hull in the process of the hull moving through the water. For most ships and boats, the on-board machinery and propeller noise comprises the majority of the generated noise that becomes radiated into the far-field [2].

When the boat is past its propeller cavitation inception, cavitation becomes the dominant source of radiated noise. Propellers cavitate when the low pressure they create drops below the local vapour pressure. Air that is dissolved in the fluid comes out of suspension in the form of bubbles. When the bubbles move into regions of higher pressure around the propeller, they collapse creating an acoustic impulse in the water. This usually is apparent as an increase in the radiated broadband levels. It can also be accompanied by tonals at the blade rates if the cavitation correlates with blade rates [3, 4, 5, 6].

There is a fair body of work on URN for large commercial and naval ships, but the focus in this project is the URN of small marine craft. Fishery vessels, crab vessels, and a significant portion of pleasure craft employ propeller cages. U.S. regulations require lifeboats and other rescue boats to be equipped with propeller cages (guards). These are used to prevent snagging of lines and to limit injury to both people and wildlife. These cages have several adverse impacts on URN. The cages can significant increase drag which negatively influences boat performance and increases fuel consumption. The cages often act as inception locations for cavitation. Fouling of the cages exasperates these issues, with operators compensating by running the propellers at higher speed generating further cavitation and URN. Propeller cage impact on performance is rarely quantified. No studies of propeller cage impact on URN are present in the open literature.

The goals of the proposed project are to measure the impact of propeller cages on URN and to provide a validated modelling environment for future assessments. This work includes four major activities:

1. Trials to measure acoustic signatures and quantify the impact of propeller cages on underwater vessel noise. This includes characterizing the vessel/propeller cage geometry and cage fouling by recording URN and vessel performance with fouled cage, clean cage, and bare propeller.

2. Development of best practices to predict URN from propeller cages systems via Computational Fluid Dynamic (CFD) analyses and other performance prediction tools. Validation of the hydroacoustic

predictions of noise generation with the results from Activity 1. This will assist in the consideration of underwater radiated noise (URN) mitigation as a design criterion for vessels.

3. Assessment of different propeller cage designs for vessel performance (fuel consumption) and URN. This effort helps increase the technology readiness level of propeller cages with respect to quantified URN levels and establishes a baseline for comparisons of future propeller cage designs. This will help to support the design of propeller cages used for fishing and whale-watching vessels, to reduce their underwater noise impacts on endangered marine mammals.

4. Assembly of the measurements, validation study results and performance predictions of the previous three Activities into a Final Report. In addition, a summary of best practice modelling guidelines will be generated to assist others with hydroacoustic modelling of propeller cages.

This report encompasses the Activity 4 tasks and details the work and results of Activities 1 (Section 3), 2 (Section 4) and 3 (Section 5). Best practice guidelines for propeller cage noise predictions are given in Section 6. In keeping with Transport Canada's desired outcomes, Section 7 summarizes the project's major achievements, Section 8 compares the project performance indicators to those originally planned, and Section 9 concludes with lessons learned in the course of this work.

2. Considered Vessels

In previous work [7], URN datasets were collected from six Cape Islanders operating in Nova Scotia, Canada. This dataset included measurements from accelerometers, a tachometer, a microphone in the engine compartment and a hydrophone. For this project, new measurements were made to specifically characterize the URN generated by the propeller cages used on these vessels. These vessels are similar to those utilized for a variety of purposes in sensitive marine environments including fishing vessels, lifeboats, whale watching charters, and pleasure craft.

An overview of the four vessels is provided in the following sub-sections.

All propeller cages were hand made from metal rods and plates. They each consisted of two parts, one on each side of the vessel. Horizontal rods start at the end of the keel (or slightly upstream of this location) and flare outwards into a U shape at the back end of the propeller. Smaller diameter rods were run vertically between the horizontal ones.

2.1 This Is It 1

Figure 2-1: Port view of This Is It 1.

Figure 2-2: Port-Aft view of propeller, cage, and rudder on This Is It 1.

2.2 Just Once

Figure 2-3: Starboard view of Just Once.

Figure 2-4: Port view of cage (backed by cardboard for scanning) on Just Once.

2.3 Bay Bliss

Parameter	Value
Length, Lpp	10.58 m
Beam	4.33 m
Draft	1.33 m
Propeller Diameter	0.7112 m (28.0 inches)
Cage Width	1.02 m (40.15 inches)
Cage Length	0.73 m (28.75 inches)

Figure 2-5: Port view of Bay Bliss.

Figure 2-6: Port view of cage (backed by cardboard for scanning) and rudder on Bay Bliss.

2.4 Brooklynn and Boys

Parameter	Value
Length, Lpp	10.73 m
Beam	4.14 m
Draft	1.08 m
Propeller Diameter	0.5842 m (23.0 inches)
Cage Width	1.06 m (41.75 inches)
Cage Length	1.28 m (50.39 inches)

Figure 2-7: Port view of Brooklynn and Boys.

Figure 2-8: Port view of cage (backed by cardboard for scanning) on Brooklynn and Boys.

3. Activity #1 - Measure Acoustic Signatures

In order to generate a predictive numerical methodology for the noise generated by propeller cages, a well-documented validation dataset is required. Numerous factors can impact both vessel performance and URN. In order to isolate the specific contributions from propeller cages, high quality measurements of both vessel performance and URN need to be generated with and without propeller cages for the same vessel. This will allow the relative performance and noise values to be determined and quantitative values assigned to the differences specifically from the cages.

In previous work, in conjunction with Transport Canada (TC) and Graphite Innovation & Technologies (GIT), URN datasets were collected from six Cape Islander vessels. This dataset included measurements from accelerometers, a tachometer, a microphone in the engine compartment and a hydrophone. Three types of measurements were collected in this set: ambient noise, static noise (URN spectrum at different engine speeds with the propeller out-of-gear) and dynamic noise (URN spectrum at different engine speeds, making two passes past a hydrophone on reciprocal headings). Observations of the propeller cages noted that they were full of marine growth that would negatively impact both the performance of the vessels and the URN.

For hydrodynamic noise generation, the flow from the hull, around the appendages and into the propeller must be properly predicted to the correct URN from downstream elements. The goal of this activity is two-fold:

1. To accurately characterize the vessel geometry, the propeller cage geometry, the cage fouling.
2. Record URN and vessel performance with a fouled propeller cage, a clean propeller cage, and a bare propeller without a cage.

This data will act as inputs to the numerical noise prediction in the subsequent activities.

Prior to conducting the trials, ship geometry data was assessed. There was no documented information available on the vessels (lines plans, propeller geometry diagrams, or appendage information). Instead, 3D photogrammetry scans were performed, as detailed in Section 4.2.

The test schedule was developed in cooperation with the 4 vessel captains interested in participating in this study. This included clarifying the need to control draft and trim (and therefore fuel levels). The recommended test location was just outside McGrath's Cove, Nova Scotia, which has a deep flat sandy bottom with no ambient noise sources. Test times were set to have the best chance of better conditions and less traffic. Sonar maps were available for the areas in which the boats normally fish. This includes not only the depth but also how "hard" the bottom is based on the reflection.

Unlike the information provided in pre-project discussions, the boat captains indicated that the cages don't typically get biofouled to the same extent as on the hull. There is typically a limited amount of growth and possible a handful of barnacles (for both coated and uncoated cages). What is problematic, is the temporary fouling of the cage (via for instance a piece of seaweed). Vessel captains noted that if there is too much blockage due to cage fouling, the boats are difficult to operate. It was noted that a piece of seaweed, the size of a hand, can cause severe vibrations and drastically slow the boats. The test plan therefore looked at adding a representative "blockage" and quantify the impact on both performance and noise. Initial thoughts were to weave in smaller (1/4") diameter rope through a few rows of the propeller cages, attaching a small plate to block some of the inflow, or to use a wire mesh over the cage. As the CFD models in the baseline analysis struggled to resolve the cage itself (while being of tractable computational size), the

finer rope/mesh approaches were deemed unsuitable. Cage fouling was achieved by attaching a small steel sheet to the cage, see Figure 3-1. The typical operational behaviour was assessed (i.e. the RPM is increased to compensate for the power decrease). Vessel stakeholders were interesting if optimized cages would have a significant impact on performance.

Figure 3-1: Artificial cage fouling on the Just Once

Since the hydrophones were located at distances of 15 and 40 m from the vessel, the numerical predictions must be capable of predicting the noise sources as well as the propagation of the noise to the far field. Similarly, the experimental noise predictions can be corrected back to the signal strength at a standard 1m distance. Both methods introduce uncertainty. To provide another point of validation data, a pressure sensor was mounted on the vessels. This allows for direct comparison of the predicted and measured quantities in the near field. There were discussions on the best location to mount the pressure sensors. The sensors are PCB 113B28 (Model 113B28 | PCB Piezotronics) and are typically mounted through the hull with the sensor face nearly flush with the hull surface. As the ship owners were unwilling to comprise their hulls, the decision was made to install the sensor on a steel plate that can be bolted to the hull using the existing hole in the hull at the open end of the cage. A strap was attached to the other end of the plate to hold it tight against the hull and to provide strain relief for the sensor cable. The sensor was located a few inches aft of the propeller and outboard of the centerline approximately 16", just a couple inches outside of the cage (when the cage is mounted), and within approx. ¼" from the hull surface (sensor is ¼" diameter, tube 5/16" dia., and steel plat thickness 1/16"), see Figure 3-2.

Figure 3-2: Pressure sensor location (in red circle) on This Is It 1.

Difficulties were encountered with the pressure sensors, with obvious damage to those retrieved from the first boats tested (Figure 3-3). Based on the accelerated corrosion at the bolt hole and the strap ring, it was theorized that there was a break in the cable and there was electricity passing to the steel base in addition to water ingress. Analysis of the pressure sensor data showed some significant differences across the boats and some smaller trends between the different run conditions, if not necessarily as expected across the whole frequency spectrum. As such, the recording of pressure data in addition to the noise data was desired for all vessels. Repairs were conducted on the sensors and cables, to enable their use on the remainder of the trials.

Figure 3-3: Pressure sensor damage

Field testing of the four subject vessels was completed successfully. For the test program, the noise was measured for ambient values, a static vessel, and dynamic runs at a variety of vessel speeds. Multiple speeds were measured to quantify the possible noise reduction that can be obtained by slowing the vessels. These include top speed (approximately 9 knots), minimum safe operating speed (approximately 3-4 knots), and 2-3 intermediary speeds. Due to the anticipated speed loss introduced by the presence of the propeller cages (and in particular fouled cages) for the same engine operation point, the trials attempted to keep similar speeds between the runs as this is more in keeping with the operational behaviour of the

vessels. This resulted in different propeller RPM values without the cage, with the cage, and with a fouled cage.

For each trial the following were measured:

- Ambient noise before static runs start, between static and dynamic runs, and after dynamic runs. Additional ambient measurements every hour as required.
- Weather: local wind speed, air and water temperature, and an estimate of wave height/sea state (with photo) at the same frequency as ambient noise measurement (more frequently as needed).
- Number of passengers.
- Approximate fuel level at start of trial.
- Latitude and longitude of static trial spot, hydrophone location, start/end of dynamic run (when speed/heading is already constant).
- Approximate depth of water at static trial spot, hydrophone location, and dynamic run route.

For each dynamic run the following were measured:

- Time.
- Underwater radiated noise at the hydrophones.
- Local pressure near the propeller.
- Vibration in the z-direction near the propeller and at the engine mount.
- Shaft RPM.
- Approximate heading and speed (GPS).

In total, 188 trials were conducted (4 vessels, ambient, static, dynamic runs without cage, with cage, with fouled cage). The measured underwater radiated noise signatures, at both the 15 m and 40 m hydrophone are presented in Figure 3-4 through Figure 3-11. There is significant scatter in the readings. All vessels exhibit the highest peak near 5 Hz at approximately 160 dB. This is reduced up to 30 Hz. A second peak is present at 200-300 Hz. Generally, the presence of the cage increased the signature (up to 20 dB in some parts of the spectrum). Additionally, fouling tended to increase the noise with a larger impact at the lower speeds.

The intention of this project was to generate a data set that may be used to assist in understanding URN interactions. As such, the experimental data is freely available. To obtain a copy of the data please contact Martec Limited via the contact information provided at the start or end of this report.

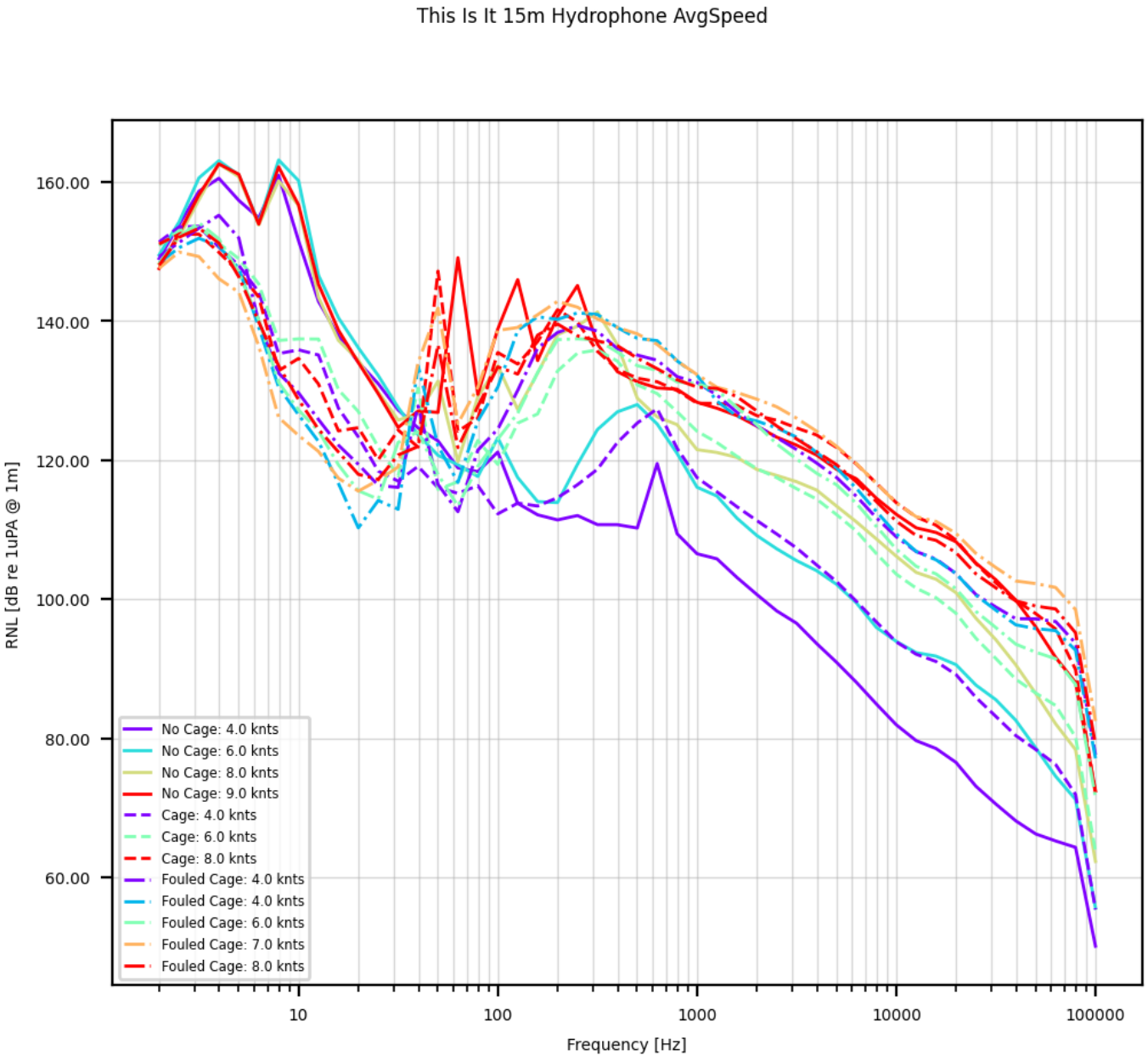

Figure 3-4: Underwater radiated noise spectrum for the “This Is It 1” from 15 m hydrophone.

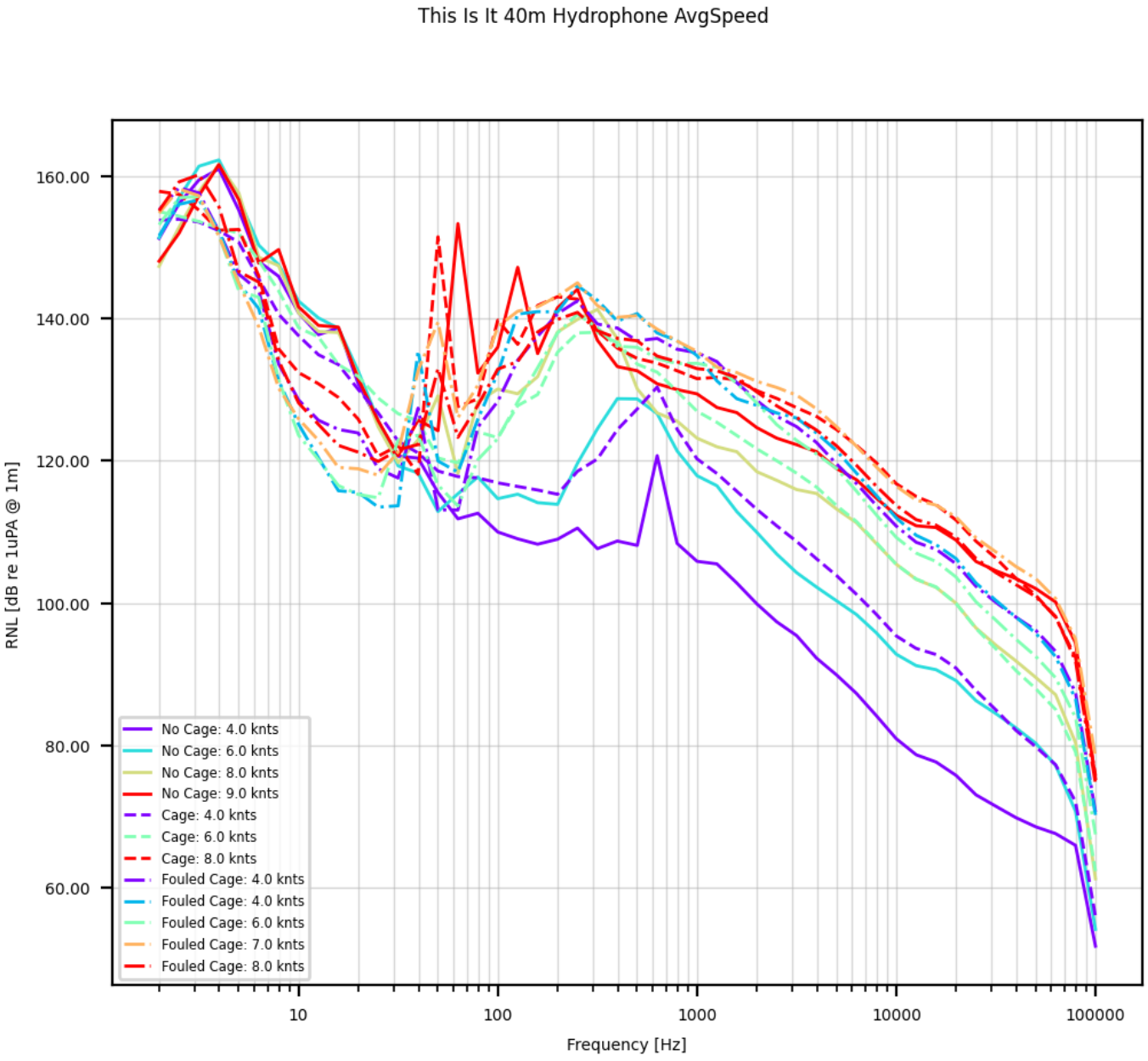

Figure 3-5: Underwater radiated noise spectrum for the “This Is It 1” from 40 m hydrophone.

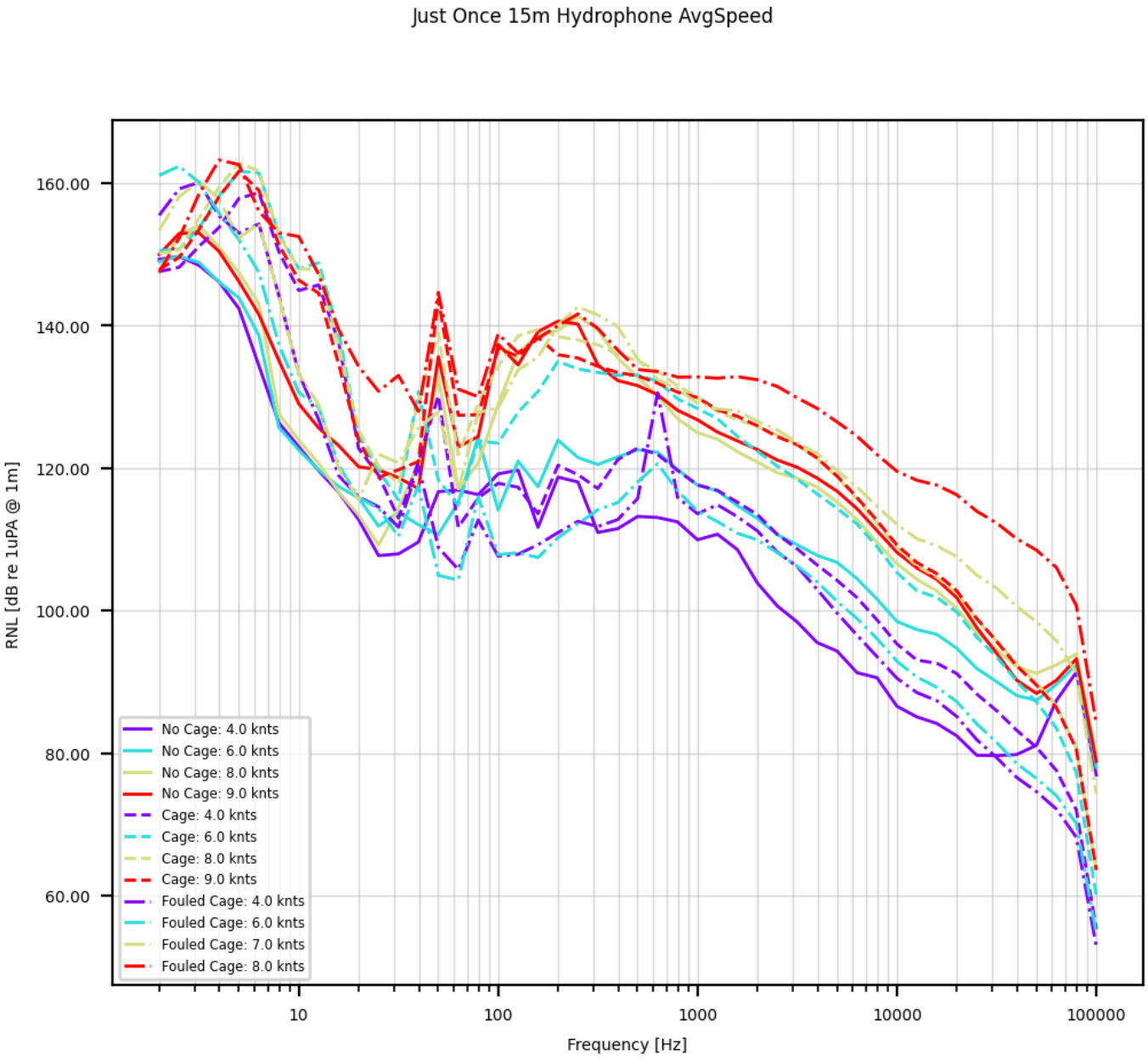

Figure 3-6: Underwater radiated noise spectrum for the "Just Once" from 15 m hydrophone

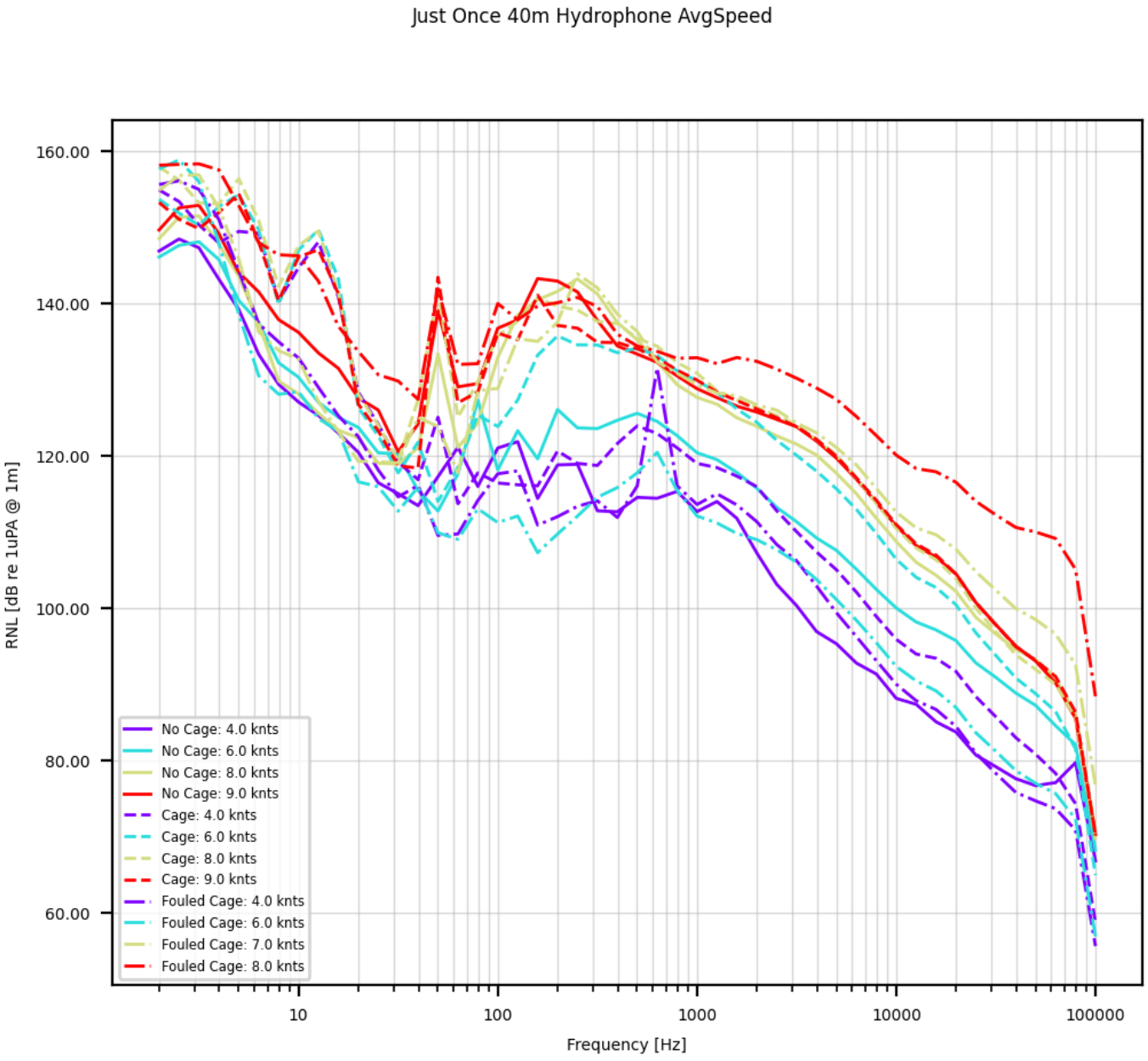

Figure 3-7: Underwater radiated noise spectrum for the "Just Once" from 40 m hydrophone

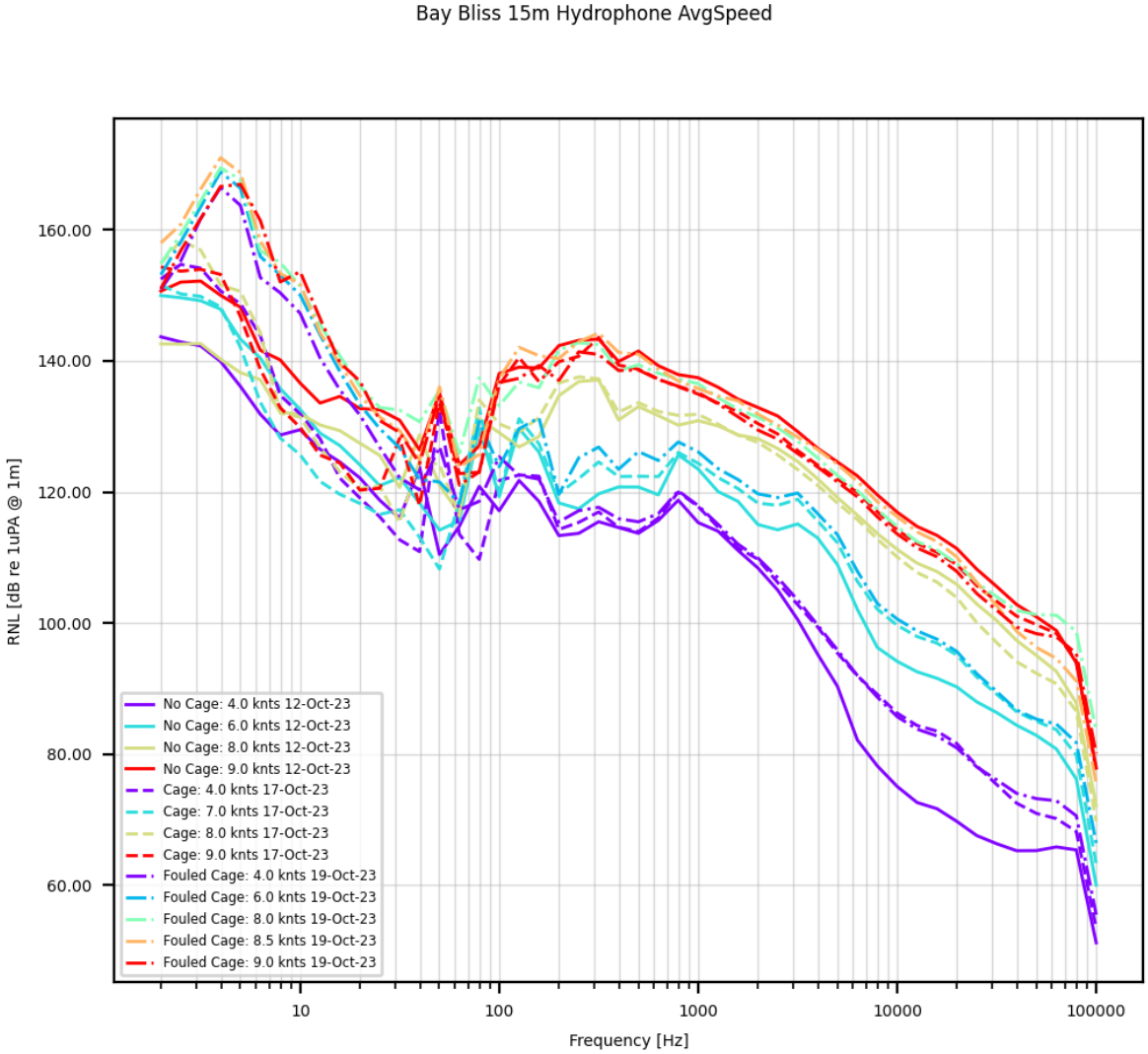

Figure 3-8: Underwater radiated noise spectrum for the “Bay Bliss” from 15 m hydrophone

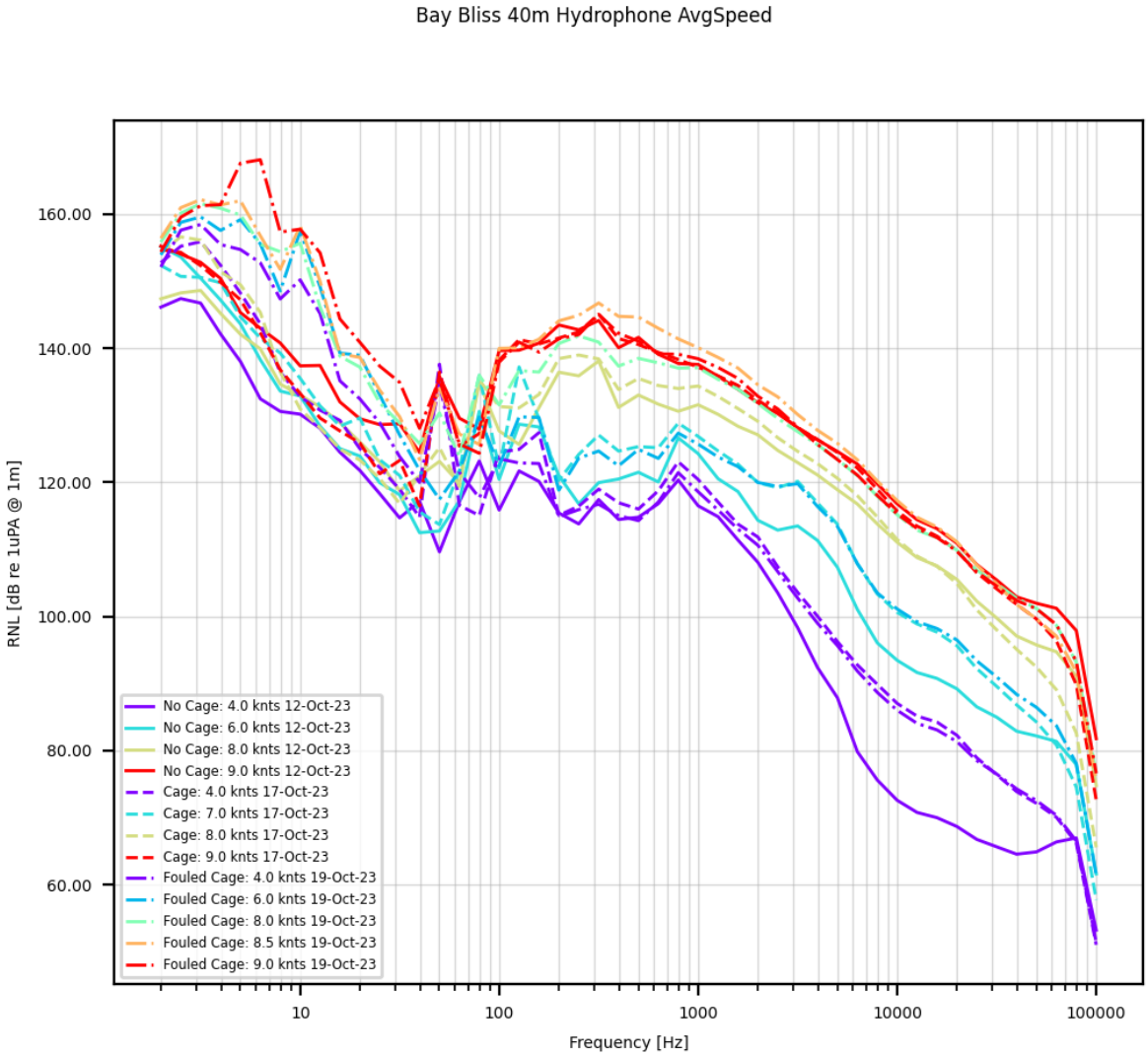

Figure 3-9: Underwater radiated noise spectrum for the “Bay Bliss” from 40 m hydrophone

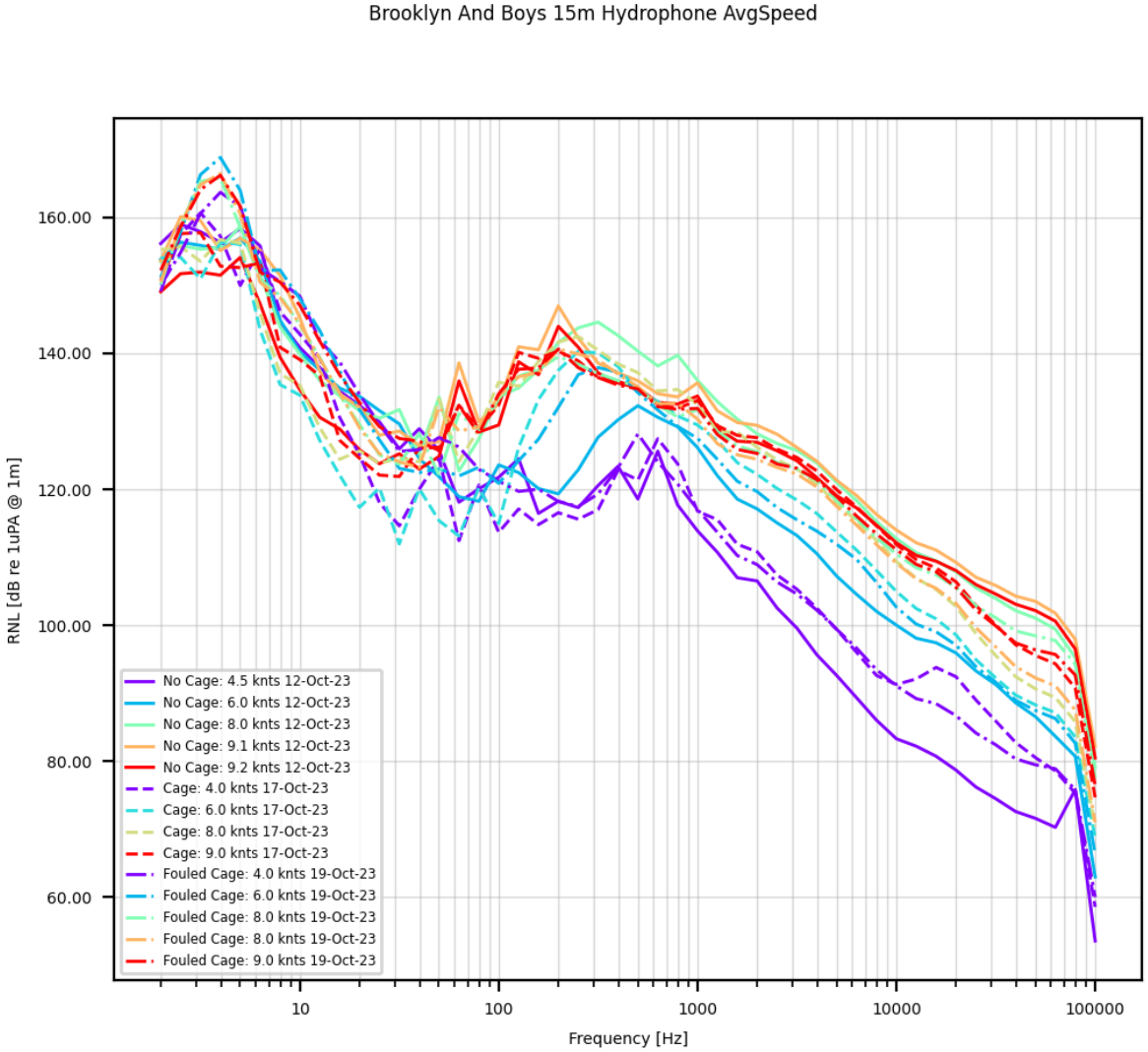

Figure 3-10: Underwater radiated noise spectrum for the “Brooklynn and Boys” from 15 m hydrophone

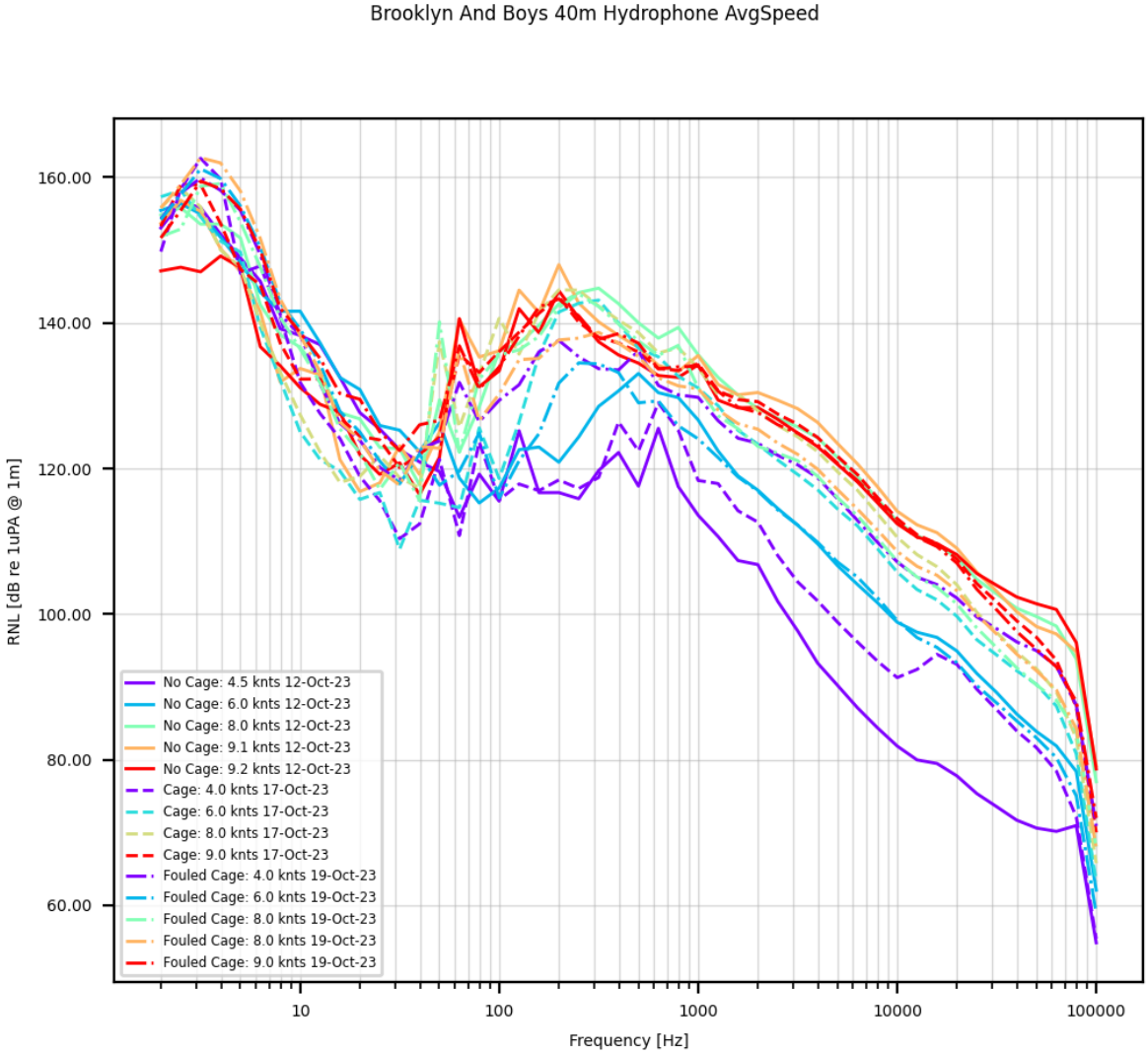

Figure 3-11: Underwater radiated noise spectrum for the “Brooklynn and Boys” from 40 m hydrophone

4. Activity #2 - Validate Hydroacoustic Predictions of Noise Generation

The second purpose of this project is to provide a validated modelling environment for future assessments of URN generated by propeller cages. Assessment of the noise generated by hydrodynamics can be performed via correlations from boundary element methods (BEM), or via a computational fluid dynamics (CFD) analysis. CFD is the analysis of fluid flows using numerical solutions of physical conservation laws. This allows for visualization and insights of hydrodynamic behaviour. While sea trials are necessary, they often address a limited number of operating conditions or geometries. Validated CFD models can be used to complement costly trial measurements and determine all desired quantities with a high resolution in space and time.

In order to have confidence in CFD model predictions not only do the correct models need to be employed, but the specific parameters of the models must be chosen correctly. Comparison of the predicted results with a validation data set allows for sensitivity studies to be conducted to verify which model parameters are important and what values provide the closest correspondence with the physical system. Once these parameters have been established, CFD allows for the exploration of alternative designs.

In current engineering practice, computations of sheared and free shear flows using the unsteady compressible Navier-Stokes equations are performed routinely. It remains challenging, however, to resolve the acoustic field of those simulations whose acoustic energy is many orders of magnitude smaller than the energy of the hydrodynamic field. Unlike the requirements imposed for resolving flow physics, the numerical mesh employed must be fine enough to resolve the acoustic frequencies of interest. This generally dictates the use of much finer meshes and higher computational costs. The physics in aeroacoustics are inherently transient and ultimately, must be solved using transient calculations. The computational run times that are associated with such simulations are high.

A goal of this activity is to develop a set of best practice guidelines for predicting both vessel performance and URN for vessels fitted with propeller cages. The guidelines will be based on the models and settings required to accurately replicate the measurements from Activity #1.

Two vessels (of the four measured) were selected for model generation and noise predictions. Section 4.2 details steps to generate CAD models of the vessels suitable for use in the numerical predictions. Due to the quality of the geometric models, the Bay Bliss was chosen as the primary vessel to be investigated. All results shown are for the Bay Bliss, except for Section 4.10 in which the same settings were applied for predictions of the Brooklynn and Boys.

Section 4.3 outlines the assumptions and chosen models for the numerical analyses. Section 4.4 shows the results of open water predictions of the propeller and cage. An overview of the self-propulsion results is shown in Section 4.5. An alternative prediction methodology treating the cages as porous membranes was explored as detailed in Section 4.6. Simulations of the stern region with and without the cage, as well as with a fouled cage are shown in Section 4.7 for a variety of prediction methodologies. Predicted URN is presented in Section 4.8. Some of the variations undertaken to improve the correspondence to the validation data are given in Section 4.9.

4.1 Numerical Noise Prediction Overview

A ship represents a very complex noise source, which consists of machinery noise, hydrodynamic flow noise and propeller radiated noise. Amongst the different noise sources, the propeller is an important one both under non-cavitating and cavitating conditions. In the presence of cavitation, pressure amplitudes increase rapidly, which results in higher noise levels at low and high-frequency parts of the noise spectrum.

The propeller URN can be predicted by using numerical methods, empirical formulations, and experiments under non-cavitating and cavitating conditions. Amongst the different methods, numerical prediction of the propeller URN by using viscous or potential based solvers together with the acoustic analogy is a relatively new research field for hydroacoustic studies. In fact, two different techniques can be employed: a direct approach (i.e., Direct Numerical Solution (DNS)) and a hybrid method (i.e., hydrodynamic solver with the acoustic analogy) for the prediction of the URN. In the DNS method, the governing equations of the flow field and all turbulent scales are directly solved to compute the sound; this makes the solutions computationally expensive. Moreover, any direct method needs a compressible flow solution to compute the sound field. The sound propagates in a medium with a finite speed under the isentropic flow hypothesis (i.e., $c_0^2 = dp/d\rho$); hence, the incompressibility assumption (i.e., $d\rho = 0$) removes the propagation phenomena due to the infinite sound speed (i.e., $c_0 = \infty$). Therefore, the DNS method is not appropriate for hydroacoustic calculations.

An alternative and more commonly used approach in hydroacoustic field is a hybrid method, which consists of an incompressible hydrodynamic solver (RANS, DES, or LES) together with the acoustic analogy. In this way, source and propagation fields can be decoupled. The source field is first determined by using an incompressible flow solver, where the propagation of the sound is provided by the aid of acoustic analogies from near field to far-field as a transfer function. The widely used acoustic analogy is Ffowcs-Williams Hawkings (FWH) equation both in the aeroacoustics and hydroacoustic fields. In the aeroacoustics field, the impermeable formulation of FWH equation (i.e., propeller blades are selected as a noise source in this approach) has been generally used for noise prediction by taking only linear terms (i.e., monopole and dipole noise terms) into account. The reason being that the flow regime is often assumed subsonic due to the low rotational speed of the blades. The non-linear term (i.e., quadrupole noise term) in the aero-acoustic field becomes important at high supersonic or transonic regimes. However, the non-linear terms are important for hydroacoustic simulations. Additionally, in the presence of cavitation, turbulent vortex structures in the propeller's wake can also give a significant contribution to the overall noise levels as non-linear noise sources even if the cavitation is more dominant. Thus, the non-linear term of the FWH equation needs to be included in the calculations, either solving the direct volume integrals or using the porous FWH (P-FWH) formulation. However, the solution of direct volume integrals is computationally expensive and more sensitive to the accuracy of the input data in original formulation. Due to this reason, P-FWH equation becomes attractive as the quadrupole volume integrals are evaluated with the solution of surface integrals.

4.2 Vessel Geometric Model Generation

A three-dimensional (3D) model of the vessel's hull, superstructure, appendages, propeller, and cage is required to model its performance and URN. The generation of a numerical vessel model is typical practice for hydrodynamic resistance of self-propulsion studies when an existing model is not available. Relevant documentation (lines plans, general arrangement, and propeller geometry) for the Cape Islander vessels were unavailable, and several of the vessels have undergone alterations subsequent to initial construction. To generate the model, a 3D photogrammetry scan of the vessel was made using Metashape (photogrammetry software) [8]. This converts the scanned images into a 3D mesh of the vessel surfaces (.OBJ and .STL formats). The resulting mesh for the Bay Bliss is shown in Figure 4-1. The superstructure contributes a small portion of the vessel drag, so it was not resolved to the same detail as the hull. Since the propeller region is critical for the URN this region was scanned in high detail – scans were taken with and without the cage installed. Several different models were developed for each vessel to appropriately capture the hull, propeller, and cage. The supporting structures of the drydock (as pictured in Figure 2-5) were then manually removed using Meshlab [9].

Figure 4-1: 3D photogrammetry scan geometries of the Bay Bliss hull (top) and propeller (bottom)

The scanned model produced a mostly complete geometry, albeit with several artifacts. The model appears appropriate, however there was a significant degree of scattering in the measurements. This produces a rough surface description, beyond the physical roughness. Due to the automation of generating a mesh from a point cloud, several regions were generated with “bridges” in the surface over other parts of the surface in what is supposed to be a smooth region. In addition, the scanning process struggled to resolve thin features, see for example the holes in the propeller in Figure 4-1. To capture the propeller cages geometry properly, they were backed with cardboard (as shown in Figure 2-6).

4.2.1 Propeller

Figure 4-2 illustrates the raw model of the propeller. Given the propeller’s critical role in predicting cavitation and subsequent broadband noise, additional effort was expended to achieve a smooth geometry that accurately represented the actual propeller.

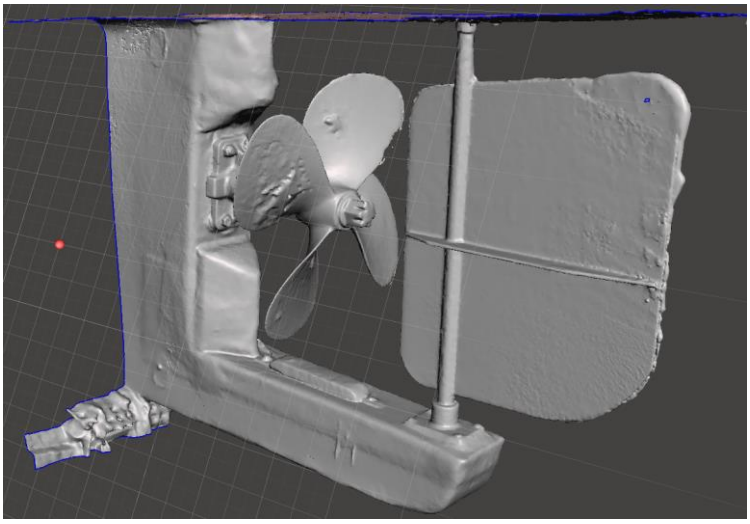

Figure 4-2: Bay Bliss scanned propeller.

The propeller model was initially processed in Rhino v7 [10], where a Grasshopper script was used to create slices of the radial cross-sections. These sections were then exported into a standard propeller format (.ppg) and imported into the tool PropART, accessible through the Cooperative Research Ships (CRS) group [11]. The .ppg file semi-parametrically represents propellers through their chord length, pitch, camber, skew, rake, thickness distributions, and radial section profiles. The raw .ppg from Rhino exhibited some artifacts from the original geometry in the distributions. These were manually adjusted in PropART using the Bezier_modify() function, which enables interactive modification of the propeller distribution curves. Figure 4-3 compares the raw and modified distributions. Changes were implemented to eliminate obvious outlier points from the distributions while preserving the original scans as much as possible.

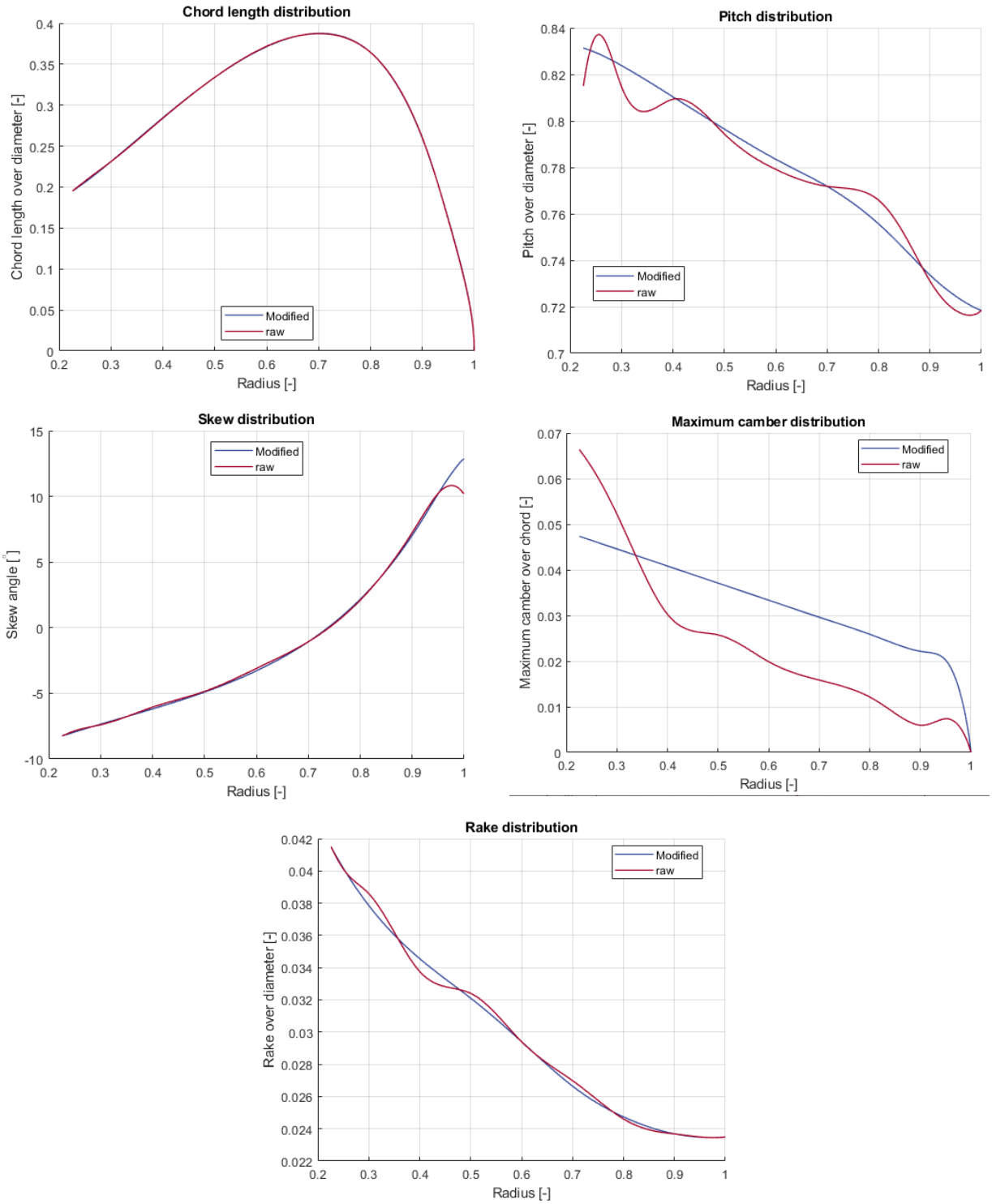

Figure 4-3: Bay Bliss propeller raw and corrected radial distributions.

Completely describing the propeller requires information about the individual radial sections and their maximum thickness in addition to the propeller radial distributions. Capturing the propeller thickness accurately proved challenging with the photogrammetry method. Therefore, a thickness distribution and a standard NACA66 section profile were assumed from a similar, standard propeller. This assumption

introduces some uncertainty in the thickness, but the assumed profiles align relatively well for most sections. Figure 4-4 shows an example at r/R = 0.7. The suction side of the propeller appears less resolved than the pressure side, likely due to the difficulty of accessing that side when the propeller is installed. Attempts to contact the propeller manufacturer regarding the thickness distributions were unsuccessful.

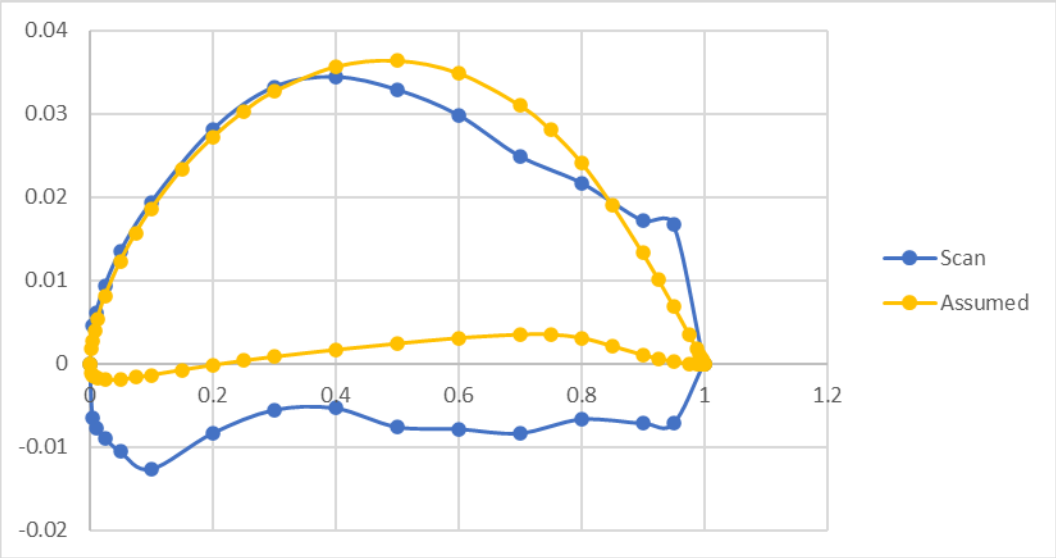

Figure 4-4: Bay Bliss scanned and assumed profiles at r/R = 0.7

4.2.2 Hull

As noted above, the photometric scans contained holes (from the support structures) and were excessively rough. Initially, smoothing was attempted in Meshlab, but was found to remove the physical features of the vessel. Instead, the mesh was processed in Rhino v7. The initial photometric mesh is shown in Figure 4-5. This was translated and rotated to place the origin on the vessel aft (x), centerline (y), and baseline (z). The draft was taken along the marked waterline. Section planes through the mesh were generated, see Figure 4-6. Smooth lines were fit through the mean of the extracted sections, see Figure 4-7. Surfaces were then created by projecting loft surfaces through the lines, see Figure 4-8. Figure 4-9 illustrates an overlay of the smooth surfaces to the original scanned mesh. The smooth surface hull can be observed to correspond well. The hull was assumed to be perfectly symmetric about the vessel centerline. Note that the superstructure recreation is not as exact, as the superstructure represents a small fraction of the vessel drag, which is mainly determined by the frontal area.

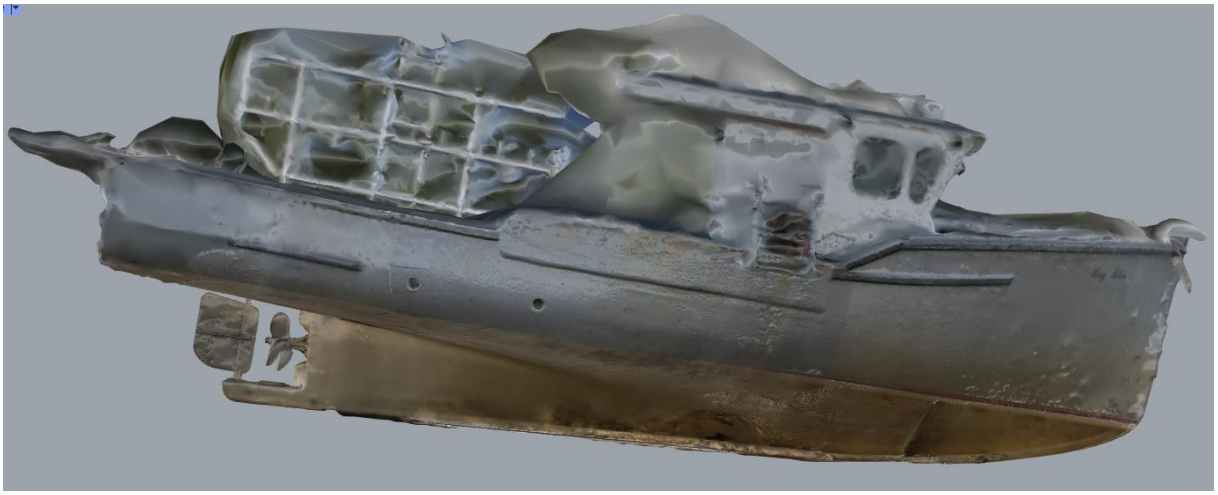

Figure 4-5: Bay Bliss hull initial photometric mesh

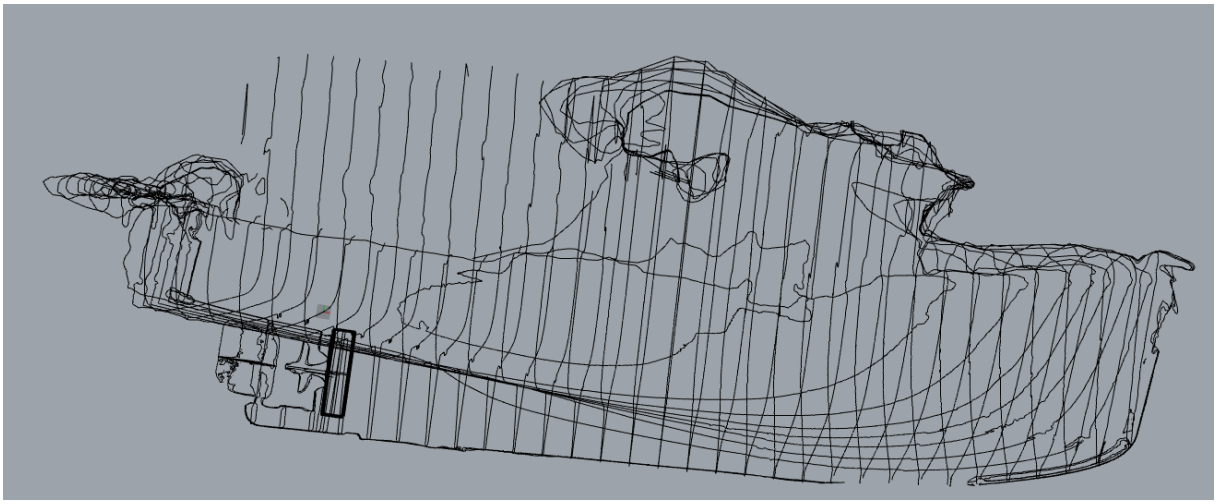

Figure 4-6: Bay Bliss hull extracted sections.

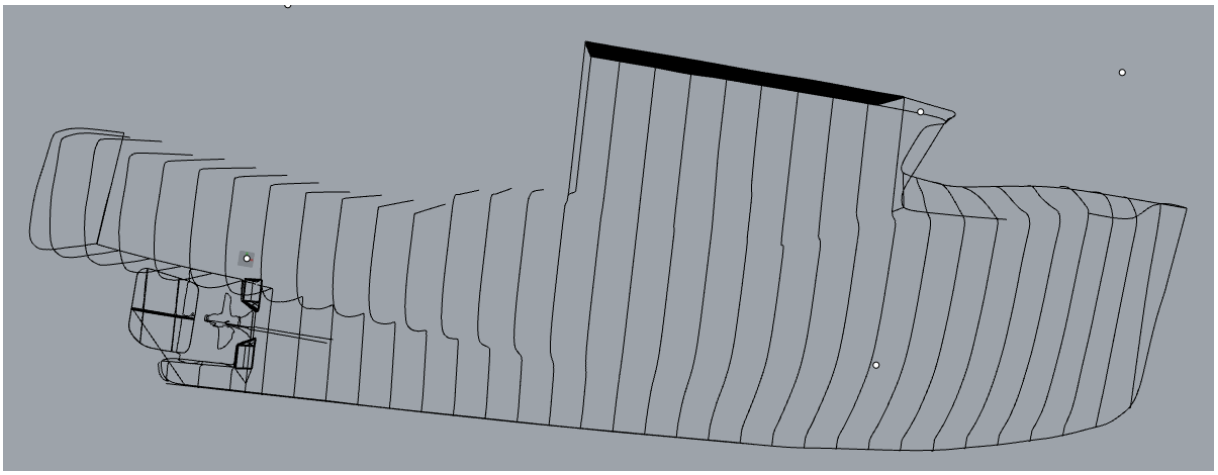

Figure 4-7: Bay Bliss hull smoothed lines fitted through extracted sections.

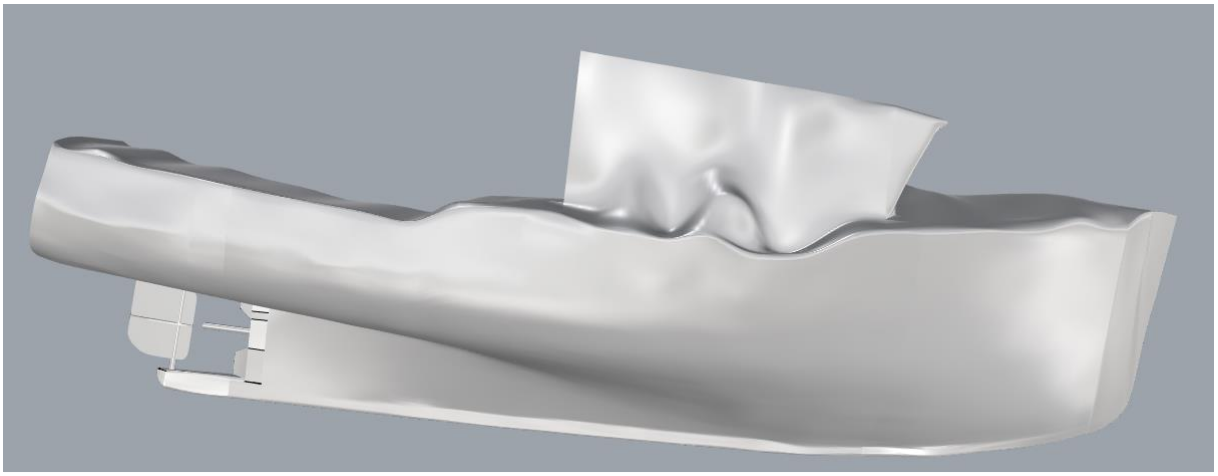

Figure 4-8: Bay Bliss hull generated surfaces.

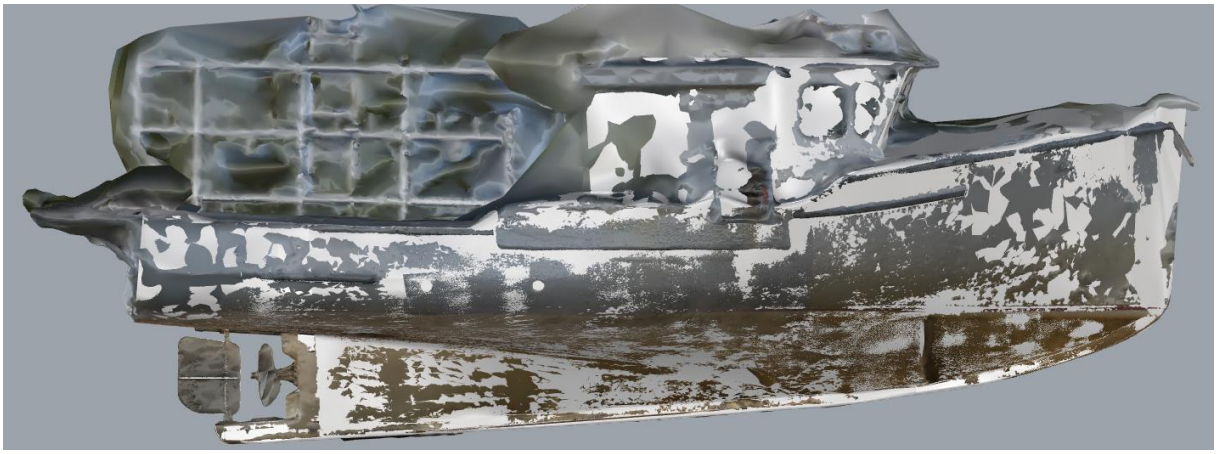

Figure 4-9: Bay Bliss hull comparison of generated surfaces to original scan.

4.2.3 Cage

Due to the difficulties in resolving thin objects, the propeller cage was lined with carboard to assist in the scanning process. The photometric scan of the Bay Bliss propeller cage is shown in Figure 4-10. Lines were fit along the cage bar and plate elements. These were then translated to an appropriate depth to lie within the scanned geometry. Cylinders of appropriate thickness were generated on the on lines. A similar methodology was utilized on the end plates. Figure 4-11 shows the generated mesh geometry overlaid with the photometric scan. The mesh geometry was taken from one side of the vessel and assumed to be symmetric on the other side of the vessel. Due to the irregularity of the cage geometries, this will introduce a slight discrepancy on one side of the vessel.

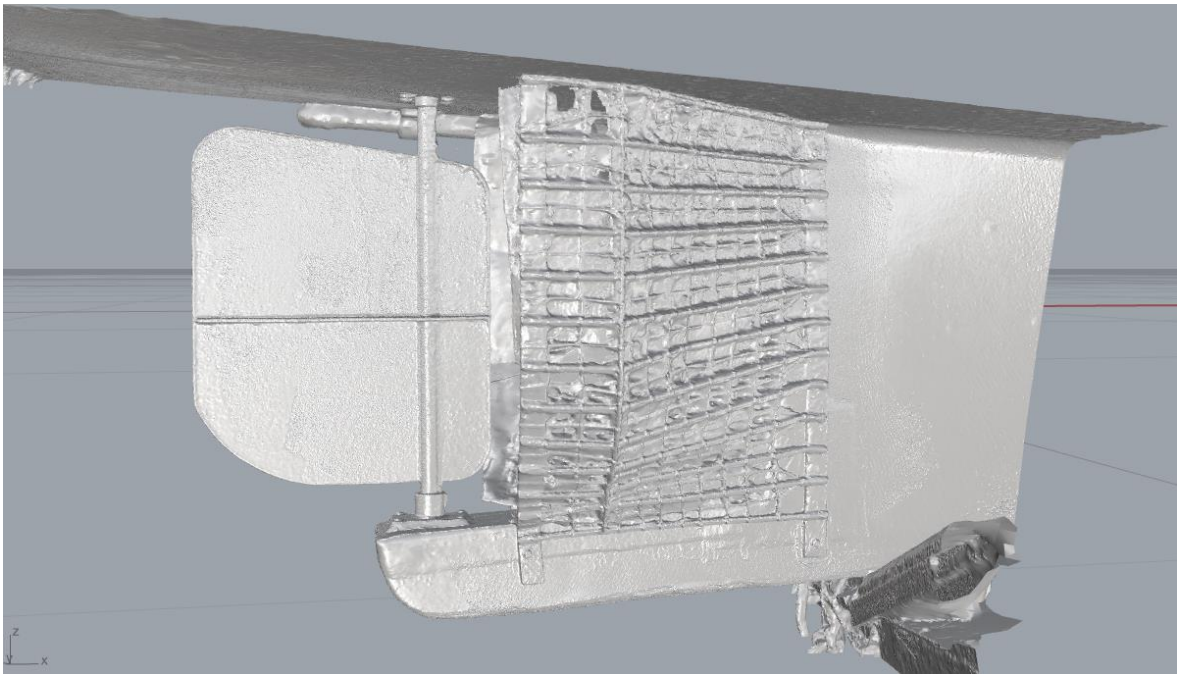

Figure 4-10: Bay Bliss propeller cage photometric mesh.

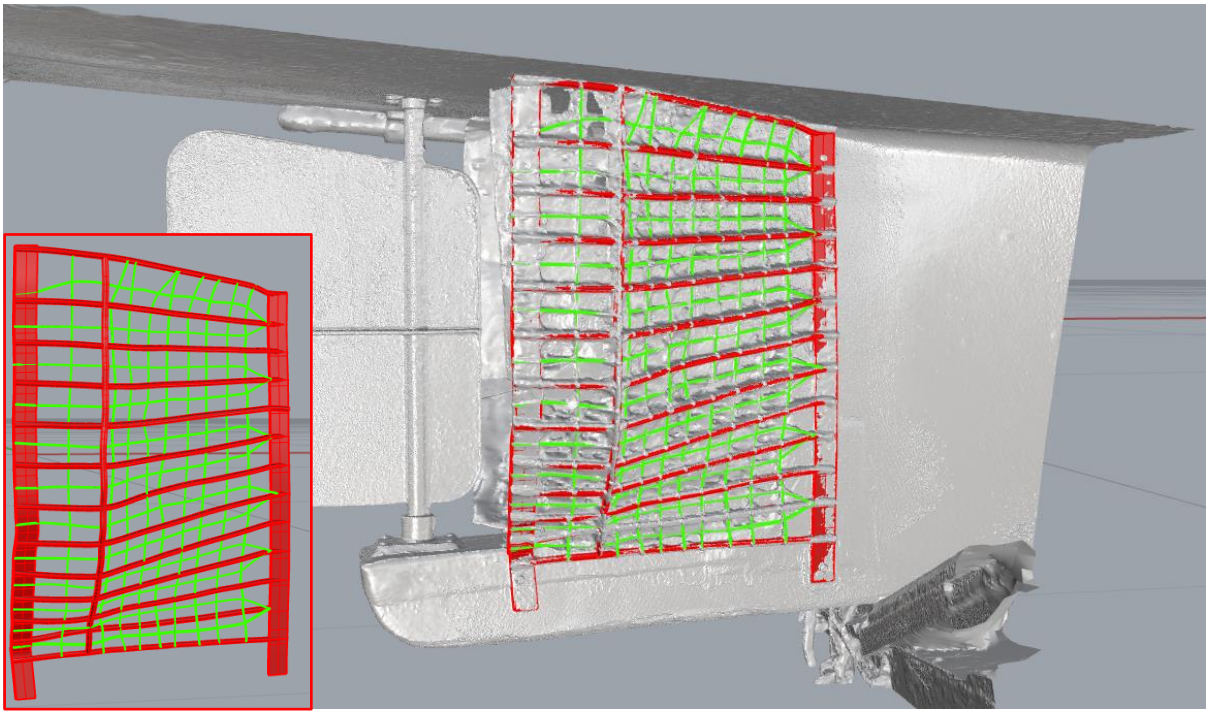

Figure 4-11: Bay Bliss generated propeller cage mesh overlaid with photometric mesh.

4.3 Numerical and Environmental Settings

The performance of two Cape Islanders (the Bay Bliss and Brooklynn and Boys) was assessed through a series of numerical predictions. The majority of the analyses were performed via computational fluid dynamics (CFD) with Star-CCM+ v18.06.007 (2310.0001) [12], see Sections 4.3.2 through 4.3.6. In addition, the Cooperative Research Ships (CRS) [11] tool PROCAL employs a boundary element method (BEM) to

simulate propeller performance and cavitation. The CRS tool PropART can be used to post-process the PROCAL results to obtain noise predictions, see Section 4.3.1.

4.3.1 PROCAL / PropART Models

Simplified method noise signatures were calculated using a combination of PROCAL [13] and PropART [14]. PROCAL was used for the fluid flow and cavitation bubble prediction and uses a boundary element method (BEM). Results from PROCAL are then used in the noise models integrated in PropART. These include a tip vortex model, ETV [15], and sheet cavitation models. Two types of sheet cavitation models are available from the work of Brown and Navais [14]. Tip vortex and sheet cavitation results were then added together to arrive at the total noise 1 m from the ship.

PROCAL requires the wake field from behind the ship to better predict cavitation in the fluid flow. The non-uniform nature of the ship wake contributes to the cavitation bubble formation and collapse as a propeller blade rotates through the wake. The cavitation collapse is the driver of the cavitation induced noise so a more non-uniform ship wake can potentially contribute to higher noise levels. For this study, wakes from the ship with no cage and the cage were generated using a Java script which samples the CFD propeller domain. Wakes were taken 0.25 radii upstream from the propeller plane. The propeller induced velocities, also calculated by PROCAL, were subtracted from the CFD simulated wake and normalized by the ship forward speed to arrive at the effective wake.

4.3.2 CFD Models

The commercial computational fluid dynamics software package Star-CCM+ v18.06.007 (2310.0001) [12] was utilized for all simulations. Star-CCM+ has been extensively validated by Lloyd's Register for marine performance.

The CFD methodology solves governing equations for the conservation of mass, momentum, and material convection. These are discretized with 2nd order accuracy on a numerical mesh. Additional models are utilized to resolve the multiple material interactions, turbulence, cavitation, and acoustic propagation.

For hydroacoustic modelling, the double precision version of Star-CCM+ is required, along with a compressible liquid equation of state to model the transmission of sound. Most analyses were conducted with the Reynolds Averaged Navier-Stokes (RANS) methodology, where the turbulence is modelled with the k-ω SST model of Menter [16] that is the recommended model for vessel hydrodynamics in Star-CCM+ and is typically employed by Lloyd's Register. This allows for the effective and efficient resolution of the boundary layer and is appropriate for the calculation of the forces and capable of capturing separation effects. Select analyses were conducted with a higher order Large-Eddy Simulation (LES) model in which the turbulent fluctuations are resolved on the numerical grid instead of being modelled. If the cavitation region is large, simpler Reynolds-Averaged Navier-Stokes (RANS) models that are industry standard for hydrodynamic predictions may provide an acceptable signature.

Simulations were conducted at full scale. A volume of fluid (VOF) strategy was utilized to distinguish between the water and air and capture the waves generated by the vessel motion. The water in all cases was assumed to have a temperature dependence based on ITTC recommendations. For the assumed 18.9 C temperature the sea water density was 1025.1 kg/m^3 and the dynamic viscosity was 0.001106 Pa·s [17]. For the same air temperature, the density was 1.209 kg/m^3 and the dynamic viscosity was 1.820×10^{-5} Pa·s [18]. All simulations assumed a standard pressure and gravitational acceleration. Initial/inflow turbulence intensity was taken as 1 % and the turbulent viscosity ratio as 10.0. The water was assumed calm in all cases.

4.3.3 Vessel Model

The center of gravity was located relative to the aft perpendicular and the keel. The moments of inertia for roll, pitch, and heave were estimated from:

$$I_{xx} = Mr_{44}^2 = M(0.4S_b)^2$$

$$I_{yy} = Mr_{55}^2 = M\left(0.25L_{pp}\right)^2$$

$$I_{zz} = Mr_{66}^2 = M\left(0.25L_{pp}\right)^2$$

where M is the vessel mass, S_b is the maximum beam, and L_{pp} is the length. Dimensions and inertial values for the Bay Bliss and the Brooklynn and Boys are given in Table 4-1 as well as Figure 4-12 and Figure 4-13. Vessel masses were determined by calculating the hydrostatic floatation to generate the draft at the known waterline.

Table 4-1: Vessel dimensions and moments

Vessel	Bay Bliss	Brooklynn and Boys
Mass, M (kg)	11072	12120
Length, L_{pp} (m)	10.58	10.73
Breath, S_b (m)	4.33	4.14
L_{cg} (m)	4.85	5.03
V_{cg} (m)	1.33	1.08
I_{xx} (kg·m^2)	3.31×10^4	3.32×10^4
I_{yy} (kg·m^2)	7.75×10^4	8.71×10^4
I_{zz} (kg·m^2)	7.75×10^4	8.71×10^4

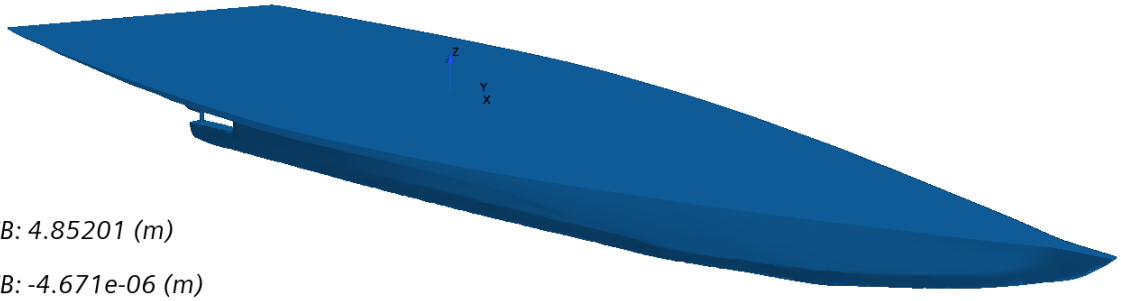

LCB: 4.85201 (m)

TCB: -4.671e-06 (m)

VCB: 1.06661 (m) *Displacement: 11071.6 (kg)* *WaterPlane Area: 31.9339 (m^2)*

LCF 4.25136 (m) *Displacement Volume: 10.8006 (m^3)* *Wetted Area Still: 42.6253 (m^2)*

Figure 4-12: Bay Bliss hydrostatic volume.

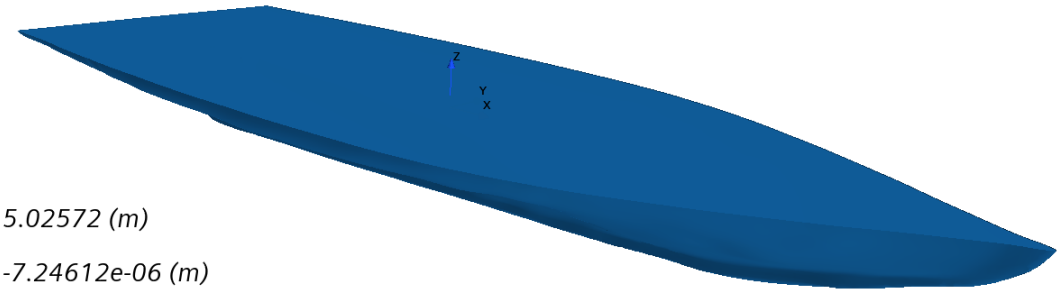

LCB: 5.02572 (m)

TCB: -7.24612e-06 (m)

VCB: 0.834033 (m) *Displacement: 12120.4 (kg)* *WaterPlane Area: 32.5918 (m^2)*

LCF 4.41943 (m) *Displacement Volume: 11.8237 (m^3)* *Wetted Area Still: 42.4516 (m^2)*

Figure 4-13: Brooklynn and Boys hydrostatic volume.

The flow-fields around the vessels were determined in all cases, including the forces, moments, and accelerations from pressure and viscous shear stress acting on the vessel. These inputs result in alterations in the vessel's mean sinkage and trim due to forward speed through water.

4.3.4 Initial Conditions and Boundary Conditions

The computational domain for the self-propulsion simulations is shown in Figure 4-14. The domain boundary downstream of the vessel was modelled as a pressure outlet, whereas all other external domain boundaries had velocity inlet conditions imposed. All hull surfaces were modelled as no-slip walls using wall functions. For the self-propulsion simulations, the propeller was represented via a source term based on the open water propeller performance. The RPM of the propeller (and hence its thrust and torque) were then varied until the vessel maintained the desired speed.

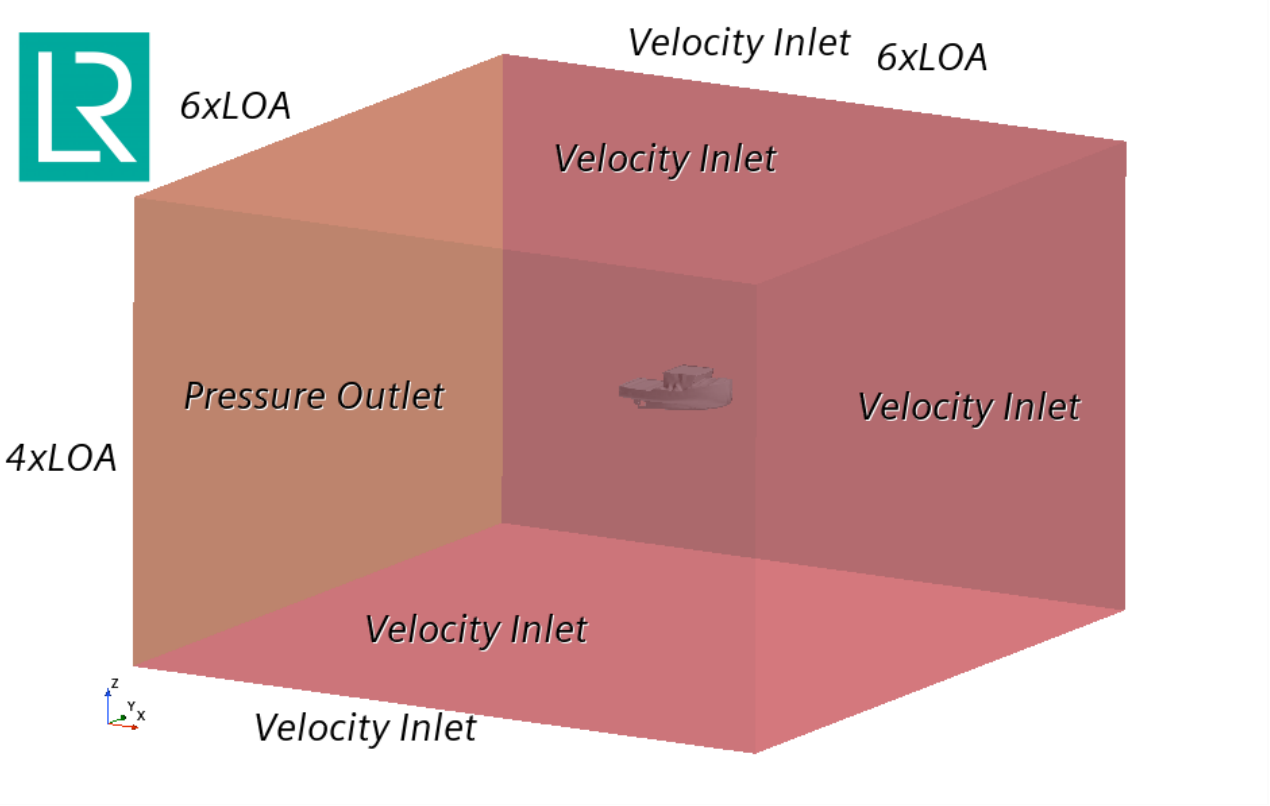

Figure 4-14: CFD self-propulsion domain and boundary conditions

All simulations are performed in a time accurate manner, with a time step of 1/50 the time it takes for the flow to pass the vessel.

4.3.5 Propeller Model

Varying levels of approximation may be used for the propeller itself which is the dominant noise generator:

- A virtual disk propeller approximation that does not include the physical propeller geometry. Instead, momentum sources are added to accelerate the flow based on the velocity field slightly ahead of the propeller location and the open water performance of the propeller. This approach was used for all the self-propulsion analyses presented in this report.
- A boundary element method (BEM) approach, in which the upstream CFD flow-field is used as input for a boundary element code (such as PROCAL). The physical geometry of the propeller is modelled in the BEM code and the momentum generated may be passed back to the CFD simulation. This has a much lower numerical cost than full CFD methods, for arguably similar accuracy in the noise predictions.

- A moving reference frame approach. The propeller geometry is physically present in the CFD model but does not rotate (only the mean rotation is captured), thus pressure peaks due to passage past the hull are lost. This methodology is used for the stern simulations in Section 4.7.2.

- A rigid body propeller rotation provides the highest fidelity modelling. All physical motions are present in the CFD model. The precision of the answer then depends on the level of discretization. This was utilized for the open water performance in Section 4.4.1.

Self-propulsion analyses are conducted in a three-step process. First the water velocity relative to the fixed vessel is applied corresponding to the sailing speed. Second the vessel is allowed to move in pitch and heave according to standard 6 degree-of-freedom methodology. Third the propeller thrust is applied via a virtual disk methodology with a variable RPM determined from the propeller open water characteristics until the thrust matches the resistive forces on the vessel.

4.3.6 Computational Mesh

The computational mesh was constructed according to LR's best practices for marine self-propulsion analyses. The Star-CCM+ "trimmed cell" mesher was utilized in all regions. This produces a Cartesian mesh region aligned to the free surface. The cells are "trimmed" around boundary layer cells extruded from the vessel surface. The computational mesh was refined around the bow, stern wave, shaft tunnels, and rudders to ensure the physics of these regions was adequately captured. The base cell size specified for Star-CCM+ was 0.42 m, with refinement regions at the propeller and rudders having 6.6 mm cells. The computational mesh around the Bay Bliss vessel center plane and water plane is shown in Figure 4-15 through Figure 4-17. Refinement regions are present around the water plane, bow, stern wave, and propeller. The mesh on the stern hull surface is shown in Figure 4-18. The mesh contained 7.9 million cells. A similar methodology was used for construction of the Brooklynn and Boys resulting in a mesh that contained 6.2 million cells.

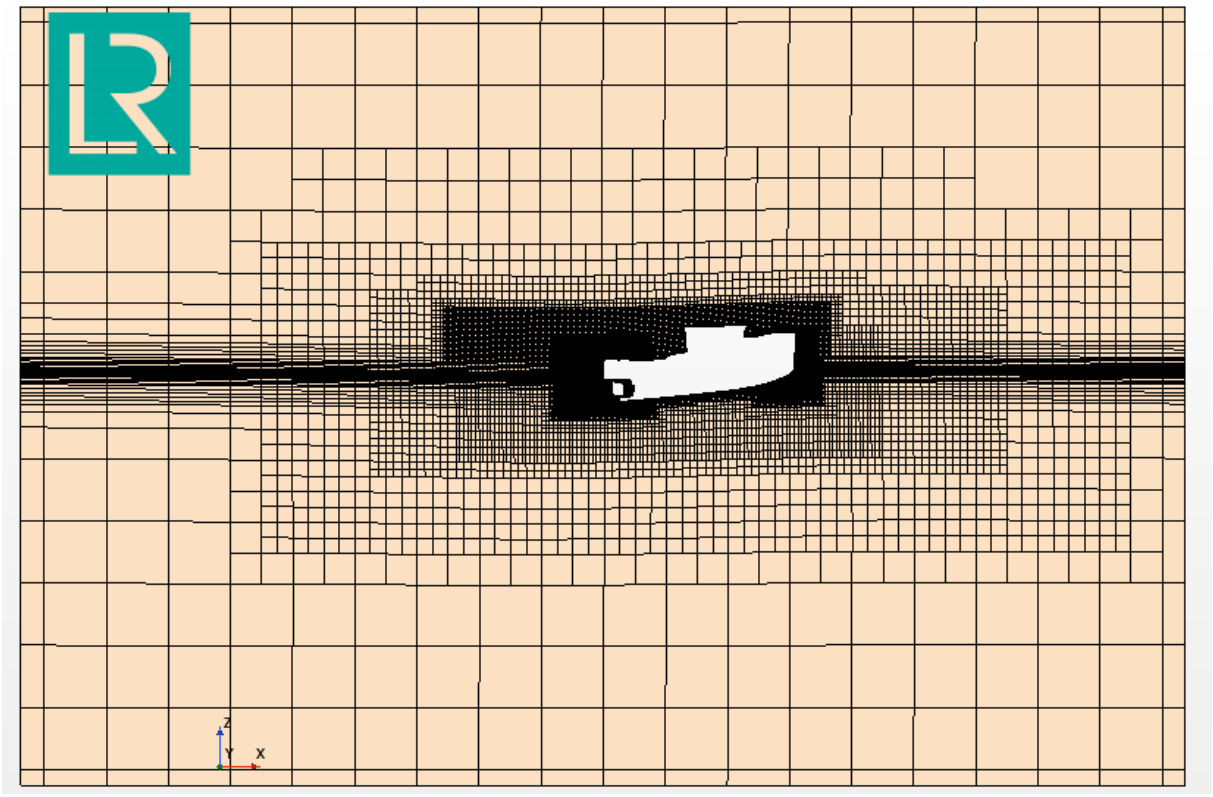

Figure 4-15: Bay Bliss self-propulsion centerline computational mesh.

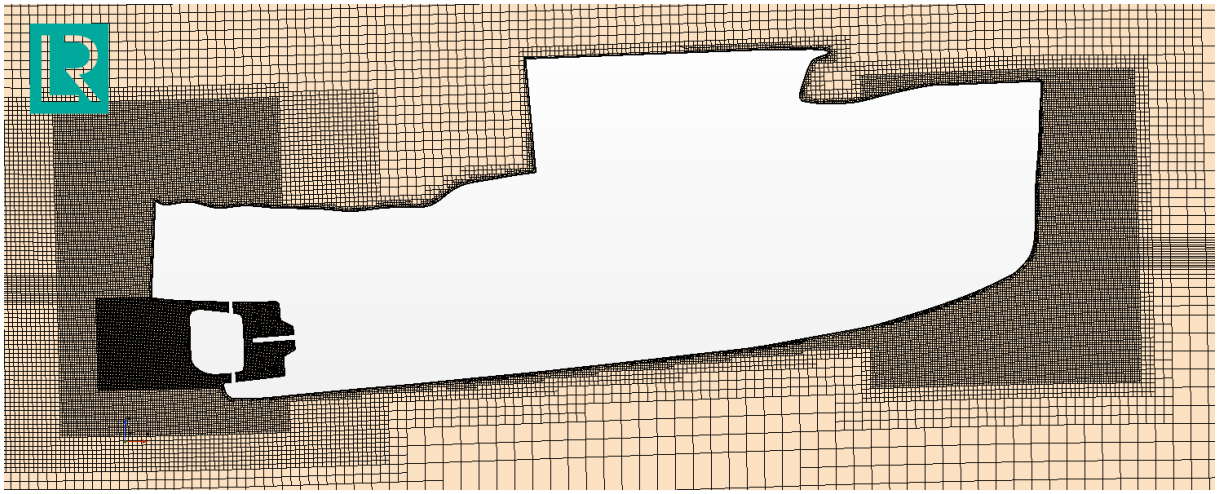

Figure 4-16: Bay Bliss self-propulsion centerline computational mesh (near vessel).

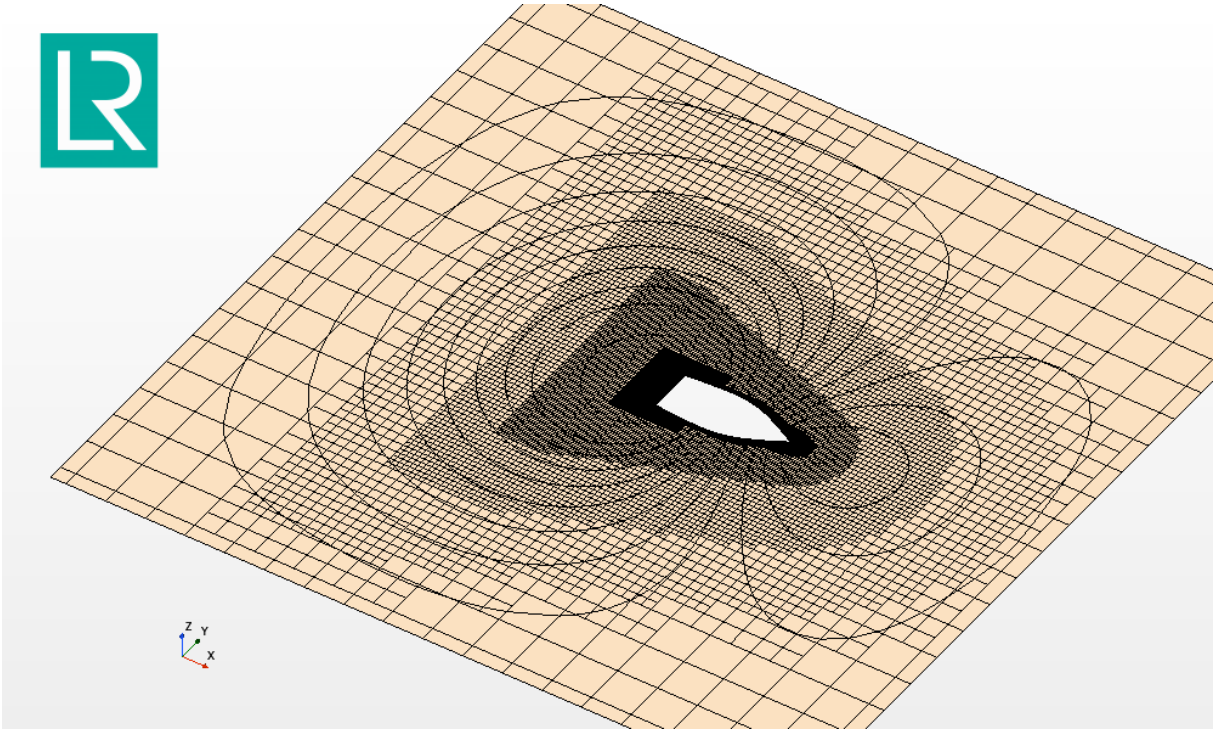

Figure 4-17: Bay Bliss self-propulsion waterline computational mesh.

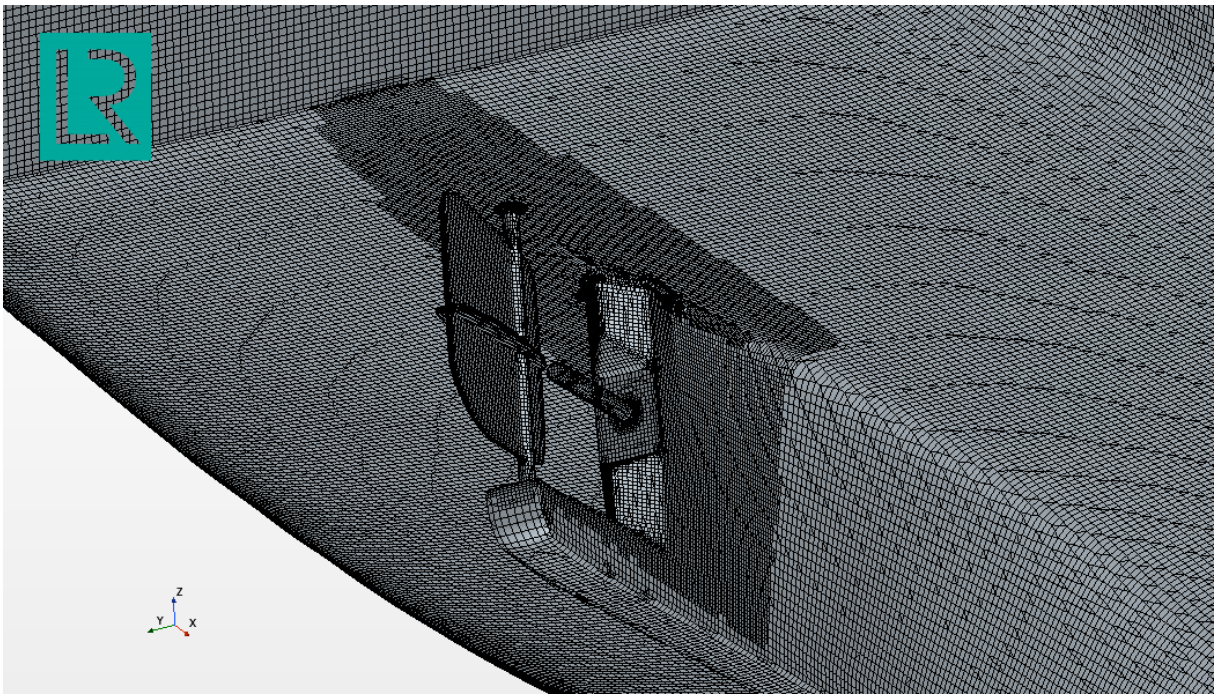

Figure 4-18: Bay Bliss self-propulsion hull computational mesh at stern.

The Star-CCM+ "all *y*+" wall functions were utilized on all ship surfaces with five cell layers extruded from the ship surface. The near-wall mesh was constructed such that y+ values remain in the range of 30-500, valid for use with wall functions. The y^+ values on the ship hull for the self-propulsion analysis is shown in Figure 4-19, with an average + value of 39 and a maximum of 365.

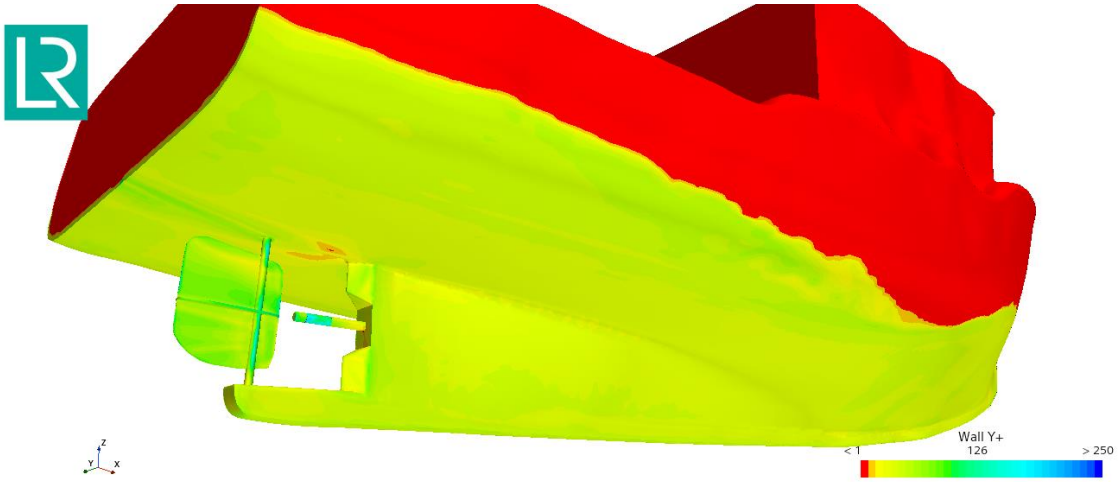

Average Wall y+: 39.488

Figure 4-19: Bay Bliss self-propulsion hull y+ values.

4.4 Preliminary Predictions

In order to understand contributions to URN, preliminary predictions of open-water performance (without the presence of the vessel hull) were made for the propeller geometry, Section 4.4.1, and the cage in isolation, Section 4.4.2.

4.4.1 Open Water Propeller

The Cape Islanders data suggested that the underwater radiated noise (URN) is primarily cavitation based. Cooperative Research Ships (CRS) [11] has several simplified models used for predicting URN and cavitation related noise as described in Section 4.3.1. The proposed approach is to use the CRS toolsets in their recommended form to determine the applicability of the current best practices to the Cape Islanders dataset. The best practices will then be altered where required to achieve the best possible agreement.

The obtained Cape Islanders data shows a strong signal up to and beyond 10 kHz. It may not be possible to fully resolve the entire frequency spectrum due to the excessive computational cost of higher frequencies. The required grid resolution is dependent on the wavelength of the sound being resolved; higher frequency content requires finer grids. This is further exacerbated by the fact that the speed of sound underwater is much higher than in atmosphere, further shortening the wavelength. It is proposed that the noise spectrum be predicted within practical limits and compared to the Cape Islanders data. There should be a sufficient range of spectral content to assess the simulation accuracy. Cavitation noise is typically broadband, meaning it spans a large frequency range, and therefore it should be reasonable to assume that if the lower frequency range shows good agreement, then the higher frequency range should also agree if it were to be resolved.

Open water simulations at a propeller rotation rate of 950 RPM and a ship speed of 6 knots were conducted in PROCAL and PropART, with the predicted cavitation extents shown in Figure 4-20. The noise calculation component of PropART predicted a maximum tip vortex sound level of 156 dB and a maximum sheet cavitation sound level of 131 dB.

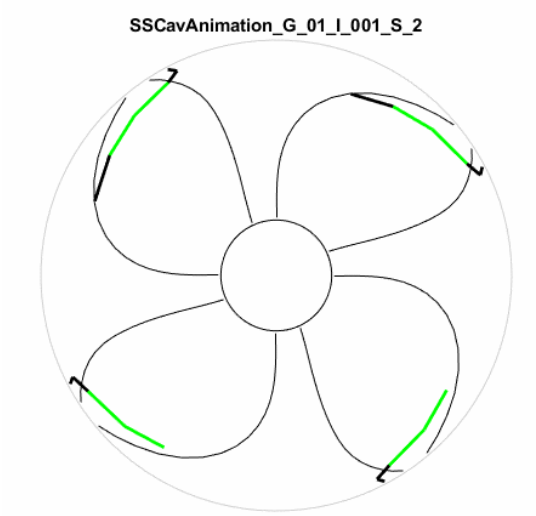

Figure 4-20: Bay Bliss propeller open water cavitation extents

An open water simulation of the Bay Bliss propeller was conducted in Star-CCM+ using a quarter symmetry model to determine the necessary setup for a high-fidelity cavitating simulation with acoustic analysis. This included adaptive mesh refinement around the cavitation bubble regions to ensure sufficient resolution. A much larger cavitation region (and hence noise) is predicted with increased resolution. This is one of the major constraints in noise prediction of a complete vessel. Very fine numerical meshes are required in conjunction with time accurate Detached-Eddy simulations in order to achieve accurate predictions. While a typical self-propulsion analysis would contain on the order of 5 million computational cells, the quarter symmetry propeller alone contained 16 million cells.

Similar predictions, of the propeller noise were generated via the Cooperative Research Ships PropART/PROCAL numerical tools. This is one avenue of dealing with the comprise between numerical cost and accuracy in predicted noise levels. The flow-field from the CFD simulations may be used as input for the BEM-based predictions. The PropART and Star-CCM+ predicted noise signatures are shown in Figure 4-21, corrected to 100 m to correspond to the numerical location of the hydrophone in Star-CCM+. The trends between the two predictions are similar, although PropART predicts a smoother signal due to the semi-empirical nature of the prediction. PropART also consistently overpredicts the signal, suggesting that while the absolute values may not necessarily be representative, the trends between similar simulations will be.

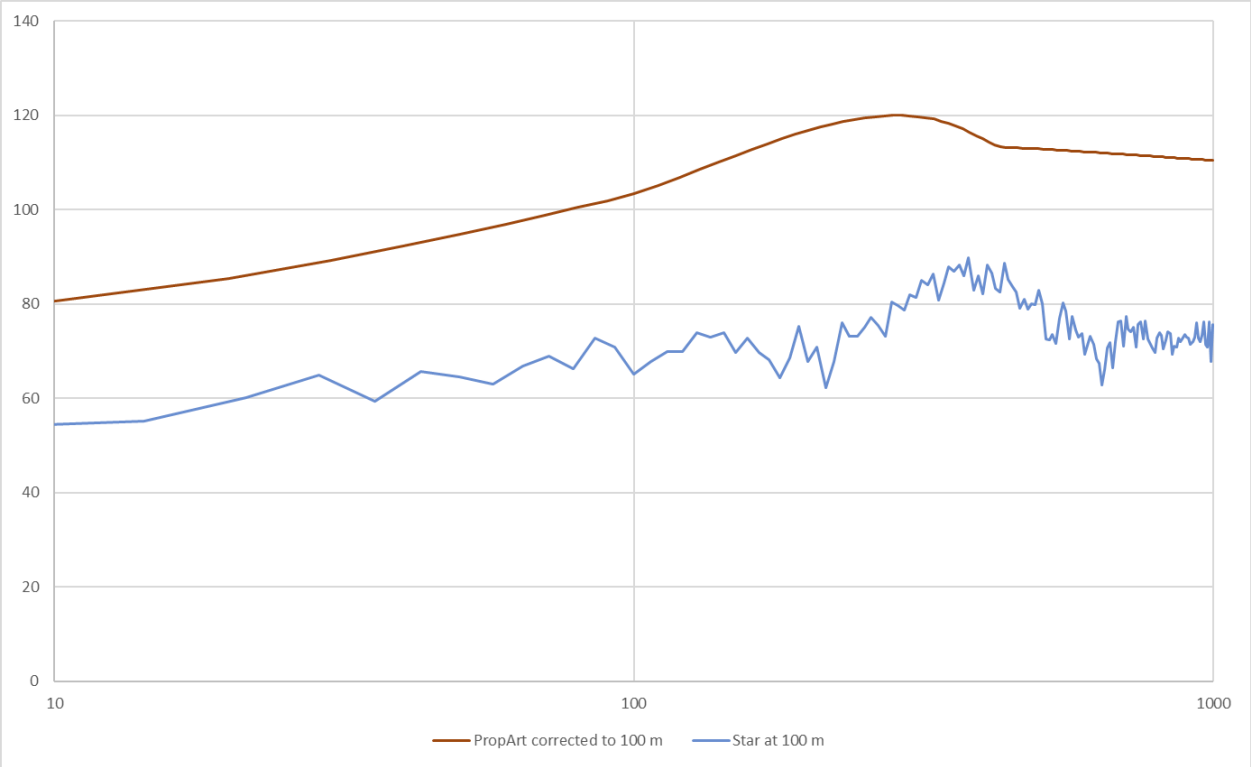

Figure 4-21: Bay Bliss open water propeller noise prediction

4.4.2 Open Water Cage

To verify noise production, the propeller cage from the Bay Bliss was simulated in isolation. The mesh had a nominal cell size on the cage of 4 mm, and a minimum of 1 mm. The entire grid contained 3.9 million cells, see Figure 4-22. As can be observed in both Figure 4-22 and Figure 4-23 the individual cage elements generate a velocity deficit directly in their wake. As expected, for the cage elements normal to the flow, the impact is smaller than in regions where multiple elements are aligned to the flow direction.

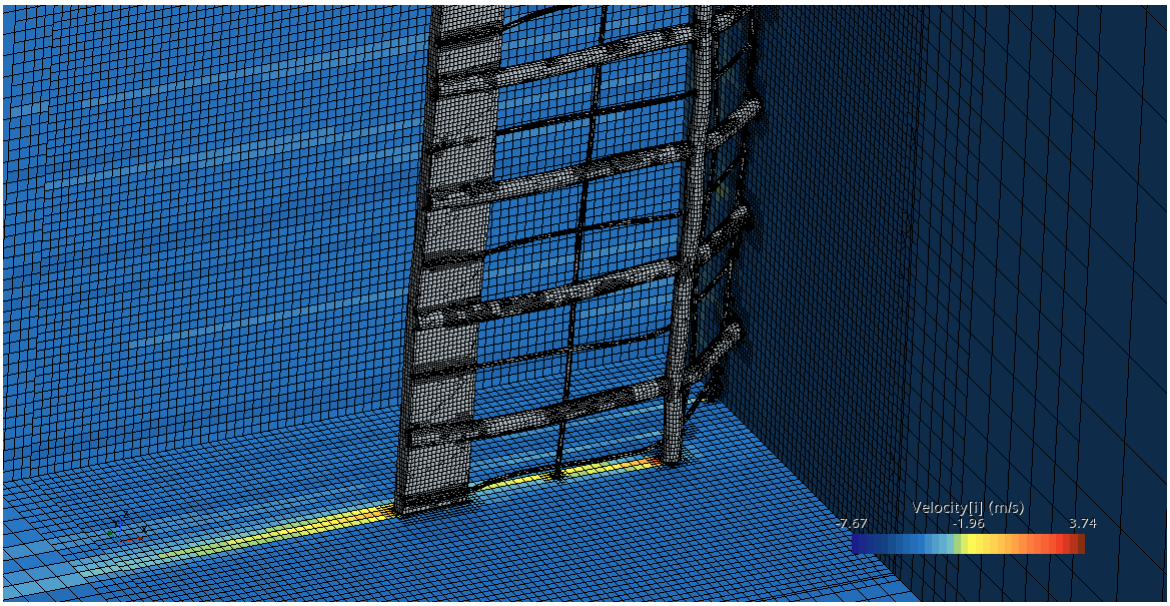

Figure 4-22: Open water propeller mesh and velocity contours (15 knots)

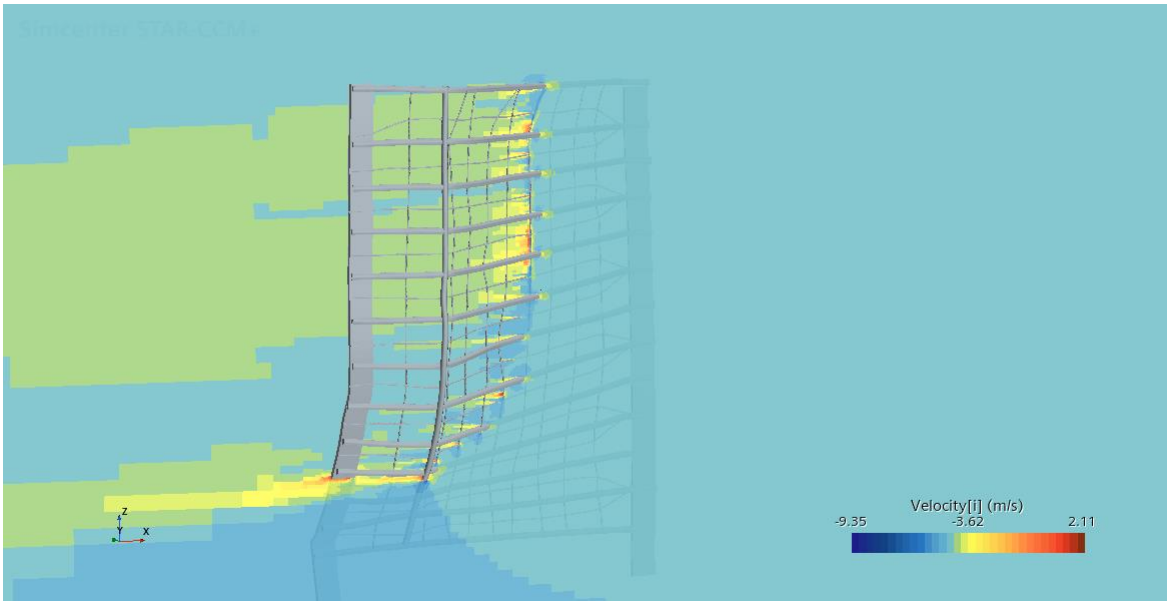

Figure 4-23: Open water propeller velocity contours

Assessment of the impact of the cage at speeds from 3 to 16 knots was made. The drag induced by the half cage simulated is shown in Figure 4-24. The drag correlates well (<1%) to velocity squared (Drag = $0.03v^2$). This is the expected result for a geometry with flow moving in one direction past its surface. The addition of the hull and induced propeller flow in the actual vessel situation is expected to alter this result. Grid convergence studies were conducted for the 9-knot case and (orange and gray dots in Figure 4-24) and showed a 6% underprediction for the coarsest grid (200% larger cells) and a 5% overprediction for the 5% overprediction for the medium grid (100% larger cells) versus the solution on the finest grid (6.0 million cells). No cavitation was generated due to the relatively low flow speeds. Sound levels were only determined at 100 m distance, and below the numerical precision.

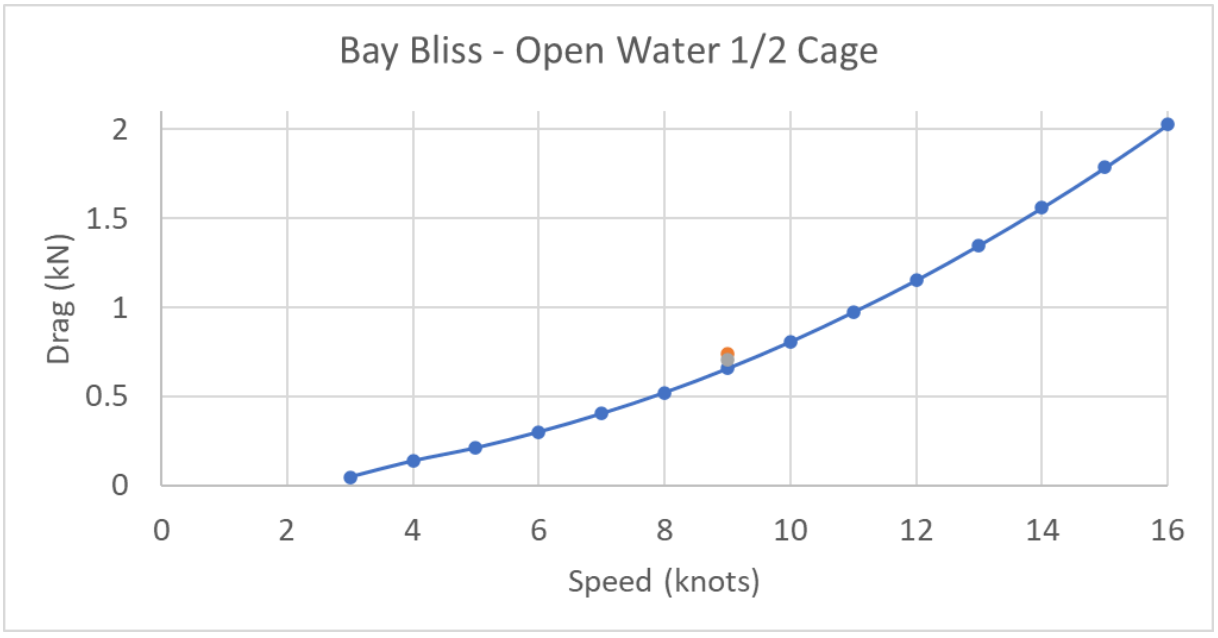

Figure 4-24: Bay Bliss open water cage induced drag.

4.5 Self-Propulsion Simulations

Baseline self-propulsion simulations of the Bay Bliss without any propeller cage were performed to verify vessel performance and URN predictions. The generated free surface elevation for a 9-knot sailing speed is shown in Figure 4-25. The typical Kelvin wake pattern is present. This dissipates after roughly a vessel length due to coarsening of the grid, since the vessel performance and near-field noise is of importance in this work.

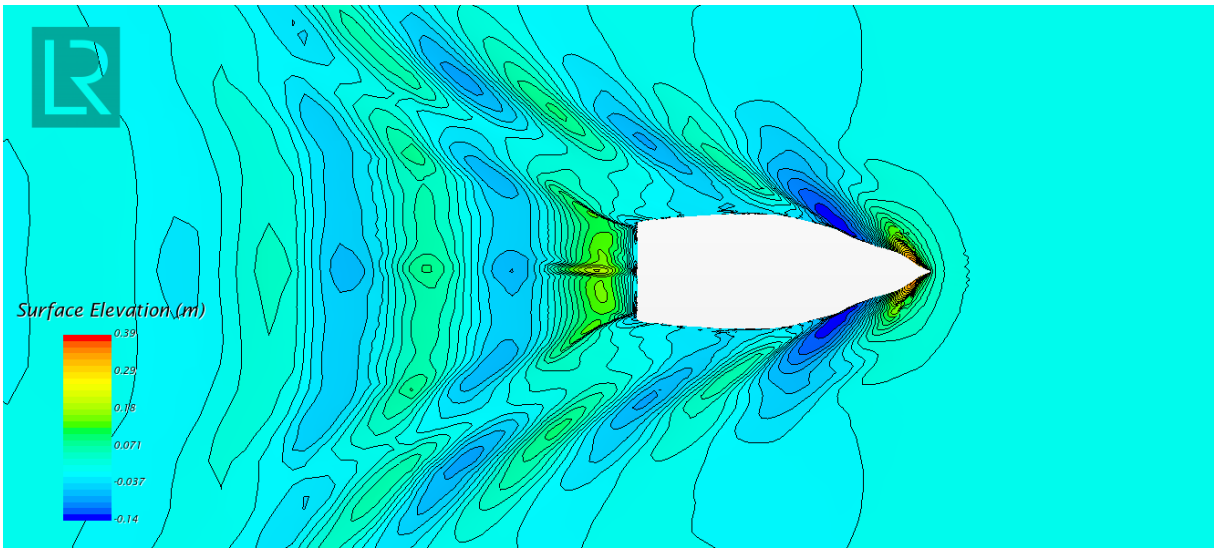

Figure 4-25: Bay Bliss self-propulsion simulation free surface (9 knots).

The volume fraction of air on the vessel centerline plane and the hull surface is shown in Figure 4-27. The bow wave is pushed up around the first 1/3 of the vessel, then the free surface starts to move slightly under the flat bottom of the hull. Finally, a stern wave is generated of approximately the same height as the aft of the vessel. The propeller and cage regions remain fully submerged.

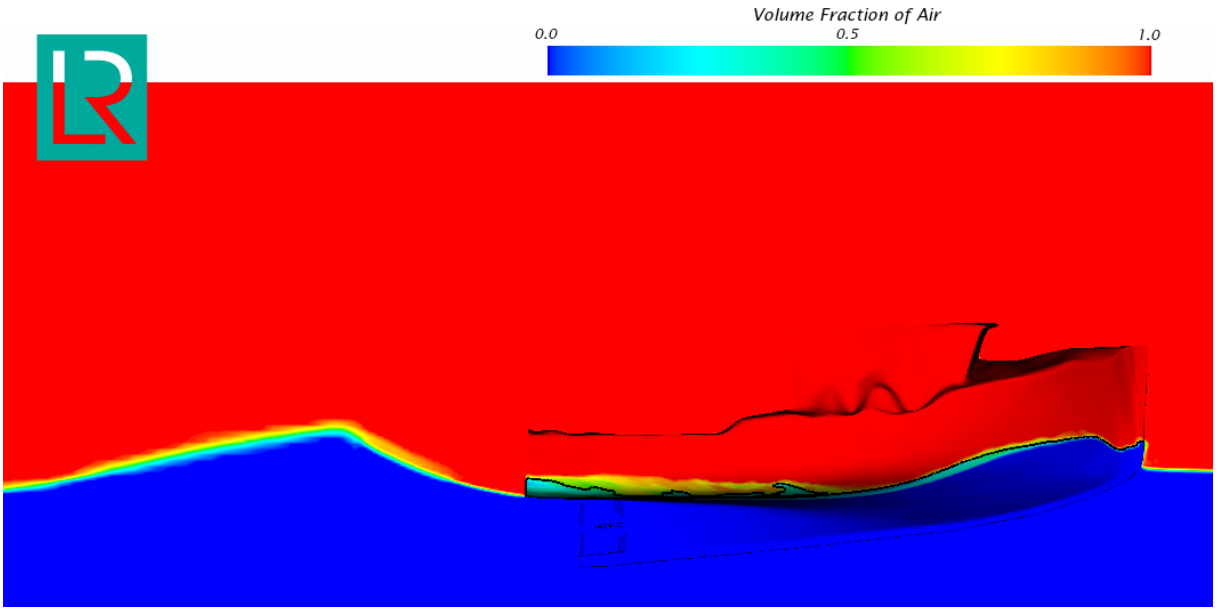

Figure 4-26: Bay Bliss self-propulsion simulation air volume fraction on centerline plane and hull (9 knots).

The velocity magnitude on the vessel centerline plane is shown in Figure 4-27. Of note is the large, induced velocity due to the propeller.

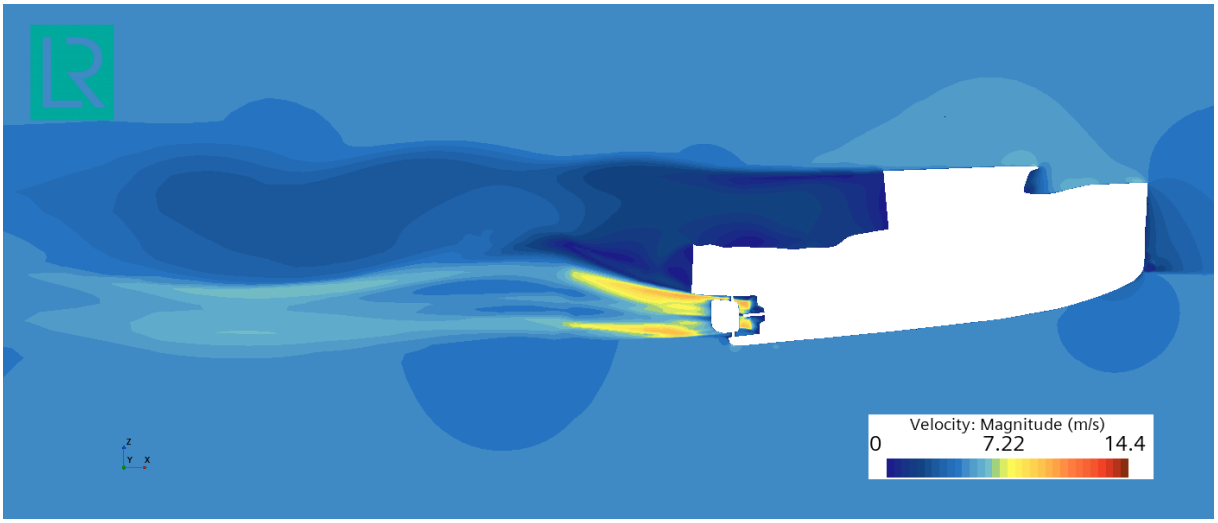

Figure 4-27: Bay Bliss self-propulsion simulation velocity magnitude on centerline plane (9 knots = 4.63 m/s).

Convergence of the governing equation residuals is shown in Figure 4-28. The time history of the sink and trim is shown in Figure 4-29, and the vessel resistance contributions in Figure 4-30. Jumps at 20 s and 40 s correspond to the release of the fixed vessel and application of the propeller thrust, respectively.

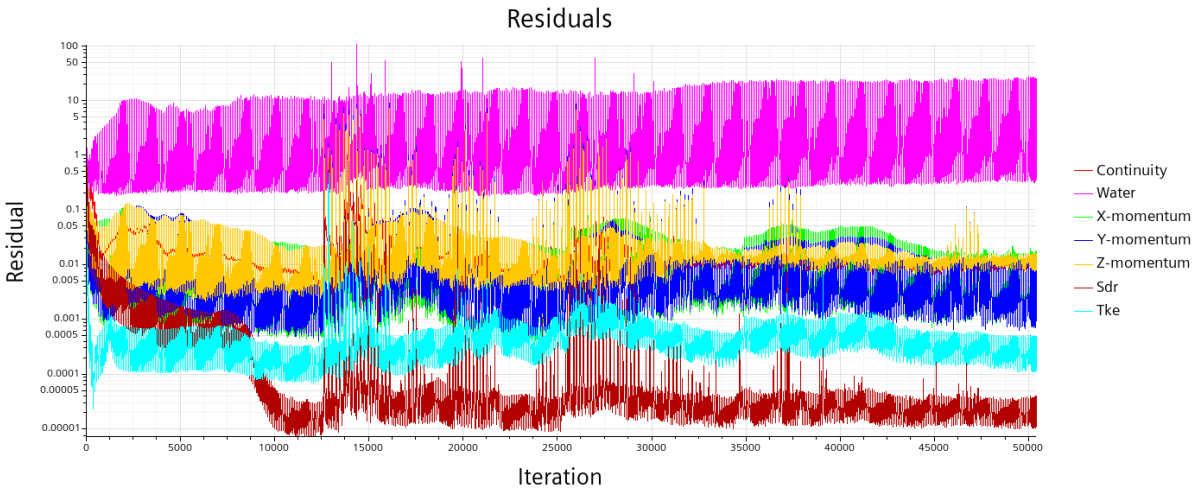

Figure 4-28: Bay Bliss self-propulsion residual convergence (9 knots).

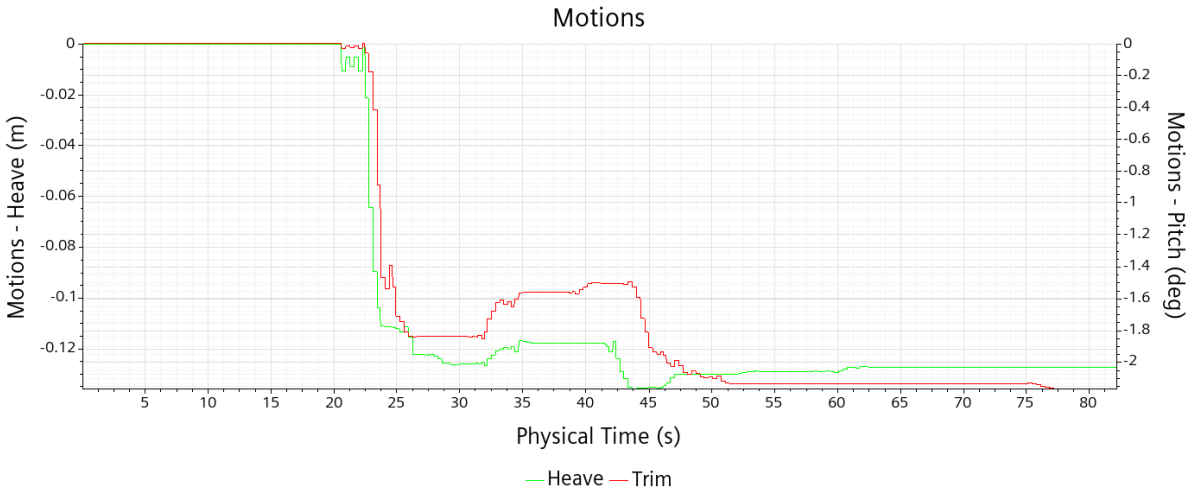

Figure 4-29: Bay Bliss self-propulsion sink and trim convergence (9 knots).

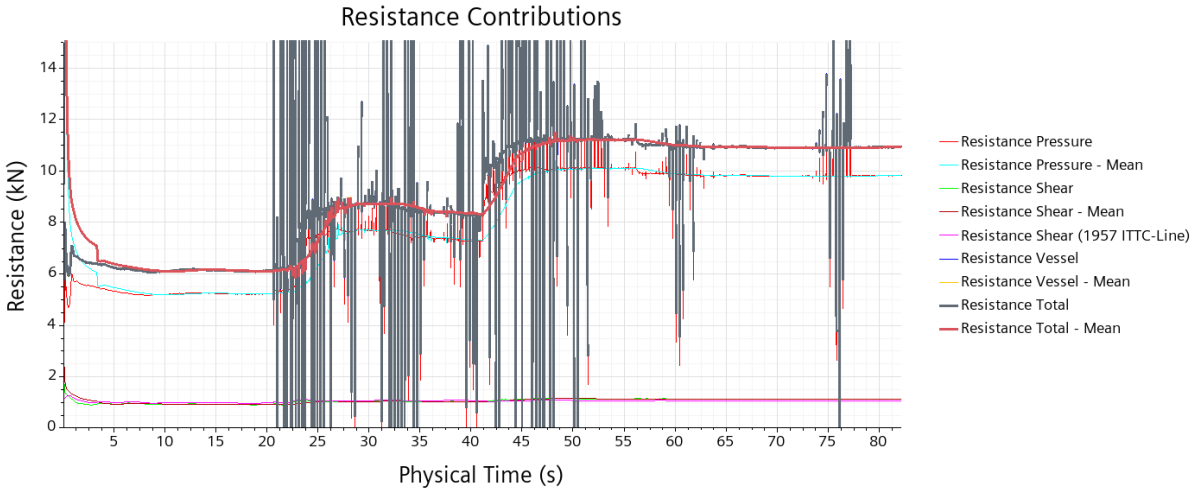

Figure 4-30: Bay Bliss self-propulsion forces convergence (9 knots).

Preliminary noise predictions for the self-propulsion scenario without the cage present were made and are given in Section 4.8. Similar self-propulsion analyses were conducted for the Bay Bliss at 3 and 6 knots, and for the Brooklynn and Boys. Results were similar to those shown in this section.

Repeated attempts were made to include the cage geometry in the self-propulsion analysis. To properly resolve the small cage rods, at least 5 cells are required across their width. With this mesh sizing, similar to that used for the cage only simulations in Section 4.4.2, the numerical grid would have been larger than practically usable (100+ million cells). Attempts were made to incorporate a growth of the cell sizing near the cage, to that needed for the ship away from the cage. All these attempts led to numerical instabilities. This was one of the objectives of this project, to isolate appropriate cell sizing requirements.

Two alternate cage performance prediction methodologies were considered to allow for predictions to be performed. These included treating the cage as a porous membrane, see Section 4.6, and simulating a smaller computational domain that only incorporated the stern of the vessel, see Section 4.7.

4.6 Membrane Approximations

The cage may be represented with a porous membrane, that would produce the same pressure loss and velocity non-uniformity as the flow around the actual cage geometry. Star-CCM+ allows for the definition of a resistance based porous membrane baffle representing thin-walled separators. These can determine the bulk effects that the baffle has on the flow, not the fine details. This baffle treatment is suitable when the flow is predominantly normal to the surface. The membrane model requires the membrane thickness, porosity (ratio of the area of the holes to the area of the surface), as tuning parameters for the inertial and viscous resistance in the normal and tangential directions and the turbulent resistance. The tuning parameters relate the pressure drop and turbulence generation to the flow velocity and density.

While a membrane approximation has the benefit that much larger computational cells could then be used in the self-propulsion analysis, generating a computational less expensive and more stable simulation. Figure 4-31 compares the physical cage geometry for the Bay Bliss to the equivalent porous surface.

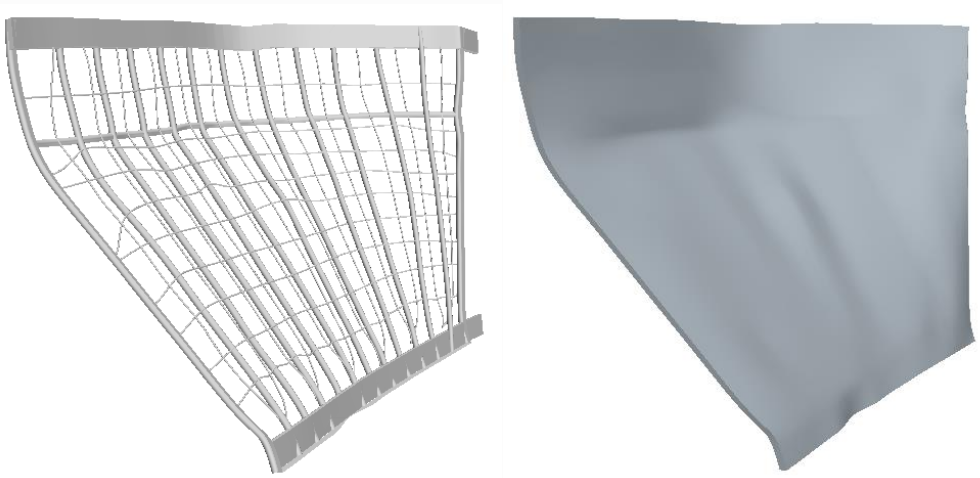

Figure 4-31: Bay Bliss propeller cage representation as a porous membrane (left: cage geometry, right: equivalent membrane).

The downside to a membrane approach is that these cage losses would be uniformly applied and hence represent an average behaviour of the cage, not the actual localized behaviour. More importantly, the values used in the model must be tuned to those produced by the physical system. As such, the membrane approach may be useful once a cage performance is well characterized to allow for computationally less expensive assessments but is not appropriate for predictive analyses.

4.7 Stern Simulations

To produce stable propeller cage performance predictions, the stern of the vessel was simulated in isolation. In this approach, the self-propulsion analysis without the cage is used to determine the flow-field near the stern of the vessel. This includes the vessel sink and trim, propeller rotation rate, and inflow boundary conditions for the stern domain. The stern region may be simulated with a much smaller cell size, in keeping with that required to resolve the cage.

The stern domain considered is shown in Figure 4-32.

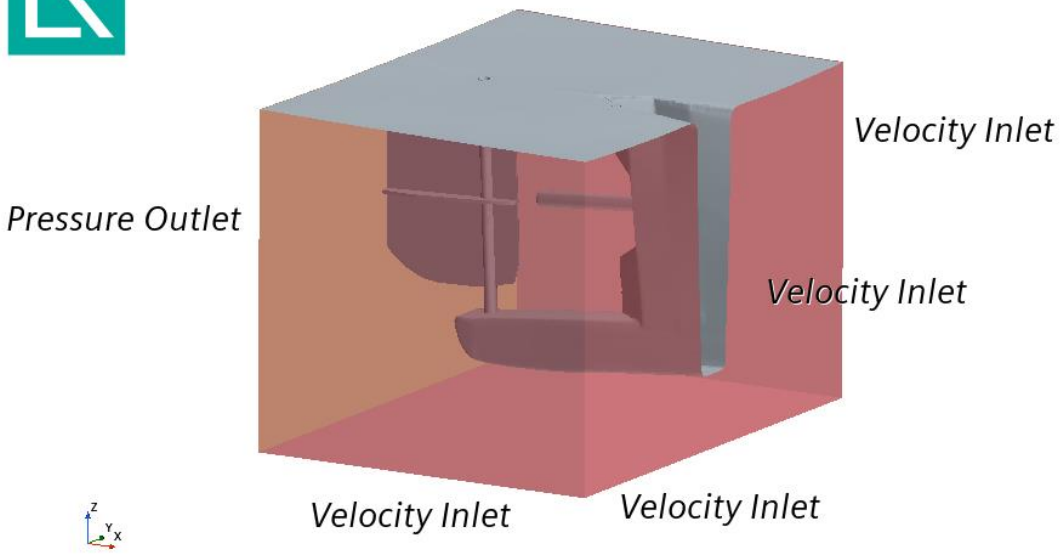

Figure 4-32: Bay Bliss stern computational domain (without propeller cage).

In the self-propulsion analyses the thrust produced by the propeller is balanced by the drag forces (CFD resolved pressure and frictional drag plus shear resistance from the surface roughness [19]).

$$Thrust_{propeller} = Resistance_{total} \quad 4\text{-}1$$

For the stern simulation with no propeller cage (and the propeller spinning at the same RPM as in the full self-propulsion case) the same total forces are present, but the CFD model only resolves a portion of them:

$$Thrust_{propeller} = Resistance_{stern} + Resistance_{fore+super} \quad 4\text{-}2$$

Under the assumption that the forces on the fore and superstructure don't change with the addition of the propeller cage, the new thrust (propeller RPM) required to compensate for the cage can be determined solely from the stern resistance simulation with the cage:

$$Thrust_{propeller,cage} = Resistance_{stern+cage} + Resistance_{fore+super} \quad 4\text{-}3$$

A variety of simulations were performed to assess the propeller cage performance and underwater radiated noise at three different speeds. Simulations were performed with different propeller representations:

1. virtual disc,
2. boundary element method (BEM),
3. moving reference frame (propeller geometry).

Simulations were performed for different cage configurations:

1. without the propeller cage
2. with propeller cage
3. with fouled propeller cage

Additional difficulties were encountered in trying to produce a stable simulation with the presence of the propeller cage even when considering only the stern section of the vessel. Further examination showed that

some of the instabilities were caused by poor resolution of the geometric features. The cage geometry generation detailed in Section 4.2.3, can produce thin gaps between the different cage bars or the bars and hull. With sufficiently small computational cell sizes the flow through these features can be resolved. However, with the cell sizes desired to keep the overall simulations of a manageable size and run time (<2 days on 120 CPUs), it is necessary to eliminate the majority of these gaps. The model of the propeller cage was therefore revised through multiple iterations to remove these gaps. Instead of metal rods modelled as they were physically constructed (a rod lying on top of the other with a weld between them), they were assumed to join perfectly at the intersections.

Results of the simulations are shown in the subsequent sections.

4.7.1 Virtual Disk Propeller

With the simplest propeller representation, a virtual disk model, the velocity magnitude on the centerline plane at a 9-knot speed is shown in Figure 4-33. While the cage (right figure) slightly slows the flow ahead of the propeller plane, the magnitude is generally faster afterward. This is a consequence of the propeller being required to spin faster to make up the drag induced by the cage.

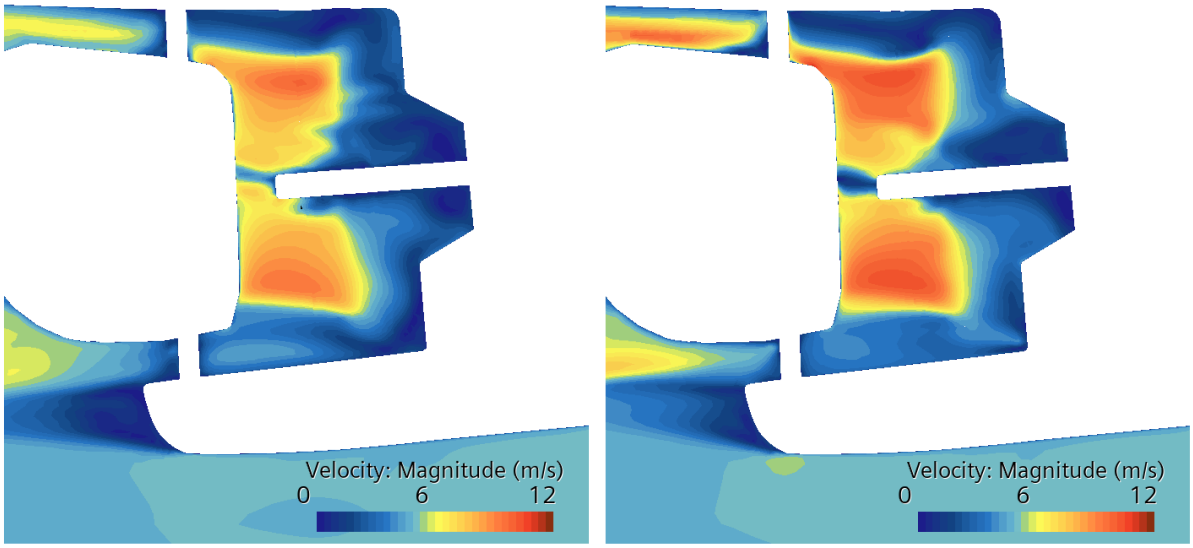

Figure 4-33: Bay Bliss stern: centerline plane velocity magnitude (9 knots) (left: without cage, right: with cage).

The wall shear stress and flow patterns on the hull and cage are shown in Figure 4-34. The presence of the cage disrupts the relatively smooth flow along the hull. This can also be observed in the crossflow plane ahead of the propeller (0.25 radius upstream), see Figure 4-35. While the influence of the cage is obvious on the velocity field, in terms of propeller performance the incoming velocity is more uniform (values closer to the mean) for this class of vessels. This is discussed further, along with the URN predictions, in Section 4.8.

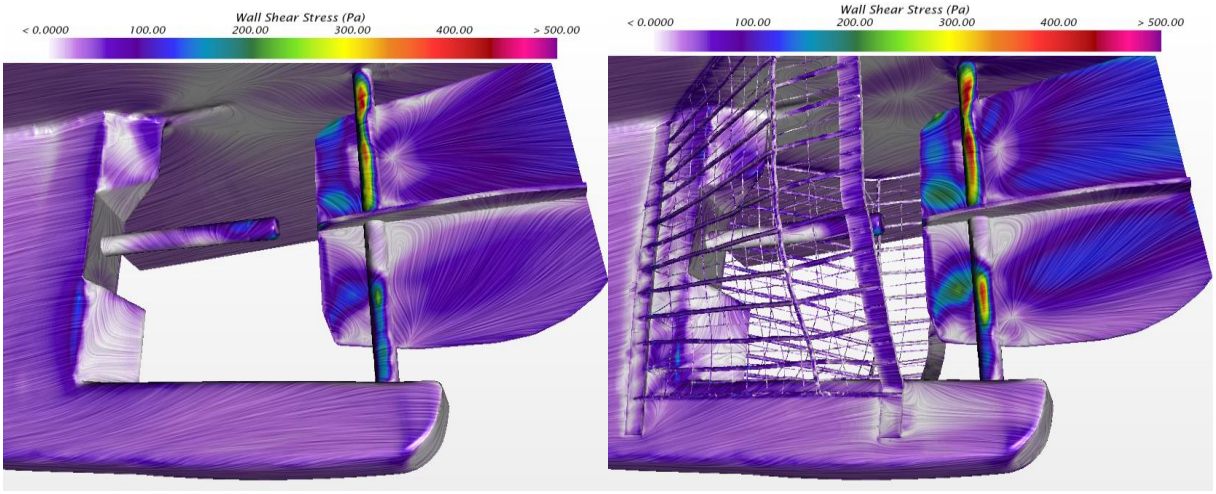

Figure 4-34: Bay Bliss stern: wall shear stress (9 knots) (left: without cage, right: with cage).

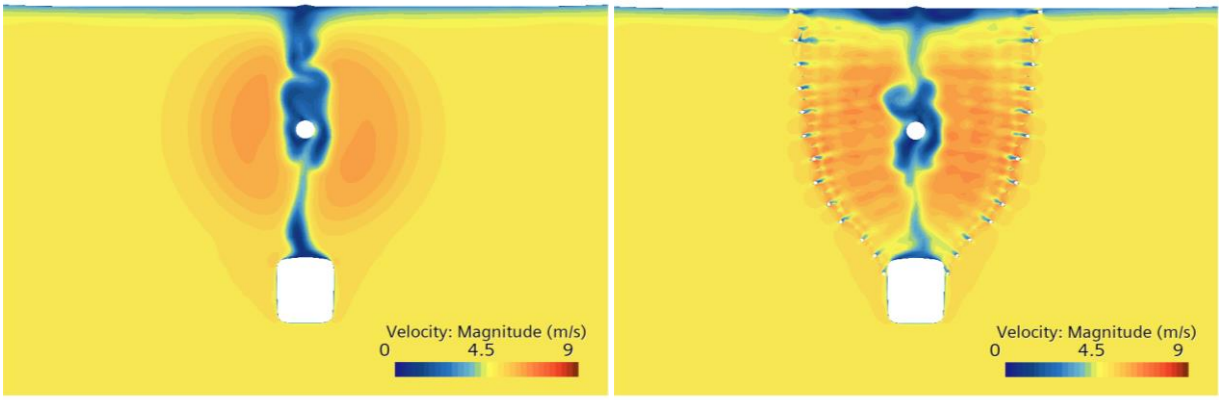

Figure 4-35: Bay Bliss stern: cross-stream plane viewed from aft (0.25 radii ahead of propeller) velocity magnitude (9 knots) (left: without cage, right: with cage).

Similar results are found for 6 knot and 3 knots sailing speeds as shown in Figure 4-36 and Figure 4-37 respectively.

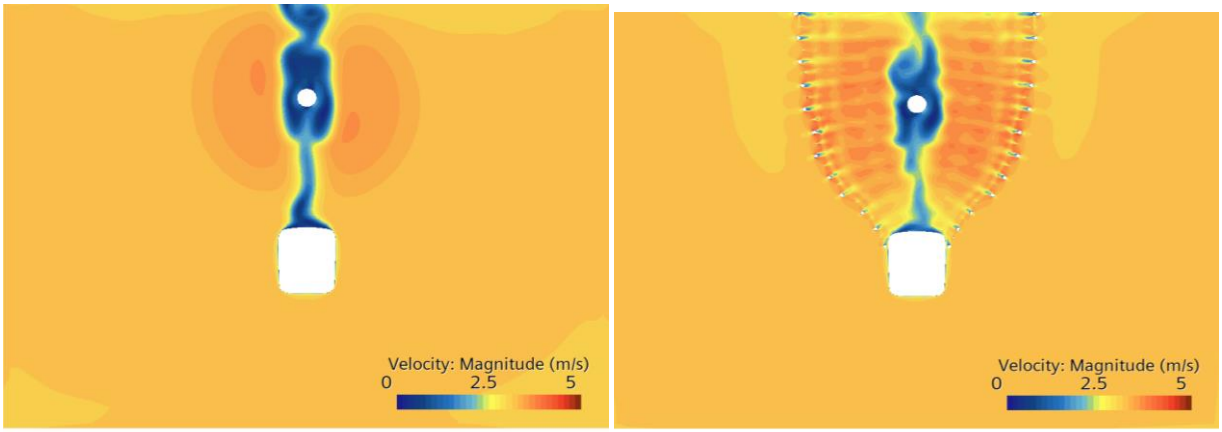

Figure 4-36: Bay Bliss stern: cross-stream plane viewed from aft (0.25 radii ahead of propeller) velocity magnitude (6 knots) (left: without cage, right: with cage).

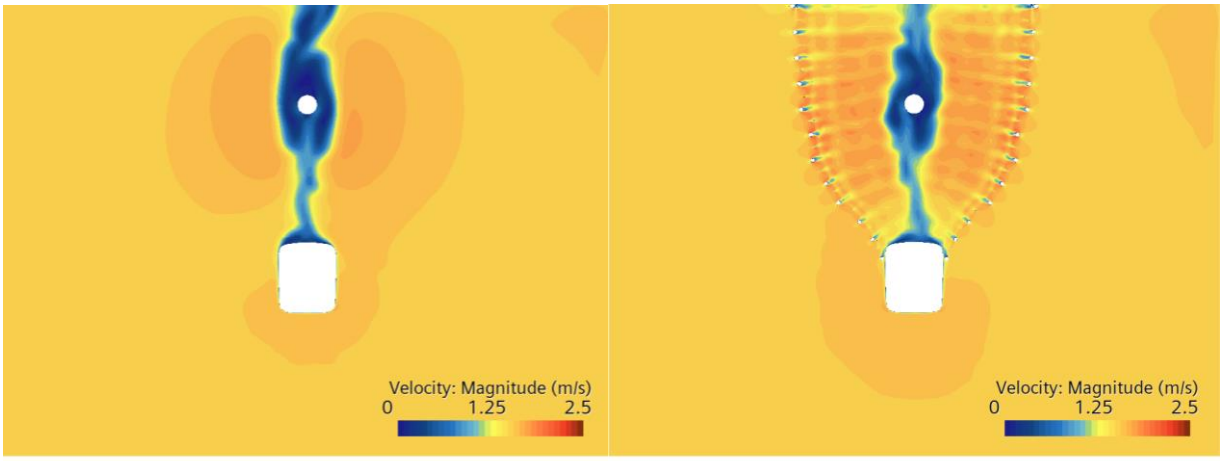

Figure 4-37: Bay Bliss stern: cross-stream plane viewed from aft (0.25 radii ahead of propeller) velocity magnitude (3 knots) (left: without cage, right: with cage).

The forces and predicted propeller RPM values are given in Table 4-2. In order to account for the extra cage drag the propeller has to spin 10 to 18 % faster. The cage drag was predicted to account for 30% of the vessel drag at the 9 knots speed. The percentage of drag from the cage increases with decreasing speed, as the wave drag over the rest of the vessel is relatively reduced.

Table 4-2: Bay Bliss forces.

Self-propulsion					
Speed (knots)	Thrust - propeller (kN)	Resistance - total (kN)	RPM	Pitch (deg)	Heave (m)
9	10.92	10.92	796	2.17	-0.13
6	2.19	2.19	391	0.12	-0.05
3	0.38	0.38	174	0.03	-0.01

Stern - no cage					
Speed (knots)	Thrust - propeller (kN)	Resistance - stern (kN)	RPM	Resistance - fore+super (kN)	
9	10.60	0.37	796	10.56	
6	2.10	-1.49	391	3.68	
3	0.37	-2.06	174	2.44	

Stern - with cage					
Speed (knots)	Thrust - propeller (kN)	Resistance - stern+cage (kN)	RPM	Cage Resistance (kN)	Cage %
9	14.17	3.61	874	3.25	30%
6	3.38	-0.29	449	1.20	55%
3	0.67	-1.77	205	0.29	78%

4.7.2 Moving Reference Frame Propeller

To assess the impact of treating the propeller as a virtual disk, as opposed to higher order approximations, the stern simulations were repeated with the physical propeller geometry modelled with a moving reference frame. For these comparisons the propeller RPM was not adjusted, and hence the cage simulations do not represent a balanced force system.

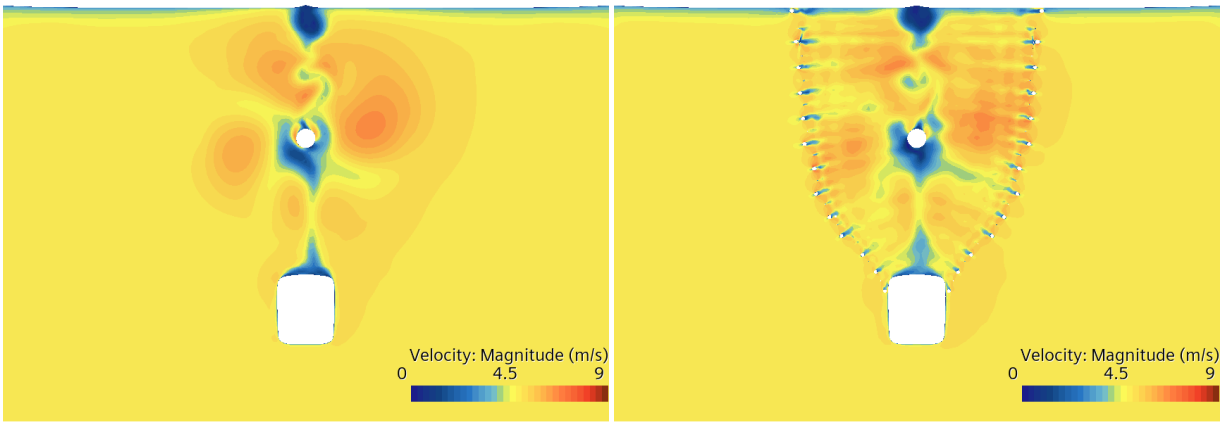

Figure 4-38: Bay Bliss stern: cross-stream plane viewed from aft (0.25 radii ahead of propeller) velocity magnitude (9 knots) (left: without cage, right: with cage).

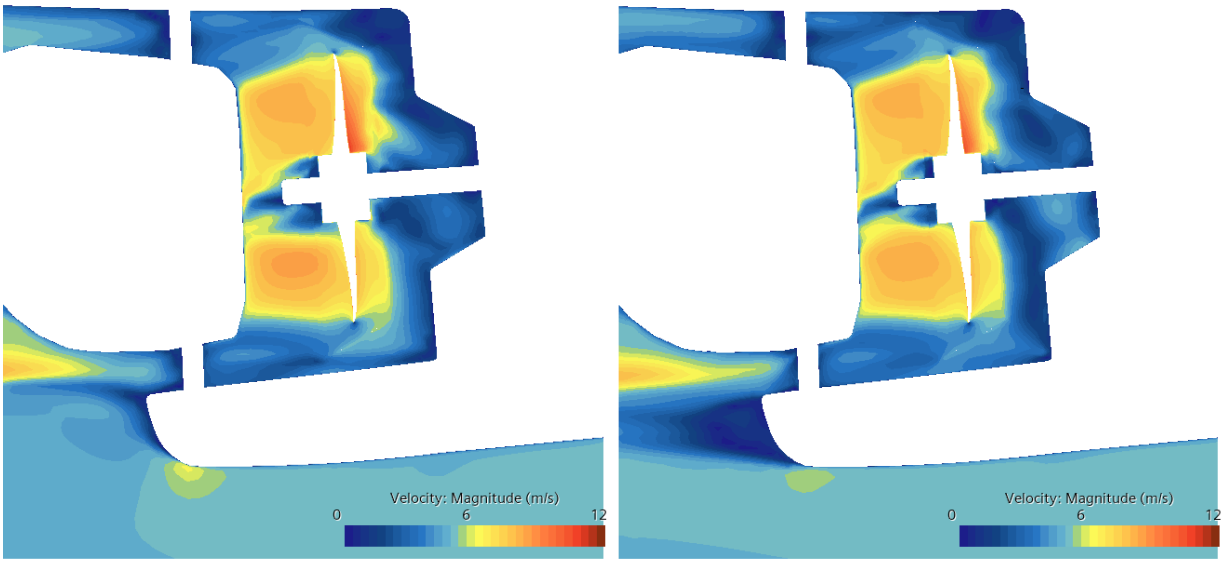

Figure 4-39: Bay Bliss stern: centerline plane velocity magnitude (9 knots) (left: without cage, right: with cage).

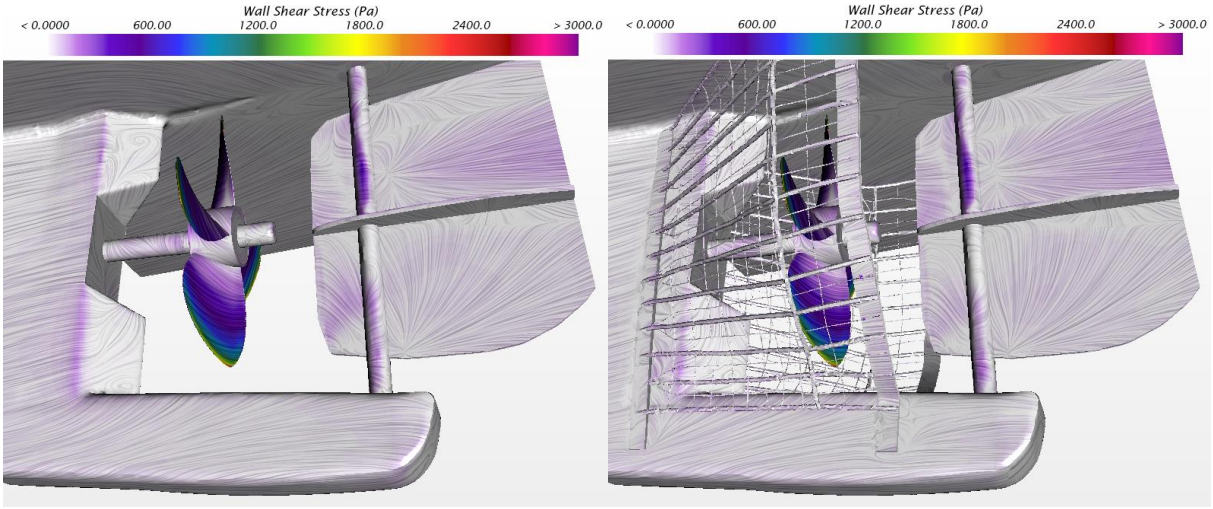

Figure 4-40: Bay Bliss stern: wall shear stress (9 knots) (left: without cage, right: with cage).

The cavitation extents on the propeller tips are shown in Figure 4-41. Due to the choice of propeller modelling and grid cell sizing appropriate for a RANS simulation, it is anticipated that these regions are underpredicted. It can be observed that the cavitation region is larger for the flow-field with the cage than without.

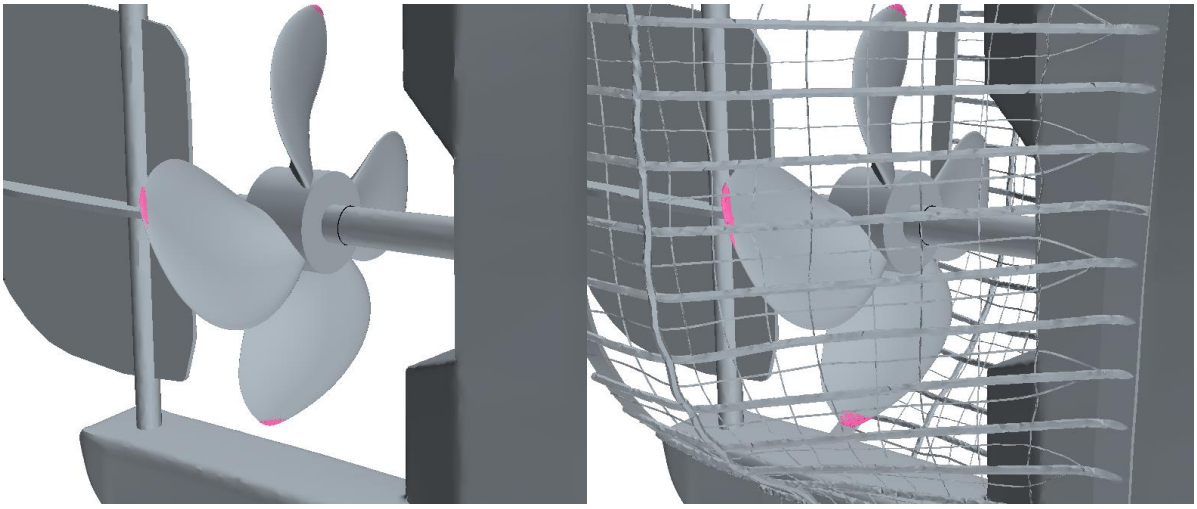

Figure 4-41: Bay Bliss stern: cavitation regions (pink), 9 knots (left: without cage, right: with cage).

4.8 Simplified Propeller Noise Calculations

For each run condition, PropART was given a target thrust based on the simulated CFD resistance and the propeller RPM adjusted until that thrust was achieved. This allowed for the propeller performance to be modelled with the higher fidelity BEM method as compared to the virtual disk model in Star-CCM+ while still incorporating the CFD ship resistance calculations utilizing the scanned real-world ship geometry.

4.8.1 9 knot Results

For the 9-knot run condition three different wake fields were considered:

- Ship without the cage,
- Ship with the cage with the propeller at the same RPM as without,
- Ship with the cage with the propeller RPM increased to compensate for the cage drag.

The *x* component of the normalized effective wakes used can be seen in Figure 4-42. The wake without the cage clearly shows the lower velocity in the centre region of the propeller plane where the ship hull is present. The cage wakes show a slightly more uniform wake field, due to the cage induced losses and diffusion of the velocity field. The drag compensated cage shows a slightly higher peak component but is overall very similar to the wake without drag compensation. This is largely due to the removal of the propeller induced velocities in the effective wake calculation. Since the differences between the two cage wakes were found to be very similar, they were considered interchangeable for the noise simulations as the impact on the final sound level result is minor.

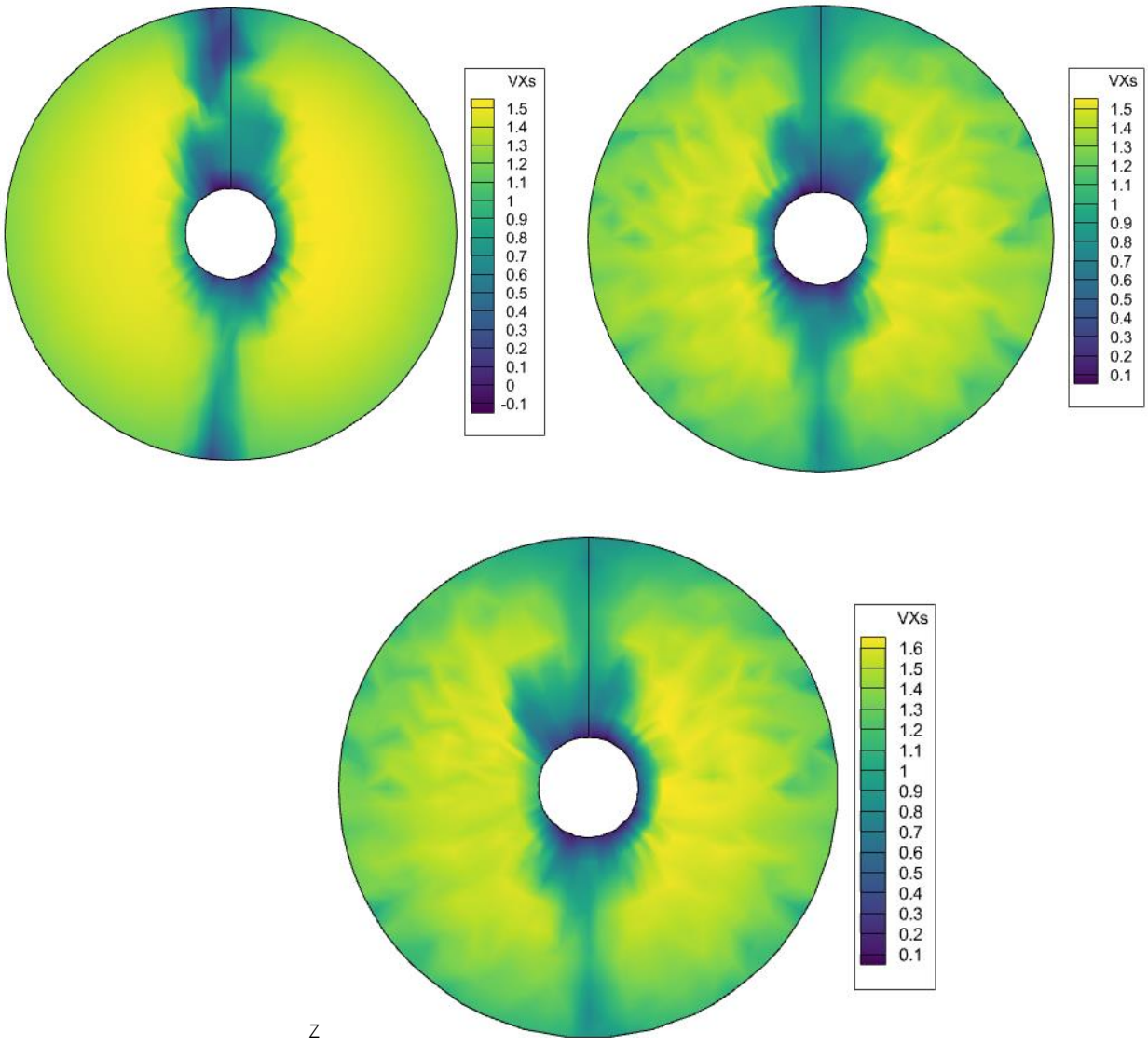

Figure 4-42 Bay Bliss 9kn effective wake fields. No cage (top left), cage with no drag compensation (top right), cage with drag compensation (bottom)

The target thrust and resulting RPM values for the 9 knot cases without and with the cage are shown in Table 4-3. Also shown is the RPM predicted by Star-CCM+'s virtual disk model. Both models predict a similar required increase in RPM to compensate for the cage, but PROCAL requires a higher base RPM to achieve the required thrust without the cage.

Table 4-3 Bay Bliss 9 knot target thrust and RPM.

Case	Target Thrust (kN)	RPM	Star-CCM+ RPM
No Cage	10.9	914	795
Cage	13.7	986	870
Difference	3.2	72	75

Individual components of the baseline noise results are shown Figure 4-43. While the face cavitation does contribute to the noise, the response is dominated by the tip vortex cavitation. Since the tip vortex is the primary contributor to the overall propeller noise, only results for the Brown sheet cavitation noise model are shown. Results for the Navais model were found to be similar with small differences in the lower sound level regions where the tip vortex noise is lower.

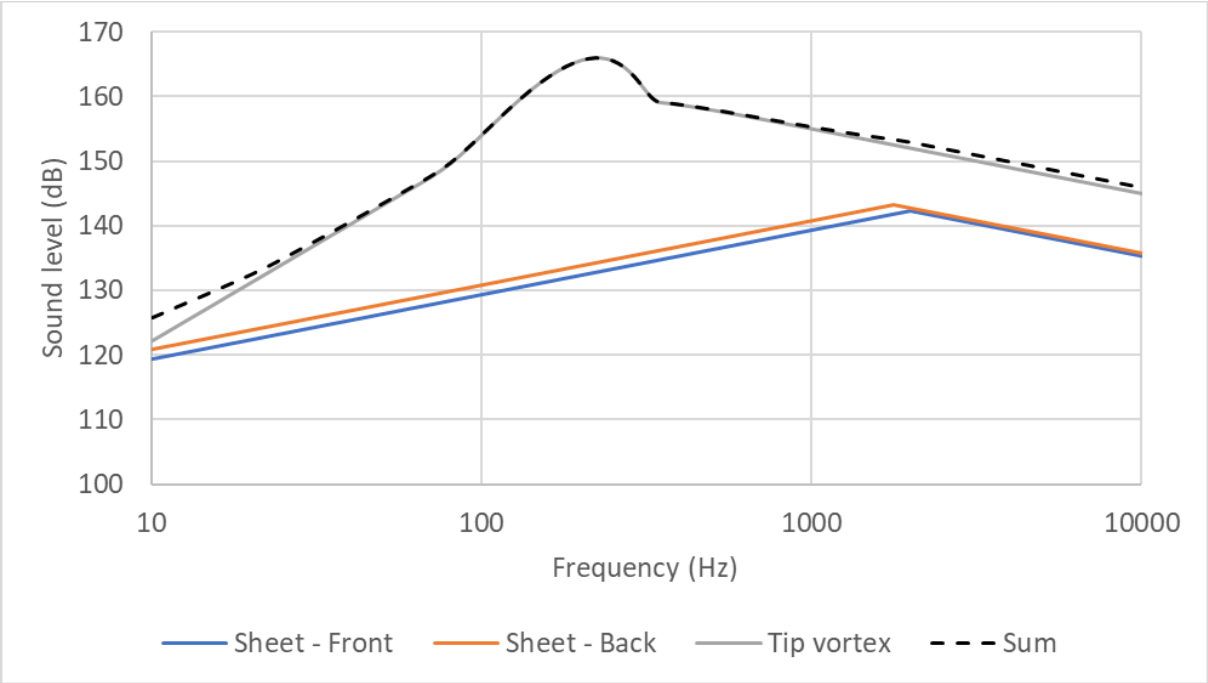

Figure 4-43 Individual propeller noise components, Bay Bliss, 9 knots, no cage

Results for the baseline, cage, and cage with drag compensation are shown in Figure 4-44. The case with cage where the RPM is held constant shows a slightly lower sound level compared to the baseline. This is due to the more uniform wake generated by the cage reducing the amount of volume change in the cavitation bubbles. The drag compensated wake shows an increase in noise due to the higher RPM of the propeller, suggesting that the primary mechanism for the increased propeller noise is simply the higher power demands due to the presence of the cage.

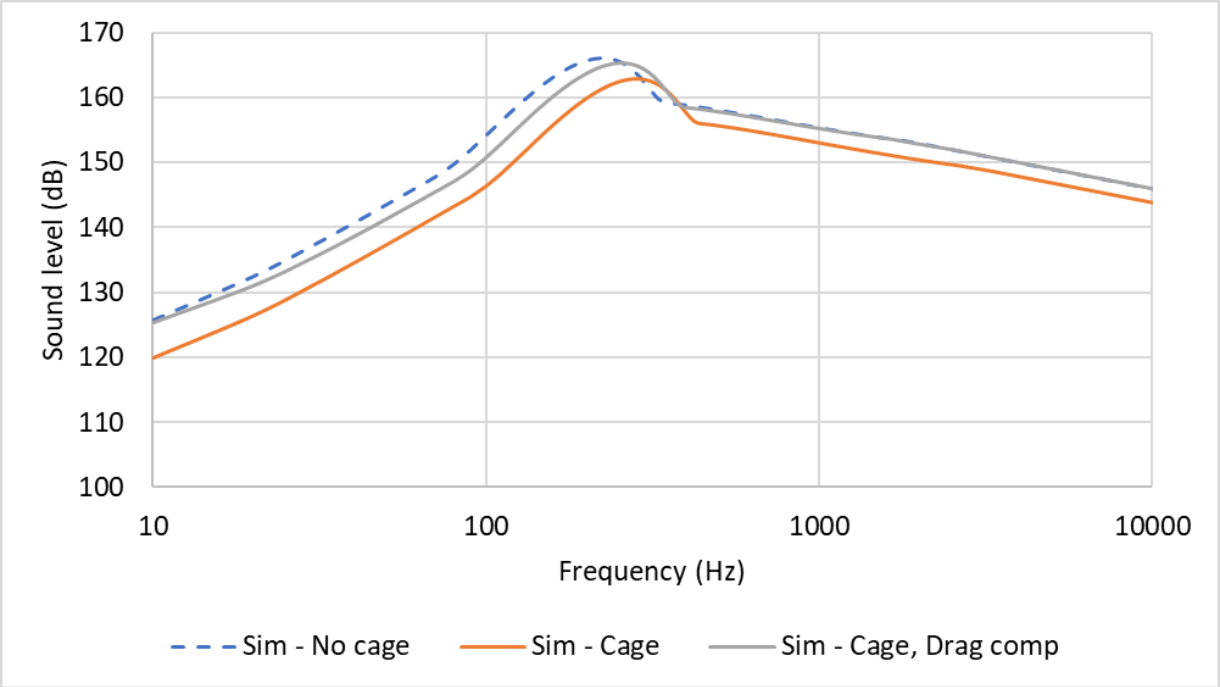

Figure 4-44 Total propeller noise, Bay Bliss, 9 knots

Cavitation extents for all three cases are shown in Figure 4-45 for a blade at top dead centre. In the images, pink indicates cavitation on the front suction side of the propeller and green/black are on the back side. All three show similar cavitation trends but the drag compensated propeller shows a larger tip region with more changing bubble volume as the propeller rotates. This corresponds to the large tip vortex component seen in the noise results and shows a trend consistent with the Star-CCM+ results.

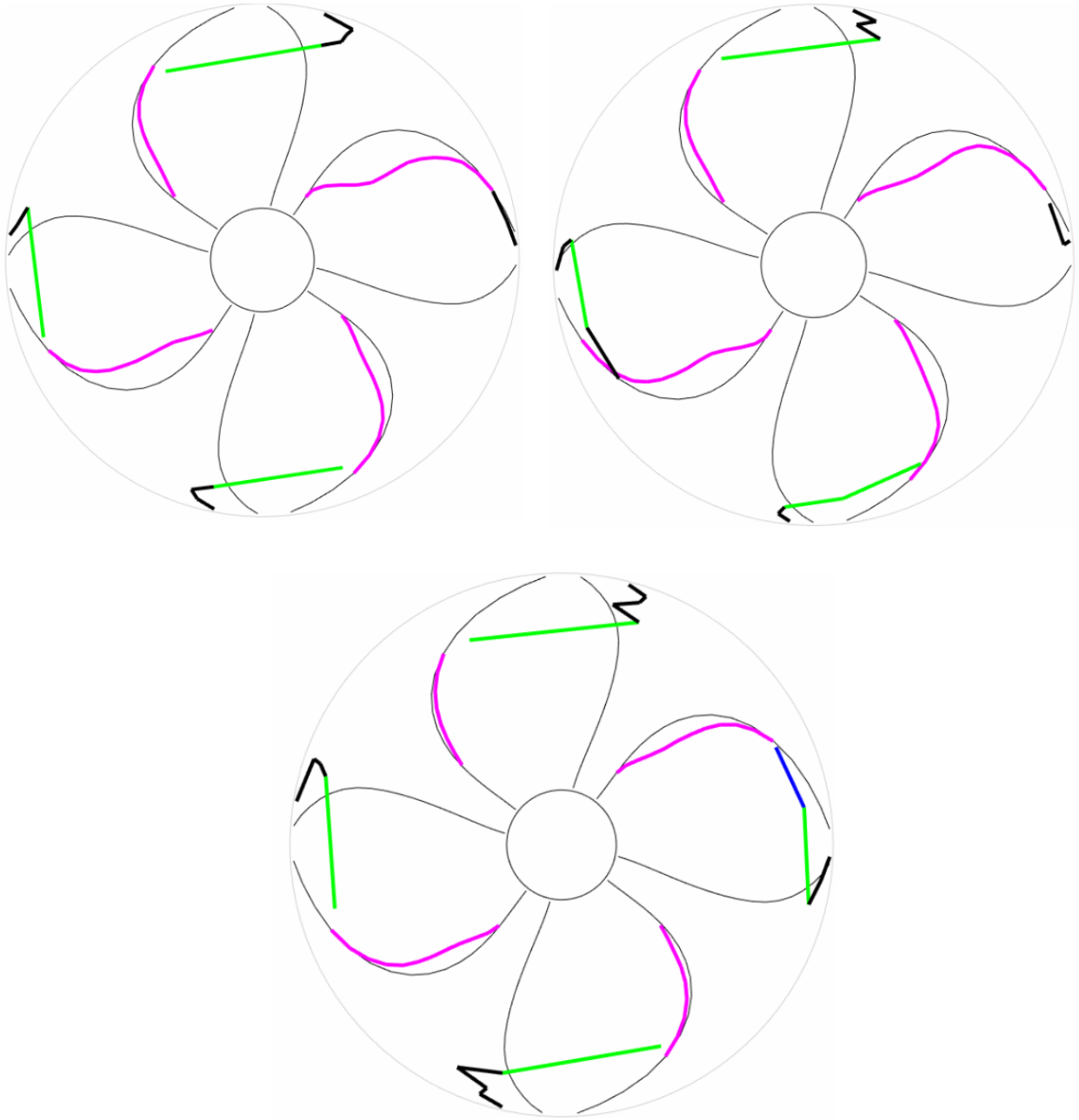

Figure 4-45 Bay Bliss 9 knot cavitation extents. No cage (top right), cage with no drag compensation (top left), cage with drag compensation (bottom)

4.8.2 6 knot Results

The wake fields for the Bay Bliss at 6 knots are shown in Figure 4-46. The same overall trend is seen as the 9-knot case but with lower peak normalized components.

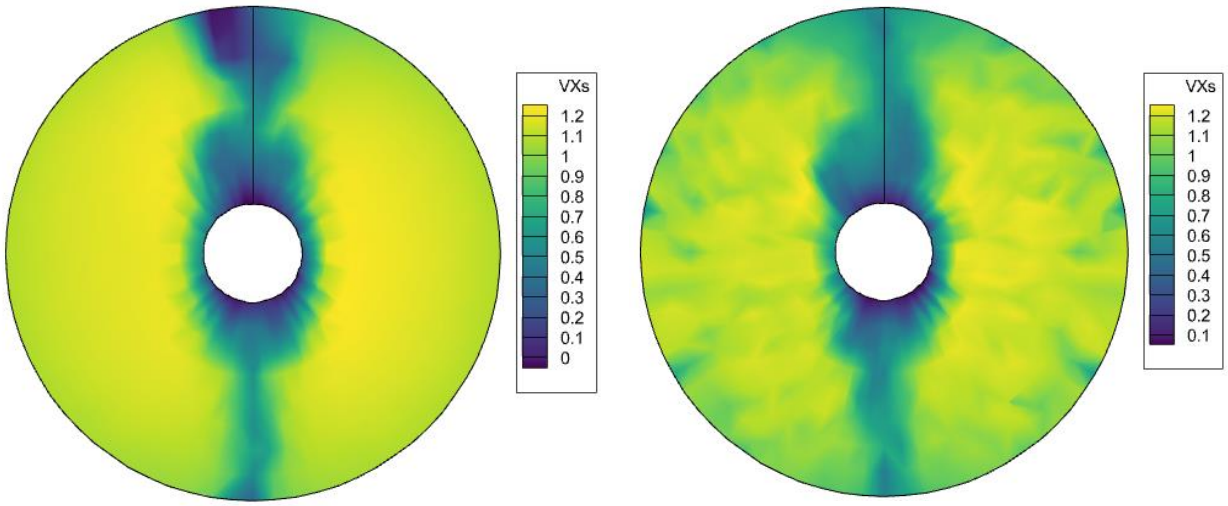

Figure 4-46 Bay Bliss 6 knot effective wake fields. No cage (left), cage (right)

The target thrust and resulting RPM values for the 6 knot cases without and with the cage are shown in Table 4-4. Also shown is the RPM predicted by Star-CCM+'s virtual disk model.

Table 4-4 Bay Bliss 6 knot target thrust and RPM.

Case	Target Thrust (kN)	RPM	Star-CCM+ RPM
No Cage	2.19	440	391
Cage	3.39	506	449
Difference	1.20	66	57

Individual noise components for the 6-knot case with no cage are shown Figure 4-47. Similar to the 9-knot case, the tip vortex noise dominates the response.

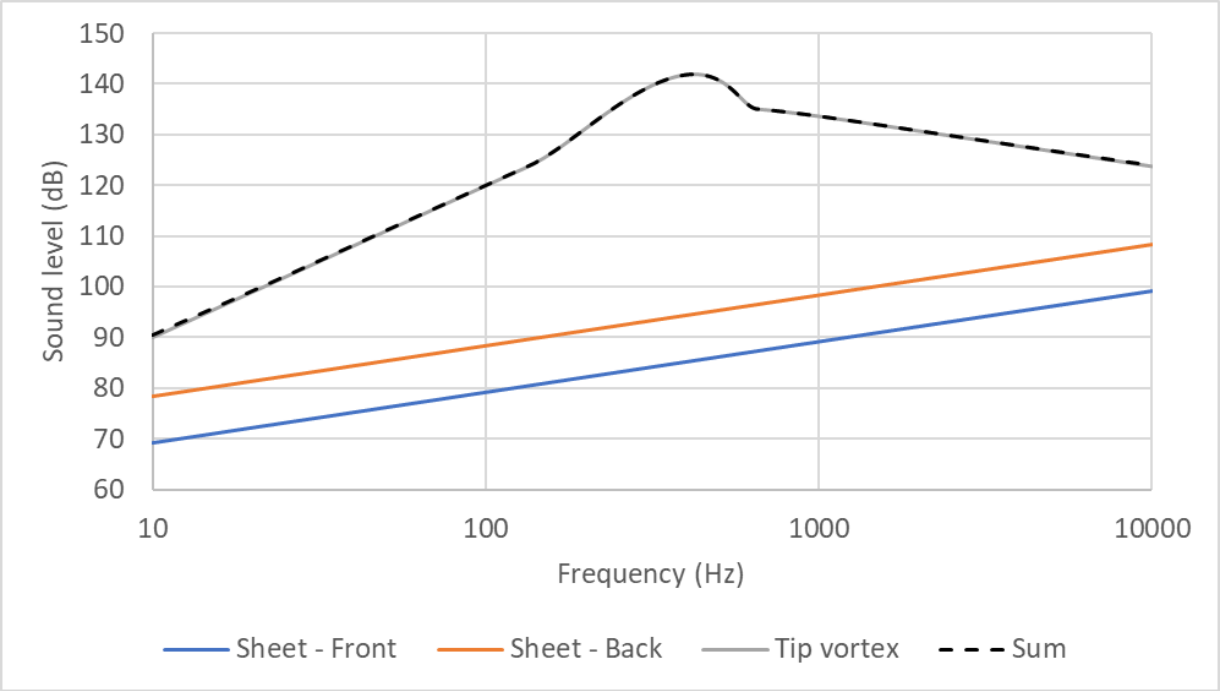

Figure 4-47 Individual propeller noise components, Bay Bliss, 6 knot, no cage.

Results for the baseline, cage, and cage with drag compensation at 6 knots are shown in Figure 4-44. The same trends as the 9-knot case are noted with the cage causing a reduction in noise if the RPM is held constant but a slight increase in noise when the additional drag is compensated for.

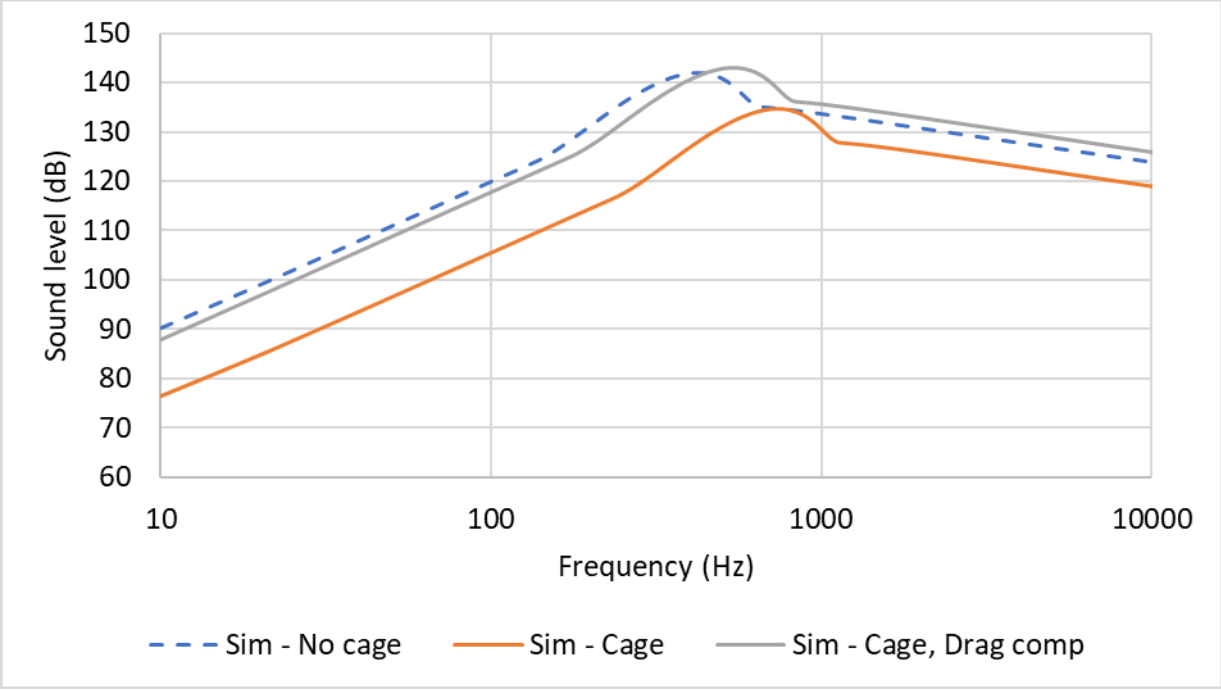

Figure 4-48 Total propeller noise, Bay Bliss, 6 knots

4.8.3 3 knot Results

The 3-knot case was not found to generate significant noise. The target thrust and resulting RPM values for the 3 knot cases without and with the cage are shown in Table 4-4 for reference.

Table 4-5 Bay Bliss 3 knot target thrust and RPM.

Case	Target Thrust (kN)	RPM	Star-CCM+ RPM
No Cage	0.380	193	174
Cage	0.675	230	205
Difference	0.295	37	25

4.9 Variations to Improve Validation

4.9.1 PROCAL/PropART Noise Parameters

The preceding results were all calculated using the default coefficients contained within PropART. The ETV model contains two parameters which control the semi-empirical fit. Since these fits were obtained from much larger vessels and propellers some tuning may be required to obtain better fits for smaller vessels. The sensitivity of the tip vortex noise to the fit factors A2 and A3 were conducted. The A3 factor was found to be the primary driver of the noise under the conditions given. Values of 0.5 and 0.25 times the nominal value were tested for the drag compensated case and are shown in Figure 4-49.

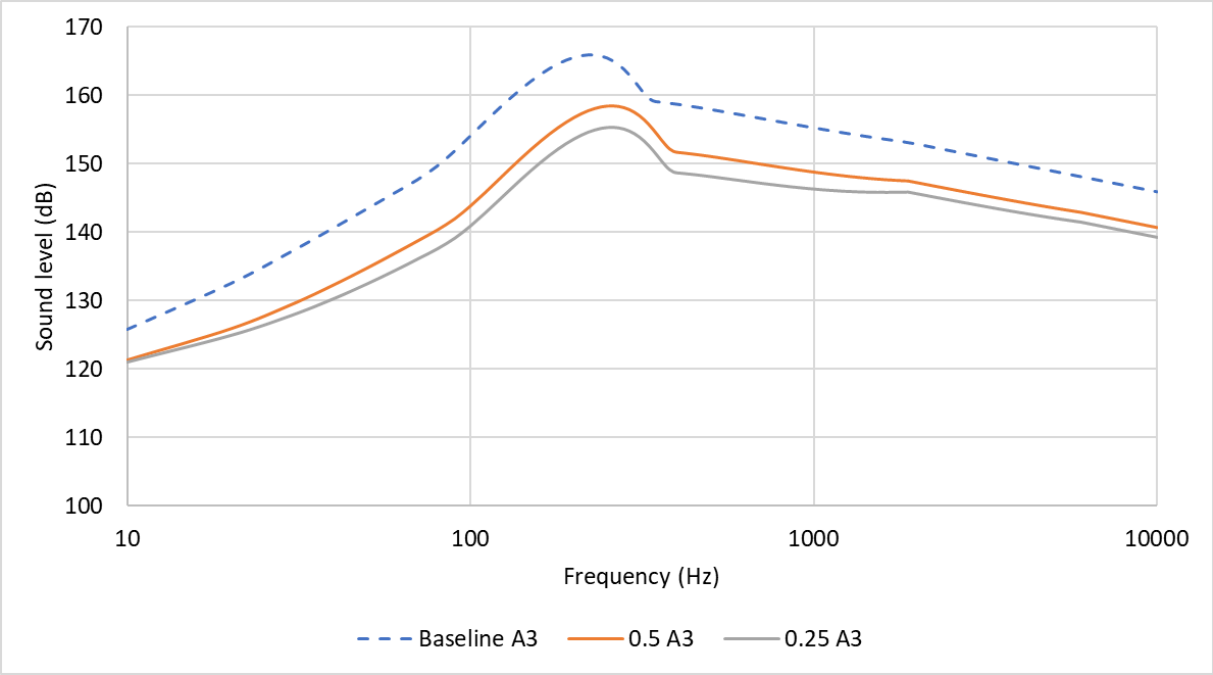

Figure 4-49 ETV model A3 parameter sensitivity, Bay Bliss, 9 knot.

Tuning the model coefficients does lower the overall noise but the results still overpredict the experimental results. However, what is more important is the trends between the ship noise without and with the cage

and the conclusions suggested by those trends. Results for all three conditions with the 0.25 times A3 factor are shown in Figure 4-50.

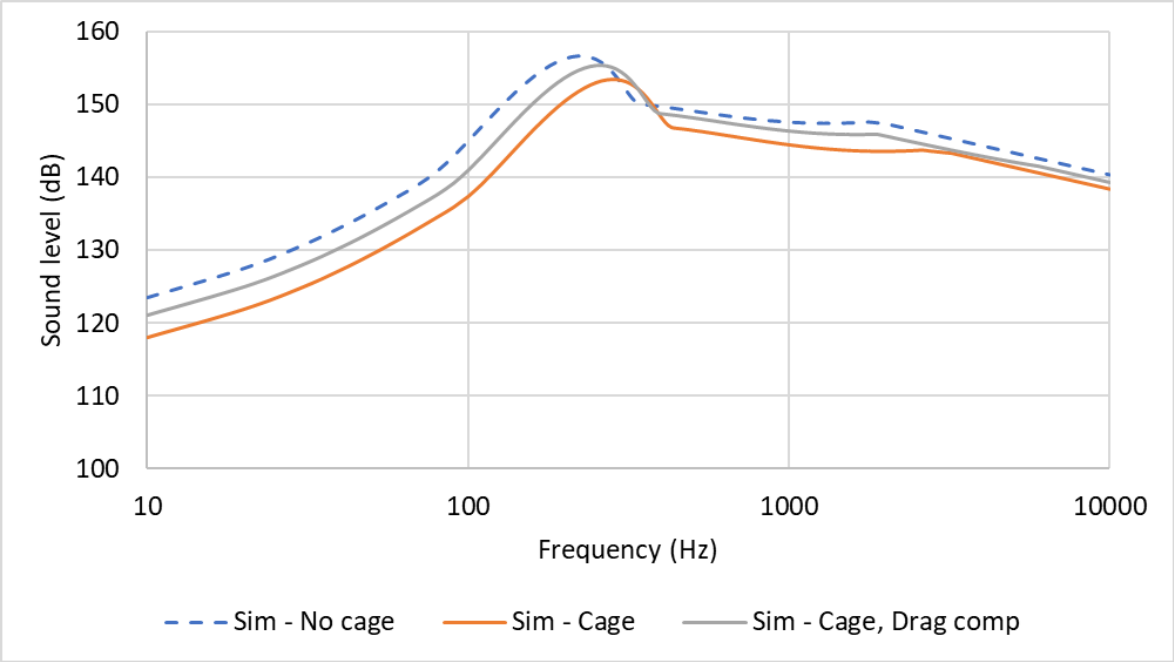

Figure 4-50 Total propeller noise, Bay Bliss, 9 knot, 0.25 A3.

All the results presented indicate that the primary driver of the increased propeller noise is due to the increased drag from the cage and the required increase in RPM to compensate for the drag. This is in addition to the known influence of a non-uniform wake that is not matched to the propeller. The trends observed were shown to be valid independent of model tuning. This suggests that while the simplified methods may overpredict the experimentally observed noise a predicted relative reduction in noise from the simplified models will translate to a reduced noise level in the real world. For the purposes of designing and optimizing a cage, the main objectives would be to minimize the drag with a secondary objective of re-distributing the ship wake such that the wake field is more uniform. A tertiary objective would be to use the cage to better match the wake field to the propeller and increase its performance, as is done in the design of energy saving devices.

4.10 Brooklynn and Boys

To verify the signature and performance predictions, a second Cape Islander vessel, Brooklynn and Boys, was simulated. Of the four vessels measured, this one was selected because it had a cage design that was the most different from the other vessels, see Figure 4-51. It was longer (extending further upstream along the hull) and had larger components and spacing.

a) This is It 1

b) Just Once

c) Bay Bliss

d) Brooklynn and Boys

Figure 4-51: Cape Islander propeller cages

The geometry of the Brooklynn and Boys was generated using 3D photogrammetry scans and a combination of software tools in a similar manner to that noted for the Bay Bliss, see Section 4.2. Following the creation of a CAD model of the vessel, a self-propulsion simulation was set up in Star-CCM+ with the same setup as that detailed in Section 4.3.

The self-propulsion simulation of the Brooklynn and Boys without any propeller cage at 9 knots is illustrated in the free surface elevation, Figure 4-52, and the velocity magnitude on the vessel centerline plane, Figure 4-53.

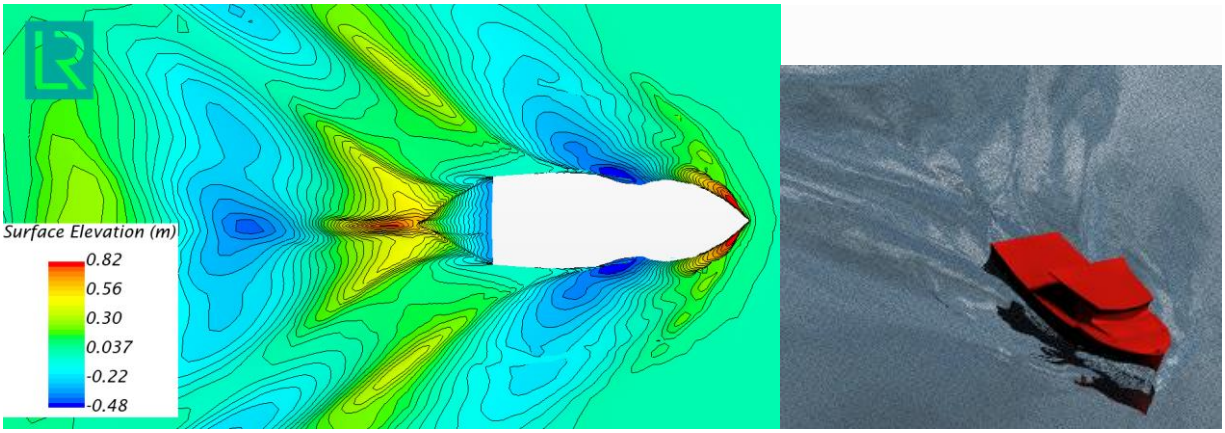

Figure 4-52: Brooklynn and Boys self-propulsion simulation free surface (9 knots).

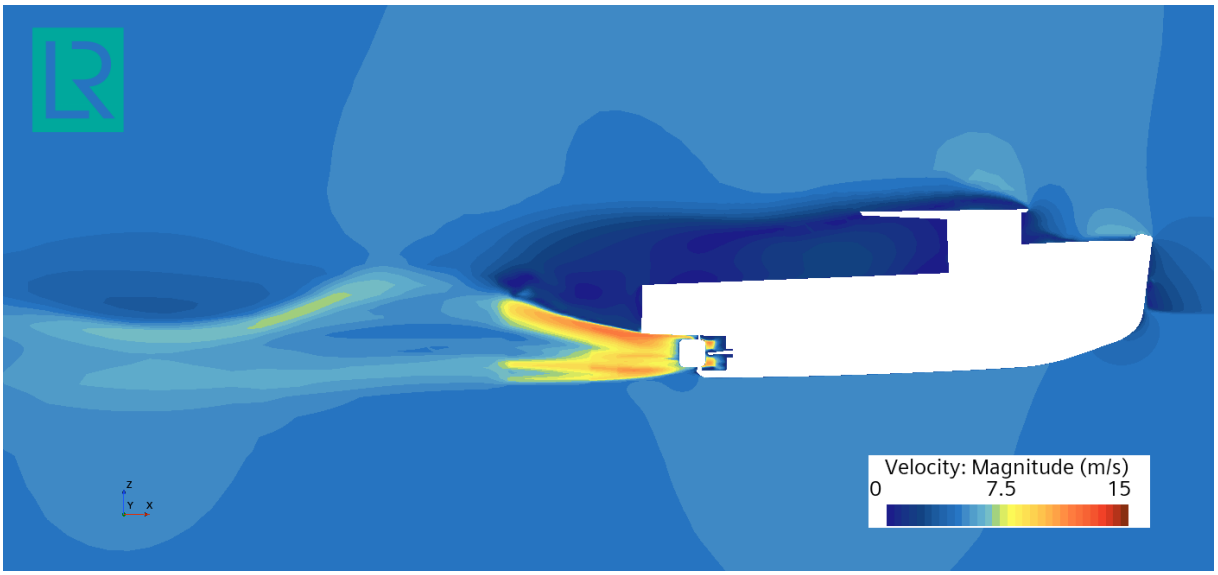

Figure 4-53: Brooklynn and Boys self-propulsion simulation velocity magnitude on centerline plane (9 knots = 4.63 m/s).

The velocity magnitude at a 9 knot speed is shown in Figure 4-54 on the centerline plane and in see Figure 4-55 on the cross-flow plane ahead of the propeller (0.25 radius upstream). The wall shear stress and flow patterns on the hull and cage are shown in Figure 4-56. Similar behaviour was observed, compared with the Bay Bliss. By moving the cage upstream from the propeller, the flow just ahead of the propeller becomes more uniform. Conversely, a longer cage will in general induce more drag.

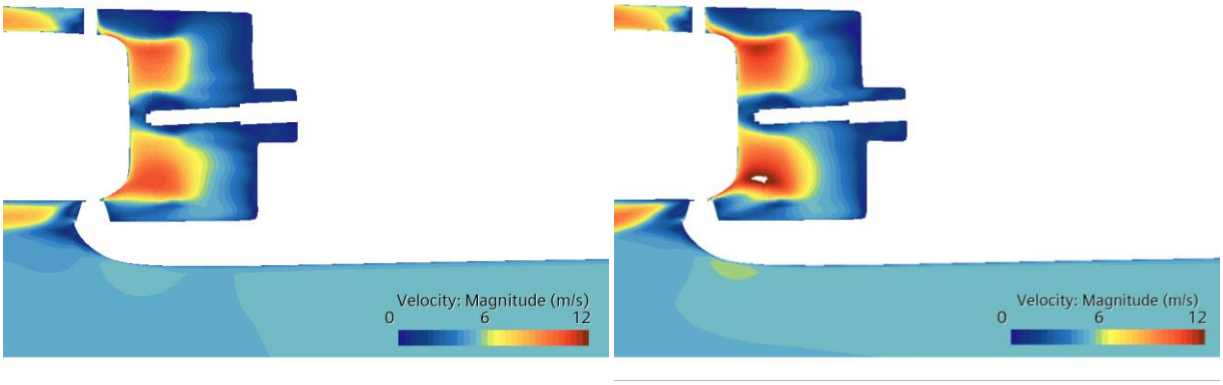

Figure 4-54: Brooklynn and Boys stern: centerline plane velocity magnitude (9 knots) (left: without cage, right: with cage).

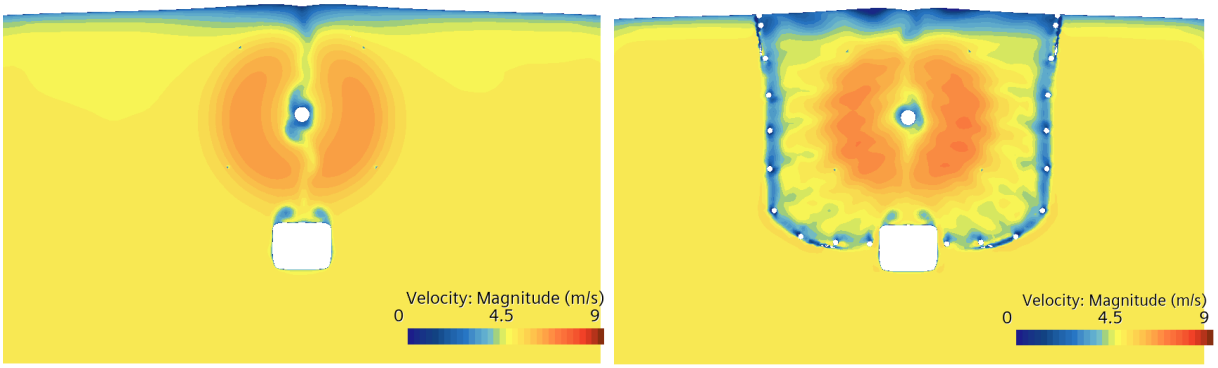

Figure 4-55: Brooklynn and Boys stern: cross-stream plane viewed from aft (0.25 radii ahead of propeller) velocity magnitude (9 knots) (left: without cage, right: with cage).

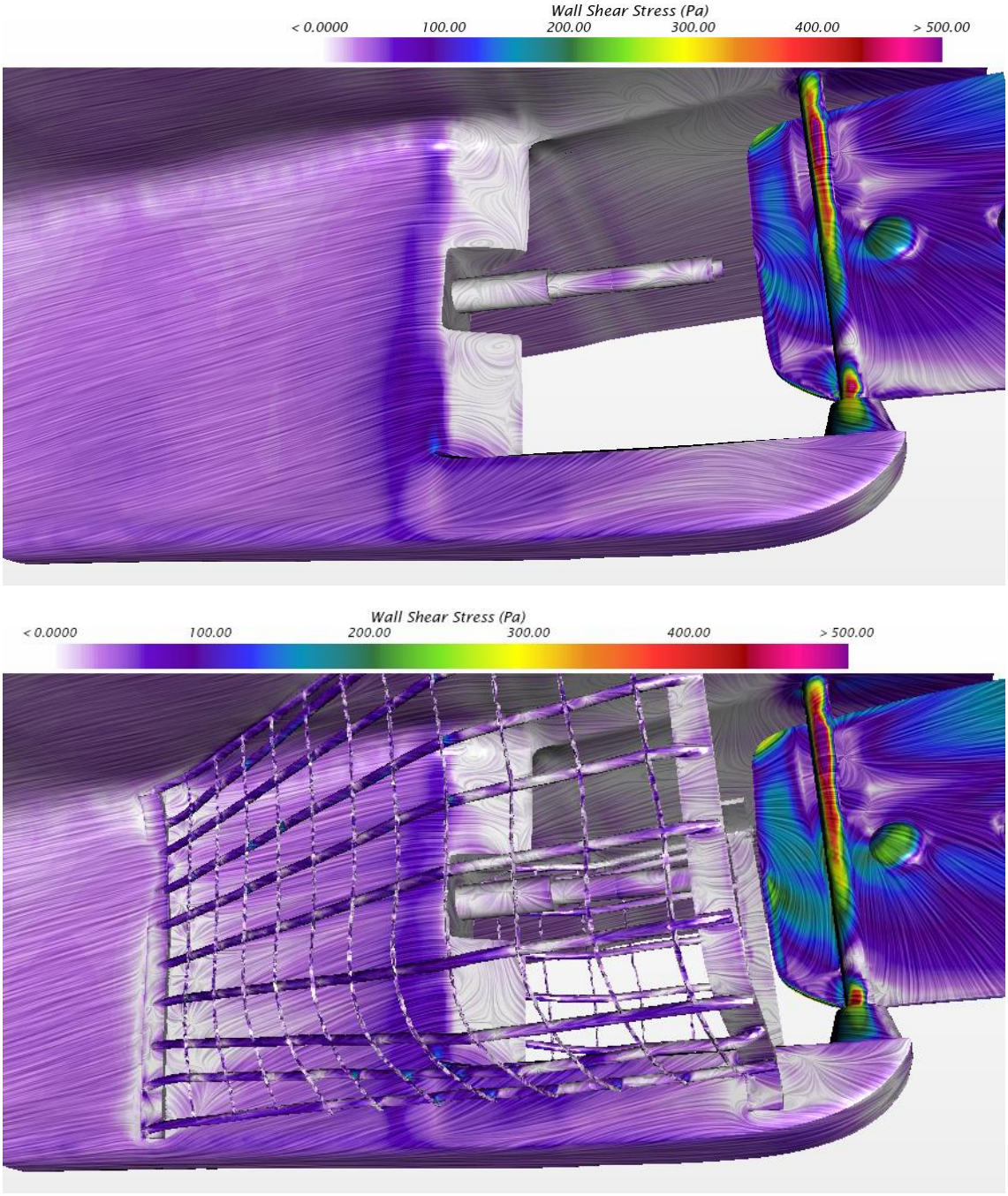

Figure 4-56: Brooklynn and Boys stern: wall shear stress (9 knots) (top: without cage, bottom: with cage).

The forces present on the Brooklynn and Boys are given in Table 4-6. The smaller diameter propeller required a higher RPM than noted for the Bay Bliss. The cage produced a similar level of drag, 27% of the total at 9 knots as opposed to 30% for the Bay Bliss.

Table 4-6: Brooklynn and Boys forces.

Self-propulsion					
Speed (knots)	Thrust - propeller (kN)	Resistance - total (kN)	RPM	Pitch (deg)	Heave (m)
9	10.95	10.97	1140	-0.75	-0.14
Stern - no cage					
Speed (knots)	Thrust - propeller (kN)	Resistance - stern (kN)	RPM	Resistance - fore+super (kN)	
9	10.43	-0.62	1140	11.585	
Stern - with cage					
Speed (knots)	Thrust - propeller (kN)	Resistance - stern+cage (kN)	RPM	Cage Resistance (kN)	Cage %
9	13.91	2.32	1257	2.94	27%

The wake fields for the Brooklynn and Boys at 9 knots are shown in Figure 4-57. The ship shows less influence from the hull than the Bay Bliss and the cage shows a more uniform flow field.

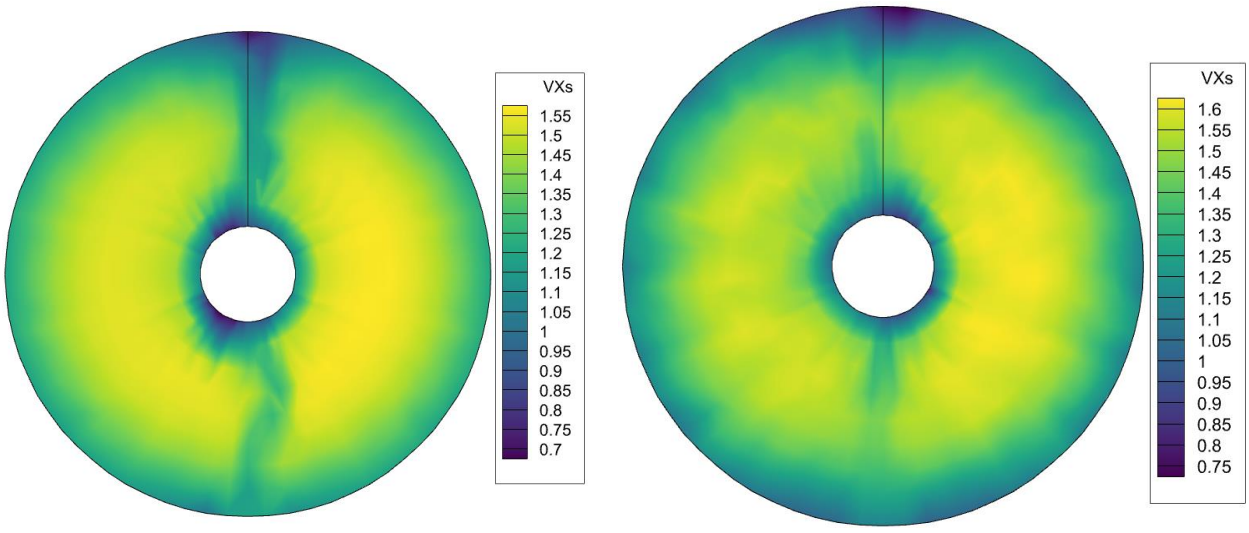

Figure 4-57: Brooklynn and Boys 9 knot effective wake fields. No cage (left), cage (right)

The target thrust and resulting RPM values for the 9 knot cases without and with the cage are shown in Table 4-7. Also shown is the RPM predicted by Star-CCM's virtual disk model. The Brooklynn and Boys propeller generally spins faster than the Bay Bliss and the same trend of PROCAL requiring a higher RPM than Star-CCM+ predictions are seen. However, the difference between the cage and no cage simulations is smaller in the case of PROCAL.

Table 4-7: Brooklynn and Boys 9 knot target thrust and RPM.

Case	Target Thrust (kN)	RPM	Star-CCM+ RPM
No Cage	10.92	1380	1140
Cage	13.92	1429	1257
Difference	3.00	49	117

Individual noise components for the 9-knot case with no cage are shown Figure 4-58. Similar to the Bay Bliss 9-knot case, the tip vortex noise dominated the response.

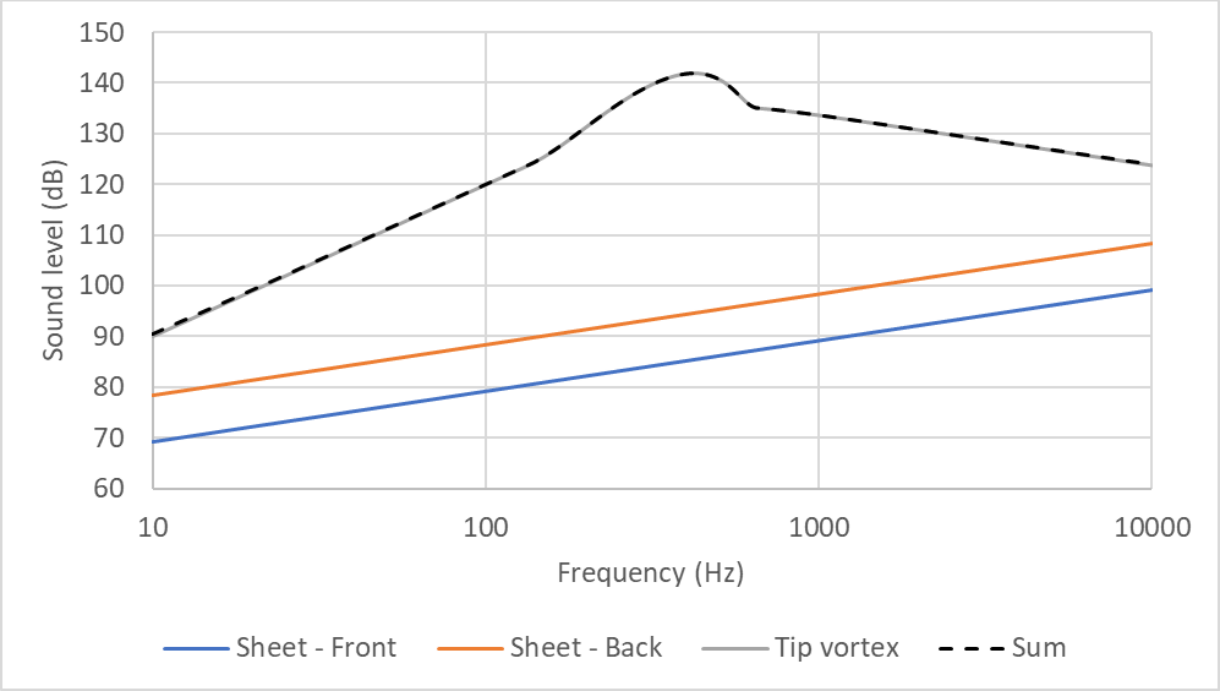

Figure 4-58: Individual propeller noise components, Brooklynn and Boys, 9 knots, no cage.

Results for the baseline, cage, and cage with drag compensation at 9 knots are shown in Figure 4-59. The Brooklynn and Boys shows less effect of the cage in the case where the drag is not compensated for. This is likely due to the fact that the wake is already considerably more uniform than the Bay Bliss and therefore the extra diffusion from the case does not influence the noise result to the same degree. The simulation where the cage drag is compensated for showed a clear increase in sound level across the full spectrum.

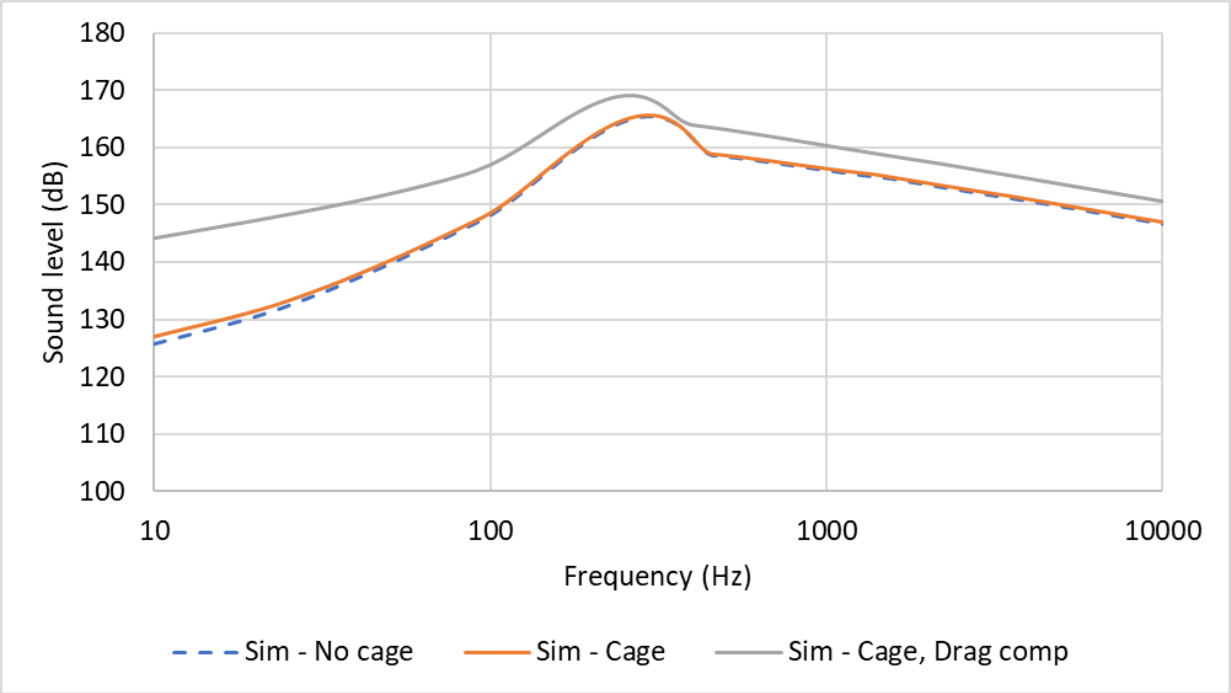

Figure 4-59: Total propeller noise, Brooklynn and Boys, 9 knots.

5. Activity #3 - Assessment of Alternative Propeller Cage Designs

A variety of propeller cage designs exist, these range from simple wire mesh cylinders with varying mesh density, metal rings (only offering protection at the propeller radius), metal rods formed to the hull, ducted propellers, and complex hybrids of all the above. There is generally a trade-off between the level of protection afforded and the impact on vessel performance. The impact on performance of these designs is rarely quantified, and no studies of the URN are available in open literature.

The goal of this activity is to assess the degree of URN expected from differing propeller cage designs. To that end, the different configurations of propeller cages (full and partial), were assessed to determine both their impact on vessel performance and to quantify the URN. The intent in this activity is not to quantify a particular device but provide evidence of broad trends linked to the overall design methodology. These results may be used as baseline for comparisons of future propeller cage designs. Recommendations can be made that add URN as a metric when propeller cages are being considered for addition to a vessel.

A review of propeller cages available commercially and in the open research literature was undertaken, Section 5.1. From the available options two were chosen to be applied as alternate designs on the Bay Bliss. CAD models were be generated for each device to the scale of the Cape Islander fishing vessels. The impact on vessel performance and URN was determined, see Sections 5.2 through 5.3. A quantitative ranking of the noise levels generated for each cage, in addition to the impact on vessel performance is provided in Section 5.4.

5.1 Review of Propeller Guard Designs

Investigations were conducted into what types of propeller cage designs were available either commercially or in other research efforts. These were found to fall broadly into the following categories:

- wire mesh (either open or closed aft)
- ring (with or without mesh or structural supports forward of ring)
- tunnel (differs from rings due to efforts to shape the flow and improve performance behaviour)

Figure 5-1: Propeller guard basic configurations

Few, if any, major suppliers were found. Some propeller sales locations also carried some form of guard. There is not a widespread market of standard products. The products are generally noted to be a niche commercial market, or improvised systems are constructed as needed (as is the case for the Cape Islander vessels). The US Coast Guard regulations do require the use of safety guards for lifeboats in their jurisdiction [20].

The simplest implementation of a propeller guard is a ring guard, see Figure 5-2. These are a metal ring that surrounds the propeller. Many have holes in the side which some manufacturers note assist in manoeuvrability. Ring guards can be very effective in protecting the propeller from damage or getting bent. In most cases, they will deflect objects away from the propeller, preventing them from coming into contact, hence preventing propeller damage and prolonging propeller life. If an object is large enough or travelling at a high speed, it may still be able to cause damage to the propeller.

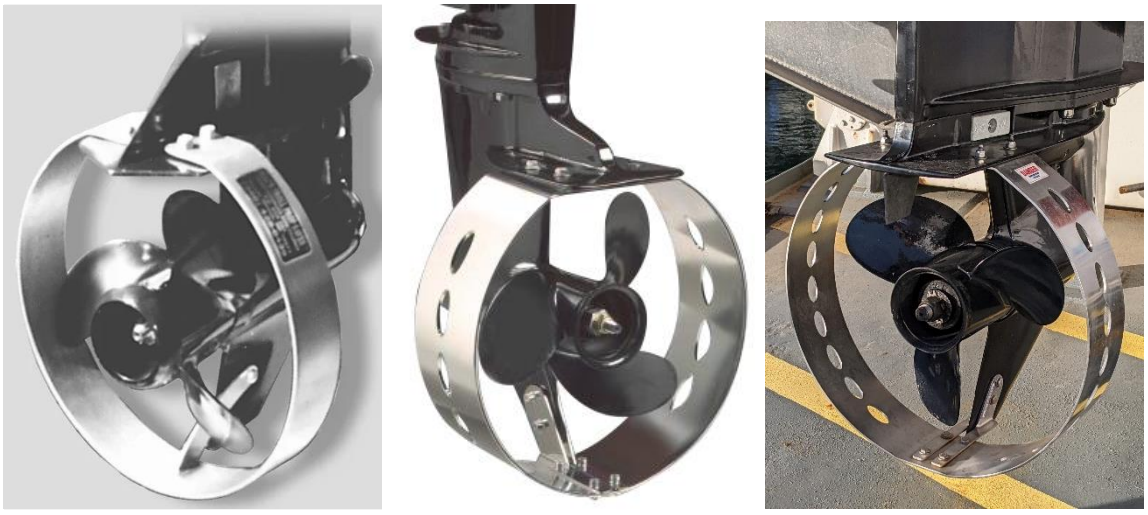

Figure 5-2: Ring guards (left: Holton Marine, middle: Adventure Marine, right: in use on BC Ferries lifeboat)

The next form are cage guards, see Figure 5-3. Cage guards are cut from a wire mesh in which the wires have a circular cross section. For larger applications, such as the Cape Islanders considered in this project, the cage is specially constructed from metal rod. These cages are used to offer the maximum protection to people and wildlife. They are also used to prevent lines from being injected into the propeller. In this case, the rear mesh is normally omitted to reduce losses. Cage guards useful on displacement boats, however they can result in considerable drag on planing boats at faster speeds.

Figure 5-3: Cage guards (left: MariTech swim guard, middle: Adventure Marine, right: Prop Guard Tech Inc.)

Often propeller guards are a hybrid of the rings and cage, see Figure 5-4. These represent an intermediate comprise in terms of less protection and performance impact. These guard provide “core” protection

(meaning the core of your body) however hands and feet may enter the propeller area. They provide the more open version in an effort to provide a balance of protection and top end speed for faster boats.

Figure 5-4: Ring / cage combination guards (left: PropGuard, middle: BH Fabrications, right: Holton Marine Ltd.)

A specialised form of the combination guard substitutes the ring for a contoured Kort nozzle, see Figure 5-5. Similar to ducted propellers, these are designed to channel the water into the propeller. For specific operating conditions such guards have been demonstrated to improve vessel performance. While some of these designs are constructed from aluminum, most are rigid plastics, which limits the size and speed of the vessel for which they are applicable.

Figure 5-5: Kort nozzle guards (left: PropGuard, middle: Thustor, right: GH Marine)

PropellerSafety.com [21] has a discussion of trade-offs when utilizing propeller guards and is an excellent source of information. However, some of the information on the website is outdated, and of the 23 guard manufacturers listed only the 8 below appear to be currently (2024) active.

1. Adventure Marine (Canada), cage & duct type propeller guards, http://adventuremarine.ca/

2. Holton Marine Ltd (New Zealand), ring guard with holes in the side of the ring, and bars to the rear of the ring. http://www.holtonmarine.com/Services/Stainless+Steel.html

3. Mac's Troll Prop Saver (USA), stainless steel ring propeller guard for smaller outboard motors, https://www.propsavers.com/

4. Midcoast Marine (Australia), stainless steel ring guards + front caging from, https://www.midcoastmarine.com.au/propeller-guards

5. OceanVier (Malaysia), ring guards and ring guards with a variety of front caging, https://oceanvier.blogspot.com/

6. Prop Guard Marine (USA) two joined polypropylene rings (duct type guard), http://www.propguardmarine.com/

7. Safe Marine Ltd. (New Zealand), ring propeller guard with two vertical bars up the back, https://propguard.co.nz/

8. Prop Guard Technologies (USA), cage prop guards with options for front and rear screens, https://www.propguardtechinc.com/

Similarly, the US Coast Guard in 2006 produced a list of twelve propeller cage devices on the market [22]. Only 3 of these are currently (2024) active, this included Safe Marine Ltd. and Prop Guard Marine from the above list, as well as:

9. Allboatproducts, Ring and cage guards, https://www.allboatproducts.com/Engine-Prop-Guards/

Research for this project also noted:

10. BH Fabrications (Southampton, UK), ring with front bars, https://bhfabrications.co.uk/prop-deflector

5.2 Alternative Design 1 - Ring

The first alternate propeller design considered was a ring guard fitted to the dimensions of the Bay Bliss, see Figure 5-6. The ring had an inner diameter of 0.7468 m (for a propeller diameter of 0.7112 m). The guard was 0.3 m in length, longer than the propeller. The ring guards reviewed above, typically do not cover the upstream and downstream extents of the propeller, so arguably a final ring design for the Bay Bliss may be shorter in length. A 1.1 cm thickness was assumed for all the guard components.

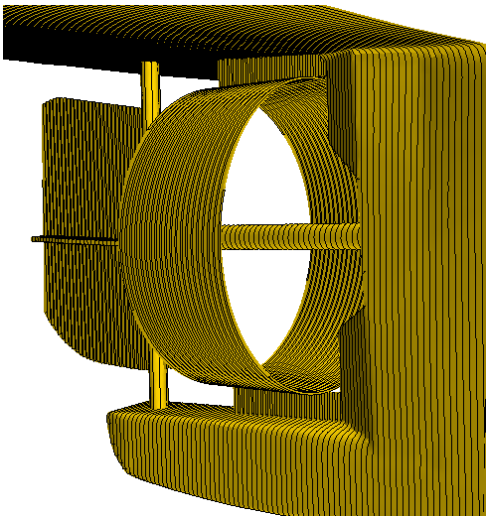

Figure 5-6: Bay Bliss alternate propeller cage 1 – ring.

The velocity magnitudes and wall shear stress are shown in Figure 5-7. The ring acts to funnel the flow to the propeller. This drops the pressure around the aft of the hull and increases the speed of the flow upstream of the propeller.

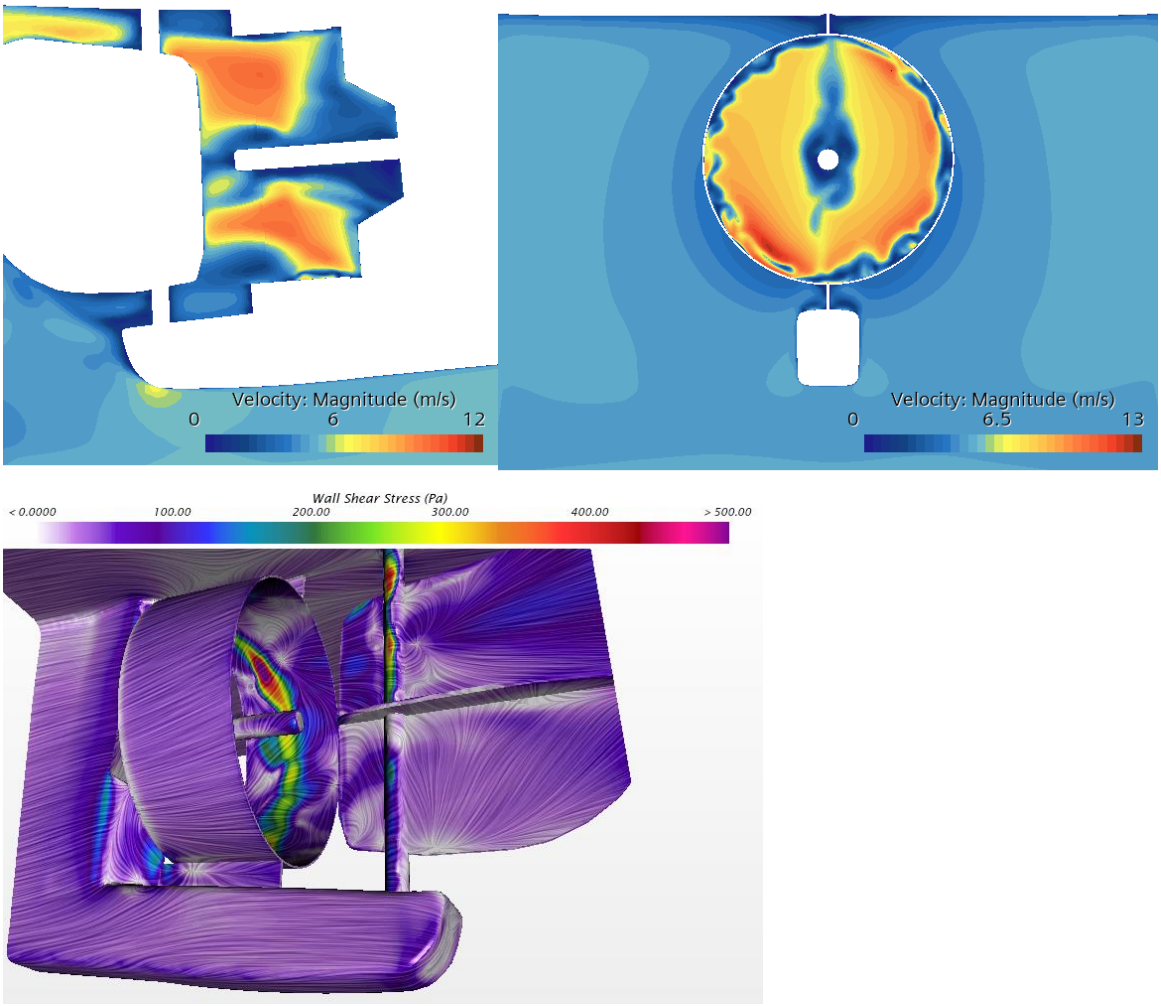

Figure 5-7: Bay Bliss alternate propeller cage 1 – ring, 9 knots (top left: centerline plane velocity magnitude, top right: cross-stream plane viewed from aft (0.25 radii ahead of propeller) velocity magnitude, bottom: wall shear stress)

5.3 Alternative Design 2 - Ring with Holes

The second alternate propeller design considered the same ring guard as given in Section 5.2, but with a series of holes, more in keeping with most ring guard designs. Eight holes with a 0.14 m diameter were chosen, see Figure 5-8.

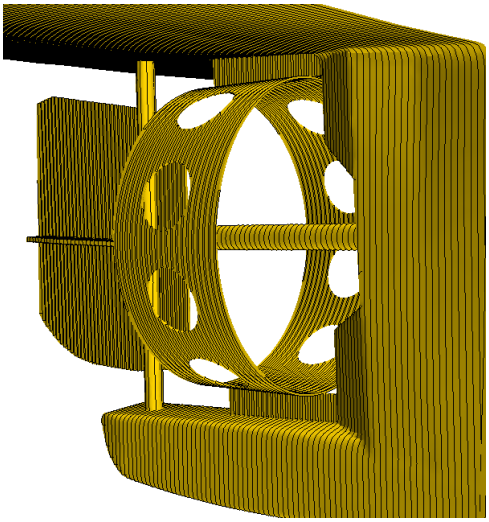

Figure 5-8: Bay Bliss alternate propeller cage 2 – ring with holes.

The velocity magnitudes and wall shear stress are shown in Figure 5-7. The ring acts to funnel the flow to the propeller. This drops the pressure around the aft of the hull and increases the speed of the flow upstream of the propeller.

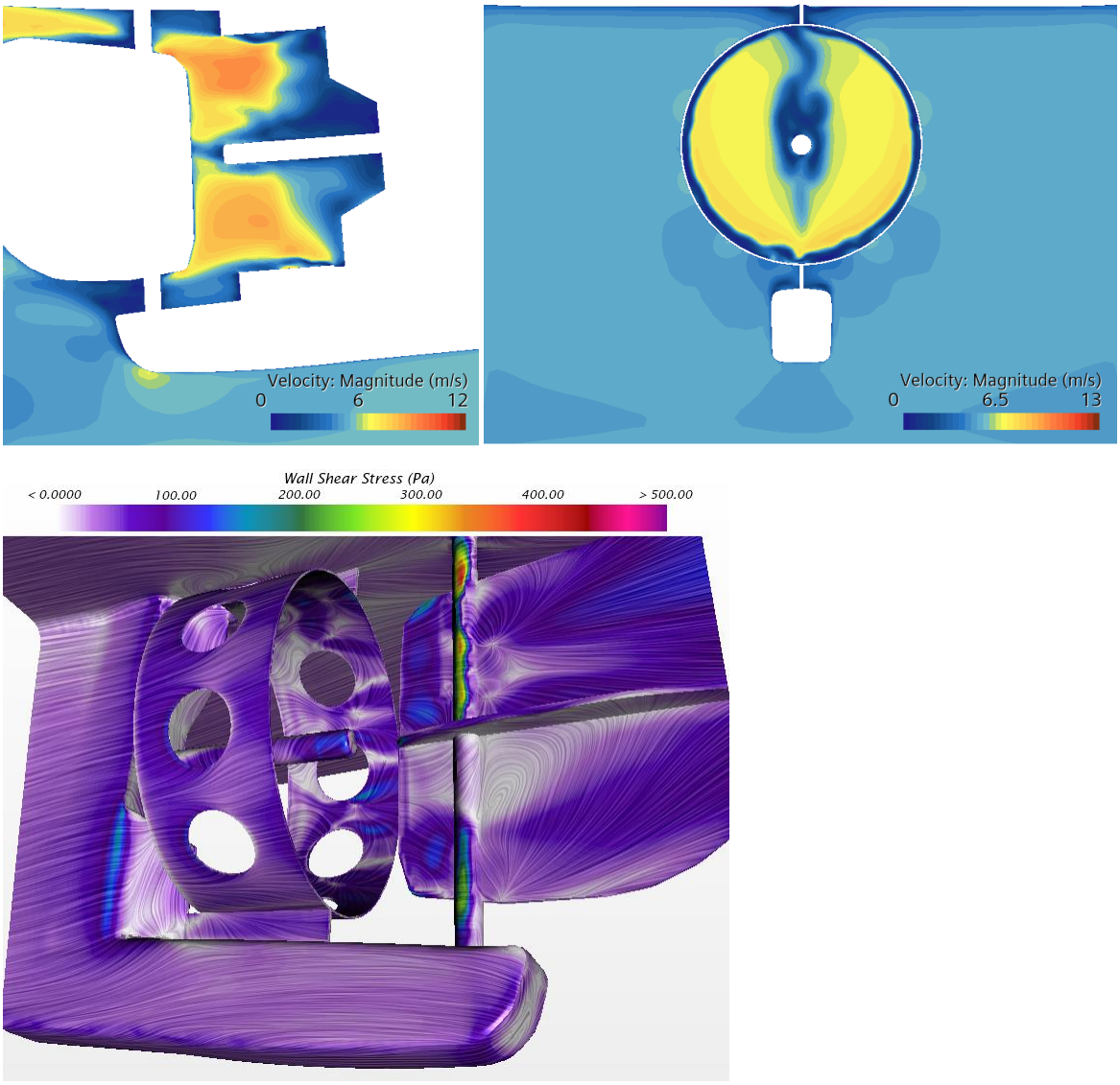

Figure 5-9: Bay Bliss alternate propeller cage 2 – ring with holes, 9 knots (top left: centerline plane velocity magnitude, top right: cross-stream plane viewed from aft (0.25 radii ahead of propeller) velocity magnitude, bottom: wall shear stress)

5.4 Alternative Design Comparison

The forces generated in the stern simulations of the alternate designs are compared to the baseline result in Table 5-1.

Table 5-1: Alternate cage design force comparison.

Stern - with cage					
Cage Design	Thrust - propeller (kN)	Resistance - stern+cage (kN)	RPM	Cage Resistance (kN)	Cage %
Baseline	14.17	3.61	874	3.25	30%
Ring	8.87	-1.71	855	-2.08	-19%
Ring with Holes	8.04	-2.54	759	-2.90	-27%

The wake fields for the Bay Bliss at 9 knots with the ring guard design variants are shown in Figure 5-10. The wakes show a strong influence from the ring around the propeller and a high level of non-uniformity as seen in the no-cage configuration. It should be noted that the PROCAL approach is not necessarily valid for this type of geometry due to the coupling approach not fully accounting for the extra influence of the rings on the propeller performance. The ring with holes design shows a less accelerated wake field compared to the first one and is expected to have better noise performance.

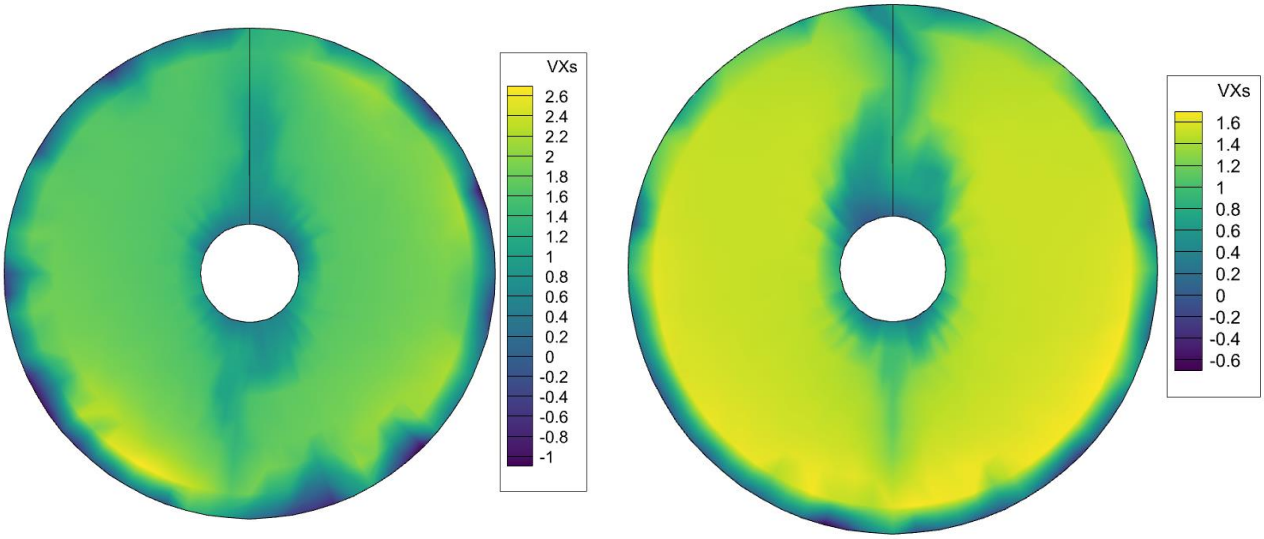

Figure 5-10: Bay Bliss 9-knot effective wake fields. Ring (left) and Ring with holes (right).

The target thrust and resulting RPM values for the 9-knot cases with the ring designs are shown in Table 5-2. The rings appear to act as a propulsive device, producing or enhancing thrust and lowering the overall drag in the system. Note again that the assumptions made for the simplified models here may not be completely valid.

Table 5-2: Bay Bliss ring guard designs, 9 knot target thrust and PROCAL predicted RPM.

Case	Target Thrust (kN)	RPM	Star-CCM+ RPM
Cage	13.7	986	870
Ring 1	8.90	954	874
Ring 2	8.06	856	759

Noise results for the baseline and two ring designs at 9 knots are shown in Figure 5-11. As predicted, the solid ring showed a higher noise result, despite the lower thrust requirement, largely due to the RPM being similar to the baseline cage design as well as the more variable wake field. The ring with holes design showed similar or slightly reduced levels of noise as compared to the original cage. This was likely due to the way the original cage made the wake field more uniform on this vessel. The ring with holes design applied to the Brooklynn and Boys would likely show a reduced noise as the cage's wake field influence had a lower impact on the noise for that vessel.

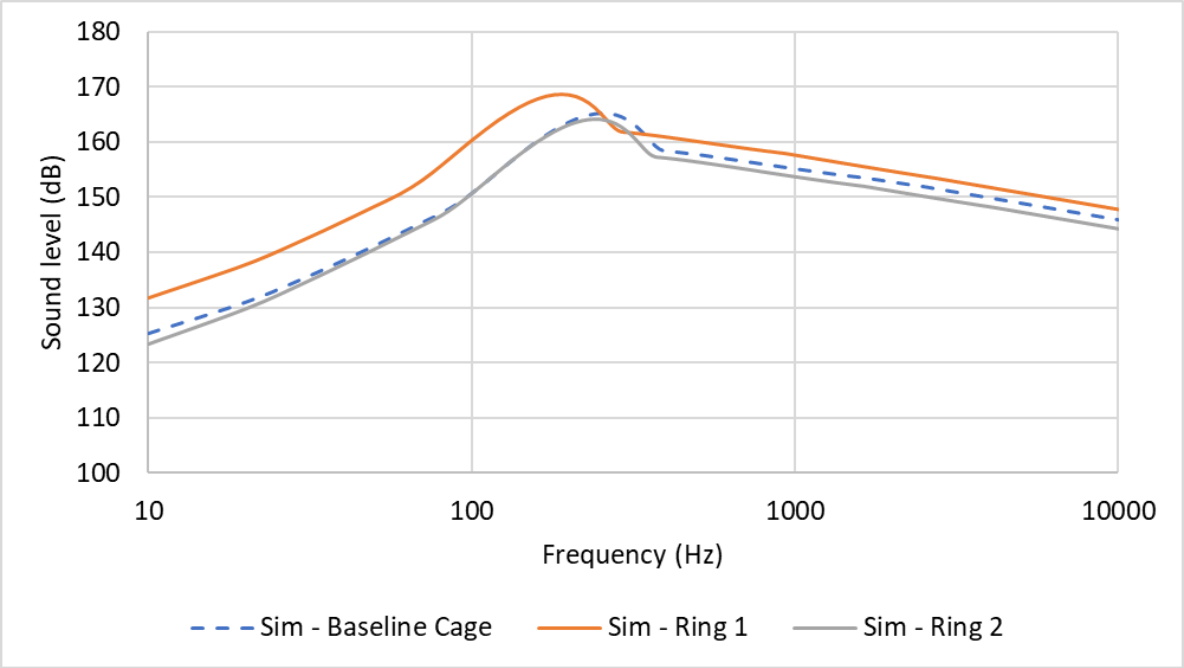

Figure 5-11: Total propeller noise, Bay Bliss with ring designs 9 knots.

6. Activity #4 - Reporting and Best Practice Guidelines

The primary action of Activity #4 was to assemble the measurements, validation study results and performance predictions of the previous three Activities into this Final Report. In addition, this work endeavoured to develop best practice guidelines for URN predictions of propeller cages to assist others with hydroacoustic modelling of propeller cages. This will assist in the consideration of URN mitigation as a design criterion for vessels.

In terms of CFD application to marine self propulsion and propeller analyses, a number of best practice guidelines are already available that incorporate far more validation than that conducted as part of this project. These include:

- ITTC – Recommended Procedures and Guidelines, Practical Guidelines for Ship CFD Applications, 7.5–03–02–03, 27th International Towing Tank Conference, 2014.
- ITTC – Recommended Procedures and Guidelines, Quality Assurance in Ship CFD Application, 7.5-03-01-02, 29th International Towing Tank Conference, 2021.
- Simcenter STAR-CCM+ Hull Performance Workflow 2302 User Guide, Siemens Digital Industries Software [12]
- P. Becchi, R. Padovan, A. Traverso, Report n. 12371, CRS-SHARCS: WP5 - CFD-calculation guidelines and conclusions, 2015 [11].

The latter reference notes that potential flow solutions or boundary element solutions neglect some physical aspects of the flow. They can only coarsely predict the macro-structures of a cavitating propeller over blades and hub without any chance to capture these phenomena in the flow field away from the boundary surfaces. Depending on the propeller being simulated this can lead to loss of accuracy. State of the art CFD modelling solves the transport equations over the entire 3D domain, allowing for full prediction of the cavitation and its development. The accuracy of a CFD prediction depends on several aspects, such as the computational domain adopted and its discretization, the numerical method, the boundary conditions imposed. The downside of the latter is that it incurs a significant computational cost.

In this project, CFD approaches were utilized to determine the overall self-propulsion performance of the Cape Islander vessels. The propulsive and URN determined via FWH were then characterized via BEM. While the original intent of this project had been to further assess CFD predicted cavitation and URN, this was not accomplished within the resources of this project. Some general guidelines developed by LR (outside this project) for these phenomena are given below.

- The accuracy of the geometry is of utmost important for the solution of the flow around the propeller. Therefore, that the leading and trailing edge of the propeller blades must be modelled properly before the meshing process.
- The propeller cavitation modelling and URN predictions are made either in open water (OW) conditions or in the presence of the non-uniform wake field. If the non-uniform wake field is of interest (i.e., behind ship condition), it is suggested to impose the calculated non-uniform wake distribution (from pure resistance simulation) in open water condition to decrease the computational cost of the solution.
- The Full-Rayleigh-Plesset equation is more correct for cavitation simulations, but it requires small timesteps and hence computational cost is high. The Schnerr-Sauer model is always preferred for

cavitation applications as it is the simplified version of the Rayleigh-Plesset equation. For this model gravity must be modelled to correctly predict the pressure term.

- Cavitation simulations require a timestep of 10^{-6} s. However, it is not possible for the marine propeller case due to the computational cost. A good compromise is to keep the timestep between 0.5 deg. and 1.5 deg. of the propeller rotation.

- If the low-frequency noise spectrum (i.e., SPL-f) and Blade Passage Frequencies (BPF) are of interest, RANS can be used. However, RANS is not capable of predicting the noise accurately in far field since the far field is highly dominated by the non-linear noise terms (i.e., turbulence and vorticity). Therefore, DES together with the k-w SST turbulence is a good compromise in terms of computational cost and accuracy.

- Always select 2nd order discretization for time and convection term to increase the accuracy of the solution.

- Always use a double precision software as acoustic pressures are small, and the accuracy may be required to capture the acoustic variations.

- Always start with steady a moving reference frame (MRF) propeller model and then switch to rigid body motion (RBM) using RANS or DES.

- Adaptive Mesh Refinement (AMR) is generally required to capture the cavitation regions. It is recommended to converge the flow on an initial mesh (i.e., without AMR). The tip vortex areas can be visualised using the threshold value of Q-criterion (vortex measure). AMR regions should then be used to refine the cavitation regions based on a Q-criterion threshold. This process may need repeated with multiple AMR levels and thresholds, see for example Figure 6-1.

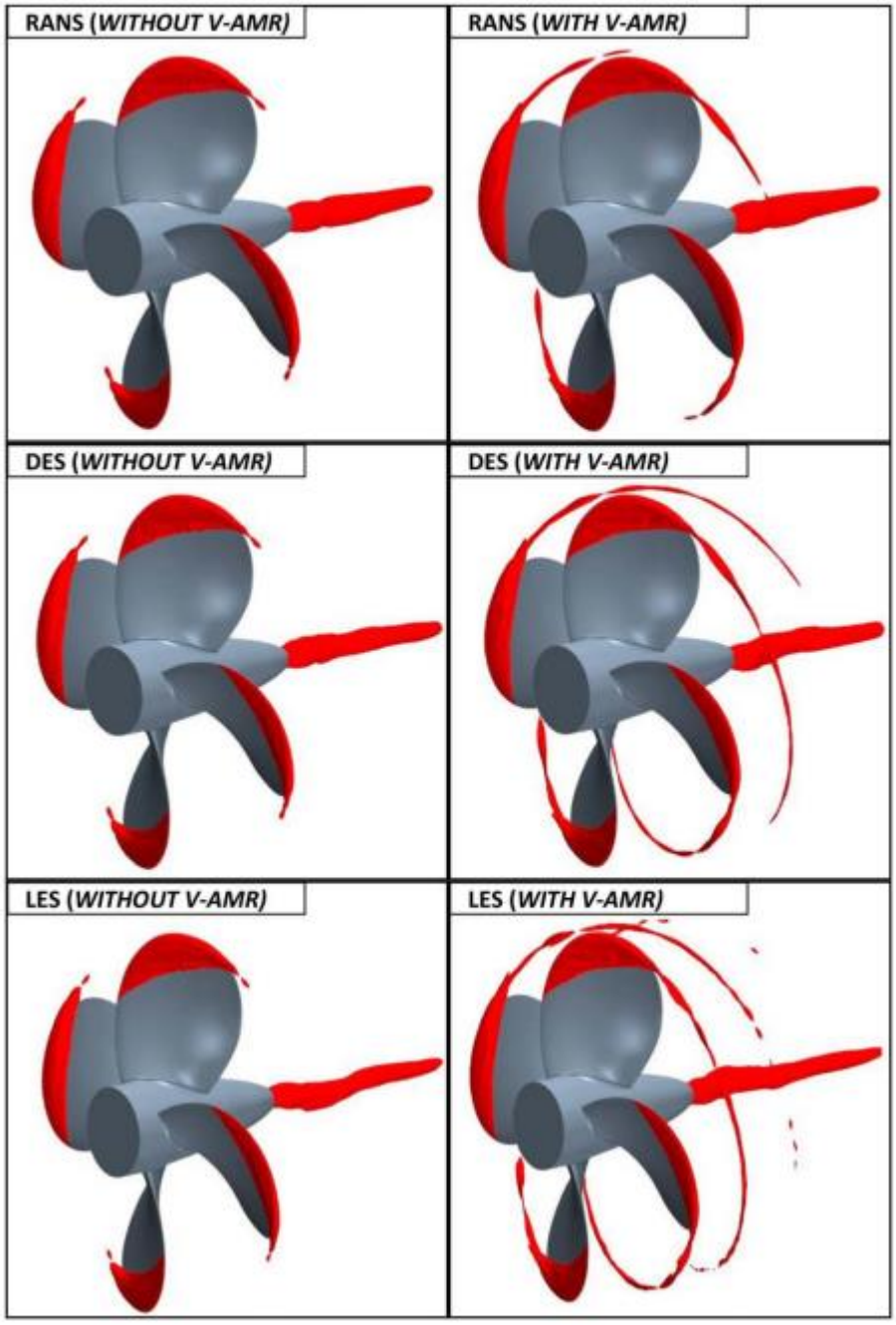

Figure 6-1: Influence of selected numerical method on tip vortex cavitation extent.

- URN is sensitive to grid resolution as it influences the propagation of sound waves. Akin to the experiments, there can be several unwanted noise sources (e.g., background noise in the tunnels). The grid structure should be well designed in the numerical solver for the accurate calculation of hydrodynamic inputs; hence, propeller URN. The low-quality cells cause deterioration of the solution accuracy, divergence, numerical and spurious noise. Therefore, the adapted mesh should be able to resolve the turbulence scales and propagate the sound from near to the far-field. Additionally, the numerical disturbances such as reflections from the domain boundaries, non-physical numerical noise generated by sliding (or rotating) interfaces, and inappropriate pressure correction methods can be considered key issues that require in-depth investigation. The artificial

reflections created by the boundaries of the computational domain can be considerably reduced with the selection of suitable domain dimensions.

- Figure 6-2 shows the example vorticity distribution in the propeller slipstream. It is adequate to include the most-energetic part of the vorticity inside the noise surface, as shown with dark red in Figure 6-2. The length of the noise surface can be increased downstream for convergence studies.

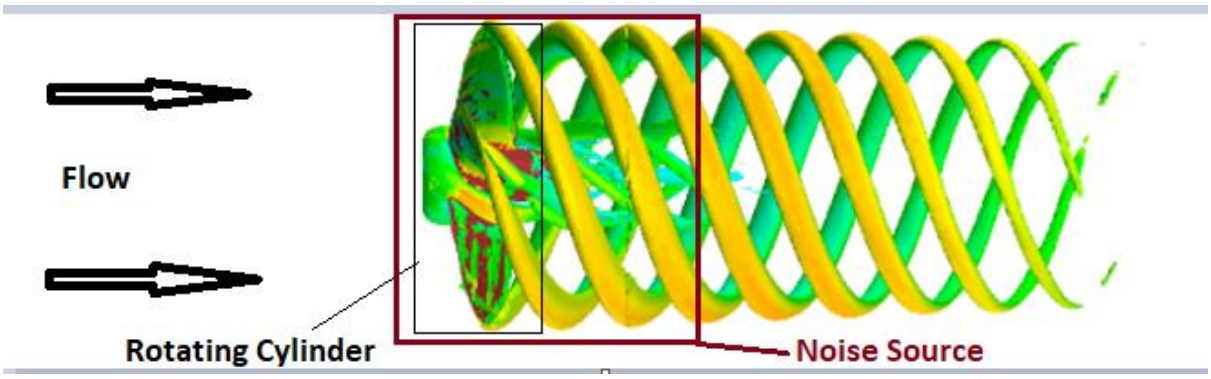

Figure 6-2: Representation of vorticity distribution, rotating and noise surfaces.

- The maximum frequency of the noise spectrum is determined according to the Nyquist theorem. For instance, for a computational timestep of 10^{-3} s, the inverse of the timestep (i.e., $1/10^{-3}$ s) makes the frequency 1000 Hz. So, the maximum frequency for the spectrum is 1000/2=500 Hz according to Nyquist theorem. Be aware of the choice of timestep and maximum frequency for the URN predictions.

- Do not activate the Quadrupole Noise under On-the-Fly FW-H (under models) since it will increase the computational cost. In practice, it is not required.

7. Project's Major Achievements

The Project's major achievements, including variation to the original activities and timelines is provided in Table 7-1 below.

This project encountered significant delays in starting, compared to the original proposed schedule as the Cape Islander vessels performed drydock ahead of schedule without informing Martec. A revised work plan was agreed with Transport Canada in November 2022 in which the vessel measurements would be completed in the spring of 2023 (with delayed timelines and cash phasing). Field testing was at this point planned for June 2023, but due to vessel commitments did not occur until September/October 2023.

Repeated attempts were made to include the cage geometry in the self-propulsion analysis with reasonable mesh sizes (to allow for the required calculations to be completed in the time and computing resources available). All of these attempts led to numerical instabilities. Alternate methodologies were adapted to allow for the project goals to be completed. These issues did prevent the full extent of sensitivity studies originally envisioned and the use of the most computationally expensive DES analyses from being completed as part of this effort.

Table 7-1: Project's major achievements.

Activity	Result	Proposed Date	Completed Date
Planning and Preparation			
Hold a kick-off meeting	Held May 12, 2022 – presentation provided to TC.	14/5/2022	12/5/2022
Organize and run periodic meetings throughout the Project lifetime	Additional meeting held November 9, 2022 and February 20, 2024, presentations provided to TC.	Monthly / as requested	9/11/2022, 20/2/2024
Activity #1: Measure acoustic signatures			
Develop a trials plan	Completed, details provided in Section 3.	22/5/2022	30/6/2023
Confirm trial vessel geometry	As detailed in Sections 2 and 4.2.	29/5/2022	30/6/2023
Activity #2: Validate hydroacoustic predictions of noise generation			
Generate vessel computer-aided design models	As detailed in Section 4.2.	11/9/2022	30/6/2023
Develop report on simulated vessel geometry	Encompassed by this report.	3/9/2022	31/3/2024
Develop baseline noise predictions	As detailed in Sections 4.4 - 4.8.	9/10/2022	31/3/2023
Develop report on final trial collected data	Encompassed by this report.	1/10/2022	31/3/2024
Run noise model sensitivity studies	Part of the baseline model development in Sections 4.4 - 4.8 plus specific studies as detailed in Section 4.9.	18/12/2022	31/3/2024

Activity	Result	Proposed Date	Completed Date
Develop report on baseline noise predictions	Encompassed by this report.	29/10/2022	31/3/2024
Develop guidelines on best practices	Part of simulation development in Section 4, guidelines as detailed in Section 6.	5/2/2023	31/3/2024
Develop report on numerical sensitivity studies	Encompassed by this report.	7/1/2023	31/3/2024
Run studies on fouled cage sensitivity	Fouled cage results as detailed in Section 4. No specific sensitivity studies developed for fouled cages.	2/4/2023	31/3/2024
Develop report on fouling simulations	Encompassed by this report.	8/5/2023	31/3/2024
Draft 2nd vessel noise predictions	As detailed in Section 4.10.	4/6/2023	29/2/2024
Finalize numerical modelling best practice guidelines	Part of simulation development in Section 4, guidelines as detailed in Section 6.	4/6/2023	31/3/2024
Develop report on 2nd vessel simulations	Encompassed by this report.	20/5/2023	31/3/2024
Activity #3: Assessment of alternative propeller cage designs			
Collect propeller cage geometry	As detailed in Section 5.1.	25/6/2023	31/12/2023
Generate propeller cage computer-aided designs	As detailed in Sections 5.2 - 5.3.	2/7/2023	31/3/2024
Develop report on alternative cage geometries	Encompassed by this report.	1/7/2023	31/3/2024
Run simulations on alternate cage designs	As detailed in Sections 5.2 - 5.4	1/10/2023	31/3/2024
Develop report on alternative cage noise predictions	Encompassed by this report.	2/9/2023	31/3/2024
Develop final report on Project results	Encompassed by this report.	2/12/2023	31/3/2024
Activity #4: Reporting and Best practices guidelines			
Document trial plan	As used for trials.	12/6/2022	30/6/2023
Verification of initial trial data	In field verification of results.	31/7/2022	31/10/2023
Run subsequent trials as required	Not required.	8/10/2022	NA
Develop report on initial trial results	Encompassed by this report.	13/8/2022	31/3/2024

8. Performance Indicators

This project developed a series of technologies and evaluated other technologies for these use in underwater radiated noise measurement and prediction. These include:

1. Generation of Cape Islander vessel computer-aided designs.

2. URN noise measurements of Cape Islander vessels that characterizes the signatures without cages, with cages, and with fouled cages across the operating speed.

3. Hull pressure measurements of Cape Islander vessels that characterizes the signatures without cages, with cages, and with fouled cages across the operating speed.

4. Generation of CFD models of the 2 Cape Islander vessels for self-propulsion.

5. Assessment of CFD for predicting propeller cage performance impacts.

6. Assessment of CFD and BEM methods for predicting URN.

7. URN noise predictions of Cape Islander vessels that characterizes the signatures without cages, with cages, and with fouled cages across the operating speed.

8. Assessment of CFD model parameters (turbulence model, mesh resolution, mesh refinement regions, geometric details, etc.) for propeller cage performance and URN impacts.

9. Generation of URN and performance predictions for alternate propeller cage designs.

9. Lessons Learned

This project encountered significant delays in starting, compared to the original proposed schedule since the Cape Islander vessels performed drydock ahead of schedule without informing Martec. A revised work plan was agreed with Transport Canada in November 2022 in which the vessel measurements would be completed in the spring of 2023 (with delayed timelines and cash phasing). Field testing was at this point planned for June 2023, but due to vessel commitments did not occur until September/October 2023. While the project schedule still allowed sufficient time for the major project goals to be accomplished, this delay did impact the number of numerical analyses that could be performed. While this project relied on the good will and willing participation of the vessel captains to proceed, written commitments from 3rd parties are recommended in the future.

Repeated attempts were made to include the cage geometry in the self-propulsion analysis with reasonable mesh sizes (to allow for the required calculations to be completed in the time and computing resources available). All of the attempts led to numerical instabilities. Alternate methodologies were adapted to allow for the project goals to be completed. These issues did prevent the full extent of sensitivity studies originally envisioned and the use of the most computationally expensive DES analyses from being completed as part of this effort. Future efforts are recommended to utilize “clean” geometries. These would sacrifice some of the fine details of the geometry such as close contact parts and welds. While this would reduce the solution accuracy, it allows for converged solutions to be generated. The degree of error introduced may be evaluated by simulations with very fine resolution.

10. Conclusions and Recommendations

The increased underwater acoustic ambient noise has had notable impacts on marine mammals that rely heavily on their generated underwater acoustic signals as a primary means to communicate, navigate, and forage in the ocean. Transport Canada's Quiet Vessel Initiative recognizes this through their Underwater Radiated Noise (URN) and Green House Gas Reduction Program for Canada's Inshore Fishing Craft. For most ships and boats, the on-board machinery and propeller noise comprises the majority of the generated noise that becomes radiated into the far-field.

There is a fair body of work on URN for large commercial and naval ships but the focus in this project is the URN of small marine craft (fishery vessels, crab vessels, lifeboats, and a significant portion of pleasure craft) fitted with propeller cages. These are used to prevent snagging of lines and limit injury to both people and wildlife. These cages have several adverse impacts on URN. The cages can significant increase drag which negatively influences boat performance and increases fuel consumption. Fouling of the cages exasperates these issues, with operators compensating by running the propellers at higher speed generating further cavitation and URN. Propeller cage impact on performance is rarely quantified, and no studies of their URN are present in the open literature.

In this project, the impact of propeller cages on URN was quantified by performing experimental measurements for 4 Cape Islander fishing vessels with bare propellers, propeller cages, and artificially fouled cages. In total 188 trials were conducted (4 vessels, ambient, static, dynamic runs without cage, with cage, with fouled cage). There is significant scatter in the measurement, however all vessels exhibited the highest peak near 5 Hz at approximately 160 dB. Generally, the presence of the cage increases the signature (up to 20 dB in some parts of the spectrum). Additionally fouling tends to increase the noise but has a larger impact on the lower speeds. The intention of this project was to generate a data set that may be used to assist in understanding URN interactions. As such the experimental data is freely available.

The second purpose of this project is to provide a validated modelling environment for future assessments of URN generated by propeller cages. While sea trials are necessary, they often address a limited number of operating conditions or geometries. Validated numerical models can be used to complement costly trial measurements and determine all desired quantities with a high resolution in space and time. Two vessels (of the four measured) were selected for model generation and noise predictions. Numerical representations of the vessel geometries were developed. Computational fluid dynamics (CFD) simulations were combined with a boundary element method (BEM) to simulate propeller performance and cavitation. Additional models were utilized to obtain noise predictions. The cages themselves were shown to have little noise generation compared to the propeller. The main issue is that the cages significantly increased the vessel drag, and hence the propeller required a higher RPM to compensate. Numerical predictions of the noise levels were higher than was determined experimentally. This may be due to a variety of factors: BEM not applicable for this class of vessel, cavitation induced noise fits not being applicable to this size/speed of propeller, insufficient resolution of the flow entering the propeller, incorrect characterization of the propeller geometry, or model settings not explored as part of this project. These are factors that should be explored in future assessments. The relative jump in noise was replicated by the numerical predictions for the bare, propeller, propeller cage, and fouled propeller. This would suggest that the relative impacts of propeller cages may be determined by the current methodology.

Best practices derived from this project and other applicable numerical analyses were presented.

The relative merits of two different propeller cages designs were assessed compared to the baseline propeller cage.

The cage drag in conjunction with propeller cavitation were identified as the primary mechanisms for increases in URN. Several CRS working groups [11] have identified that stator designs can potentially be used to reduce cavitation. Ducted propellers can also be designed to minimize cavitation. Both of these geometric features can potentially be incorporated into a cage design with the goal of increasing propeller efficiency, reducing cavitation and therefore URN while also maintaining the practical objectives of a propeller cage.

11. References

[1] G. V. Frisk, "Noiseonomics: The relationship between ambient noise levels and global economic trends," *Scientific Reports,* vol. 2, no. 1, p. 437, 2012.

[2] R. W. Fisher and N. A. Brown, "Factors Affecting the Underwater Noise of Commercial Vessels Operating in Environmentally Sensitive Areas," in *OCEANS, Proceedings of MTS/IEEE*, Washington, D.C., USA, 2005.

[3] G. Wenz, "Acoustic ambient noise in the ocean: spectra and sources," *The Journal of the Acoustical Society of America,* vol. 34, p. 1936, 1962.

[4] S. Nilsson and N. P. Tyvand, "Noise Sources in Ships: I Propellers, II Diesel Engines," Nordic Cooperative Project: Structure Borne Sound in Ships from Propellers and Diesel Engines, Nordforsk, Norway, 1981.

[5] T. Sasajima, N. Nakamura and A. Oshima, "Model and Full Scale Measurements of Propeller Cavitation Noise on an Oceanographic Research Ship with Two Different Types of Screw Propeller," in *In: Buiten, J. (eds) Shipboard Acoustics*, 1986.

[6] J. Hallander and B. Göran, "Influence of acoustic interaction in noise generating cavitation," in *24th Symposium on Naval Hydrodynamics*, Fukuoka, Japan, 8-13 July 2002.

[7] Lloyd's Register & GIT , "Results from underwater acoustic measurements from the application of XGIT coatings compared to the previous baseline conditions," Transport Canada Project (TR-22-33) - URN & GHG Reduction Program for Canada's Inshore Fishing Craft.

[8] "Agisoft Metashape 2.1.0," Agisoft LLC, 64 Kirochnaya street, St. Petersburg, Russia, 191015, [Online]. Available: https://www.agisoft.com/.

[9] "MeshLab 2022.02," [Online]. Available: https://www.meshlab.net/.

[10] "Rhino 7," Robert McNeel & Associates, 146 N Canal St, Suite 320, Seattle, WA 98103 USA, [Online]. Available: https://www.rhino3d.com/.

[11] "Cooperative Research Ships (CRS)," [Online]. Available: https://www.crships.org/#.

[12] "Star-CCM+," Siemens Aktiengesellschaft, [Online]. Available: https://plm.sw.siemens.com/en-US/simcenter/fluids-thermal-simulation/star-ccm/.

[13] MARIN, "PROCAL V2.0 User's Guide," 2009.

[14] MARIN, "CRS Propagate II: T131 PropART User Guide V1.800," 2023.

[15] MARIN, "Empirical cavitating Tip Vortex (ETV) model version 3; Incorporating tonals and cavitating flow results; CRS ONBOARD, Task 1.3," 2020.

[16] F. R. Menter, "Two-Equation Eddy-Viscosity Turbulence Models for Engineering Applications," *AIAA Journal,* vol.

32, no. 8, pp. 1598-1605, August 1994.

[17] "ITTC – Recommended Procedures: Fresh Water and Seawater Properties," in *7.5-02-01-03 (2011 Rev. 02), International Towing Tank Conference*, 2011.

[18] "U.S. Standard Atmosphere, 1976," U.S. Government Printing Office, Washington, D.C., USA, 1976.

[19] "ITTC Recommended Procedures and Guidelines: 1978 ITTC Performance Prediction Method," 7.5-02-03-01.4, 27th International Towing Tank Conference , 2017.

[20] *United States Coast Guard Lifeboat Regulations: 160.135-7 Design, Construction, and Performance of Lifeboats,* 2012.

[21] May 2023. [Online]. Available: https://www.propellersafety.com/.

[22] U. C. Guard, "2006-03-21 USCG Prop Intervention Devices," 2006.

Contact person
Derrick Alexander
237 Brownlow Ave, Suite 200, Dartmouth, NS, Canada, B3B 2C6

Registered name Martec Limited

t: +1 (902) 417 2471
e: derrick.alexander@lr.org
w: lr.org